Solid Earth, 12, 2735–2771, 2021
https://doi.org/10.5194/se-12-2735-2021

Solid Earth Open Access EGU

Chronology of thrust propagation from an updated tectono-sedimentary framework of the Miocene molasse (western Alps)

Amir Kalifi[1,2], Philippe Hervé Leloup[1], Philippe Sorrel[1], Albert Galy[3], François Demory[4], Vincenzo Spina[2], Bastien Huet[2], Frédéric Quillévéré[1], Frédéric Ricciardi[2], Daniel Michoux[2], Kilian Lecacheur[1], Romain Grime[1], Bernard Pittet[1,†], and Jean-Loup Rubino[2]

[1]Laboratoire de Géologie de Lyon, Terre Planètes et Environement, Univ Lyon 1, ENSL, CNRS, LGL-TPE, 69622 Villeurbanne, France
[2]Total SA, CSTJF, Avenue Larribeau, 64000 Pau, France
[3]CRPG, 15 rue Notre Dames des Pauvres, 54500 Vandœuvre-lès-Nancy, France
[4]Aix Marseille Univ, CNRS, IRD, INRAE, Coll France, CEREGE, Aix-en-Provence, France
[†]deceased

Correspondence: Amir Kalifi (kalifi.amir@gmail.com)

Received: 20 April 2021 – Discussion started: 8 June 2021
Revised: 31 October 2021 – Accepted: 8 November 2021 – Published: 15 December 2021

Abstract. After more than a century of research, the chronology of the deformation of the external part of the western Alpine belt (France) is still controversial for the Miocene epoch. In particular, the poor dating of the foreland basin sedimentary succession hampers a comprehensive understanding of the deformation kinematics. Here we focus on the Miocene molasse deposits of the northern subalpine massifs, southern Jura, Royans, Bas-Dauphiné, Crest, and La Bresse sedimentary basins through a multidisciplinary approach to build a basin-wide tectono-stratigraphic framework. Based on sequence stratigraphy constrained by biostratigraphical, chemostratigraphical (Sr isotopes), and magnetostratigraphical data between the late Aquitanian (∼ 21 Ma) and the Tortonian (∼ 8.2 Ma), the Miocene molasse chronostratigraphy is revised with a precision of ∼ 0.5 Ma. The Miocene molasse sediments encompass four different paleogeographical domains: (i) the oriental domain outlined by depositional sequences S1a to S3 (∼ 21 to ∼ 15 Ma), (ii) the median domain characterized by sequences S2 to S5 (∼ 17.8 to ∼ 12 Ma), (iii) the occidental domain in which sequences S2a to S8 (∼ 17.8 to ∼ 8.2 Ma) were deposited, and (iv) the Bressan domain where sedimentation is restricted to sequences S6 to S8 (∼ 12 to ∼ 8.2 Ma). A structural and tectono-sedimentary study is conducted based on new field observations and the reappraisal of regional seismic profiles, thereby allowing the identification of five major faults zones (FZs). The oriental, median, and occidental paleogeographical domains are clearly separated by FZ1, FZ2, and FZ3, suggesting strong interactions between tectonics and sedimentation during the Miocene. The evolution in time and space of the paleogeographical domains within a well-constrained structural framework reveals syntectonic deposits and a westward migration of the depocenters, allowing for proposing the succession of three deformation phases at the western Alpine front. (i) The first is a compressive phase (P1) corresponding to thrusting above the Chartreuse oriental thrust (FZ1), which was likely initiated during the Oligocene and rooted east of Belledonne. This tectonic phase generated reliefs that limited the Miocene transgression to the east. (ii) The second is a ∼ WNW–ESE-directed compressive phase (P2) lasting between 18.05 ± 0.25 Ma and ∼ 12 Ma, with thrusts rooted in the Belledonne basal thrust. Thrusts were activated from east to west: the Salève (SAL) and Gros Foug (GF) thrusts and then successively FZ2, FZ3, FZ4, and FZ5. Along two WNW–ESE balanced cross sections the amount of horizontal shortening is of ∼ 6.3 to 6.7 km, corresponding to average shortening rates of ∼ 1.2 km Myr^{-1} and migration of the deformation toward the west at a rate of ∼ 2.9 km Myr^{-1}. Dur-

ing ∼ 6 Myr, the Miocene Sea was forced to regress rapidly westwards in response to westward migration of the active thrusts and exhumation of piggyback basins atop the fault zones. Phase P2 thus deeply shaped the Miocene paleogeographical evolution of the area and appears as a prominent compressive phase at the scale of the western Alps from the Swiss molasse basin to the Rhodano–Provencal one. (iii) The third is a ∼ 300 m phase of uplift in the Bas-Dauphiné (P3) of probable Tortonian age (∼ 10 Ma), which would have induced southward sea retreat and been coeval with the folding of the Jura in the north and possibly with back-thrusting east of the Chartreuse massif.

1 Introduction

Foreland basins result from the flexural warping of the lithosphere in response to the orogenic load induced by a continental collision (Dickinson, 1974; Beaumont, 1981). Along the flexural profile of the foreland basin, the accommodation space increases progressively towards the orogeny and is maximal near the deformation front (DeCelles and Giles, 1996). As the deformation front advances, the entire flexural profile is forced to migrate, and additional secondary controls interact with the flexural migration. Thrust systems are activated synchronously with the sedimentary infill between the deformation front and the inner part of the orogenic wedge. There, small-scale basins are carried on top of growing thrusts and constitute "piggyback basins" (Ori and Friend, 1984). As a result, foreland basin strata (including piggyback basins; DeCelles and Giles, 1996) are among the most reliable witnesses of the geometry and kinematics of growing structures (Suppe et al., 1992) and thus of the advance of the deformation front.

The arcuate form of the western Alps results from a N-NW-directed continental collision from Eocene to earliest Oligocene (Ford and Lickorish, 2004; Dumont et al., 2008, 2011, 2012) then W-directed motion driven by extrusion of the internal western Alps, leading to the radially propagating arc (Butler, 1992a; Dumont et al., 2011, 2008). This evolution was recorded in the foreland basin strata. From the Oligocene to the Aquitanian, the larger flexural basin was located in the North Alpine Foreland Basin (NAFB, Fig. 1A) where molasse deposits are very thick (up to 4 km; Bonnet et al., 2007; Burkhard and Sommaruga, 1998). During the middle to late Miocene, the NAFB was uplifted (Ford and Lickorish, 2004), and the depocenter migrated to the west along the western Alpine foreland basin in France (Allen and Bass, 1993; Lamiraux, 1977) (Fig. 1A). The present study focuses on the transitional area between these two domains (Fig. 1A), which correspond to the southern prolongation of the NAFB (southern Jura synclines) constituted by lower Miocene strata and the northern termination of the western Alpine foreland basin (Bas-Dauphiné basin) constituted mainly by middle to upper Miocene deposits (Latreille, 1969; Nicolet, 1979; Kwasniewski et al., 2014). The Bas-Dauphiné basin is located in front of the Vercors and Chartreuse subalpine massifs and southern Jura synclines (Fig. 1B) where Miocene deposits outcrop in piggyback basins above NNE–SSW-trending Miocene thrusts that root in a basement thrust below the External Crystalline Massif (ECM) (Laubscher, 1992; Bellahsen et al., 2014; Deville and Chauvière, 2000; Deville et al., 1994, 1992). In the NAFB and the southern Jura synclines, Miocene syntectonic deposits date from the late Burdigalian (e.g., Allen and Bass, 1993; Beck et al., 1998; Deville et al., 1994; Garefalakis and Schlunegger, 2019) and a westward depocenter migration occurred between the early and the middle Miocene (Lamiraux, 1977; Bass, 1991). Further south, in the Vercors–Chartreuse and Bas-Dauphiné basins, syntectonic deposits are, however, still insufficiently described. Hence, this hampers a comprehensive understanding of the onset and the chronology of the Alpine deformation over the Miocene.

This study aims at reappraising the Miocene deformation history of the western Alpine foreland basin. Based on $^{87}Sr/^{86}Sr$ dating combined with new sedimentological fieldwork, new sequence stratigraphy interpretations for upper Aquitanian to lower Langhian sedimentary successions outcropping in piggyback basins of the subalpine massifs and the southern Jura synclines have been proposed (Kalifi et al., 2020). Here, we complete this work with data from the Bas-Dauphiné, Crest, and La Bresse basins, and we propose an updated chronostratigraphy for the whole area based on integrated biostratigraphical, magnetostratigraphical, and new chemostratigraphic dating of well logs and field sedimentological sections. A new structural analysis is also conducted based on fieldwork data along with a reinterpretation of available seismic lines, geological maps, and published cross sections. Taken together, the sedimentological, chronostratigraphical and structural approaches enable an updated calendar of the subalpine massifs and southern Jura deformations and shortening phases as a response to the western propagation of the Alpine orogen during the Miocene.

2 Geological setting

The western Alpine foreland basin corresponds to a part of the peripheral foreland basin of the Cenozoic Alpine orogeny (Fig. 1A). The Alpine orogeny originates from the closure of the Tethyan Ocean and subsequent continental collision between Eurasia and Adria (or Apulia) (Nicolas et al., 1990; Pfiffner et al., 1997; De Graciansky et al., 2011). The study area (Fig. 1B) includes (i) the subalpine massifs (i.e., Vercors, Chartreuse, and Bauges massifs) and the French southern Jura, where the Miocene "molasse" deposits are preserved within synclinal structures and constitute the infill of piggyback basins and (ii) the Bas-Dauphiné, La Bresse, and Crest basins (Fig. 1B), where deposits are poorly deformed

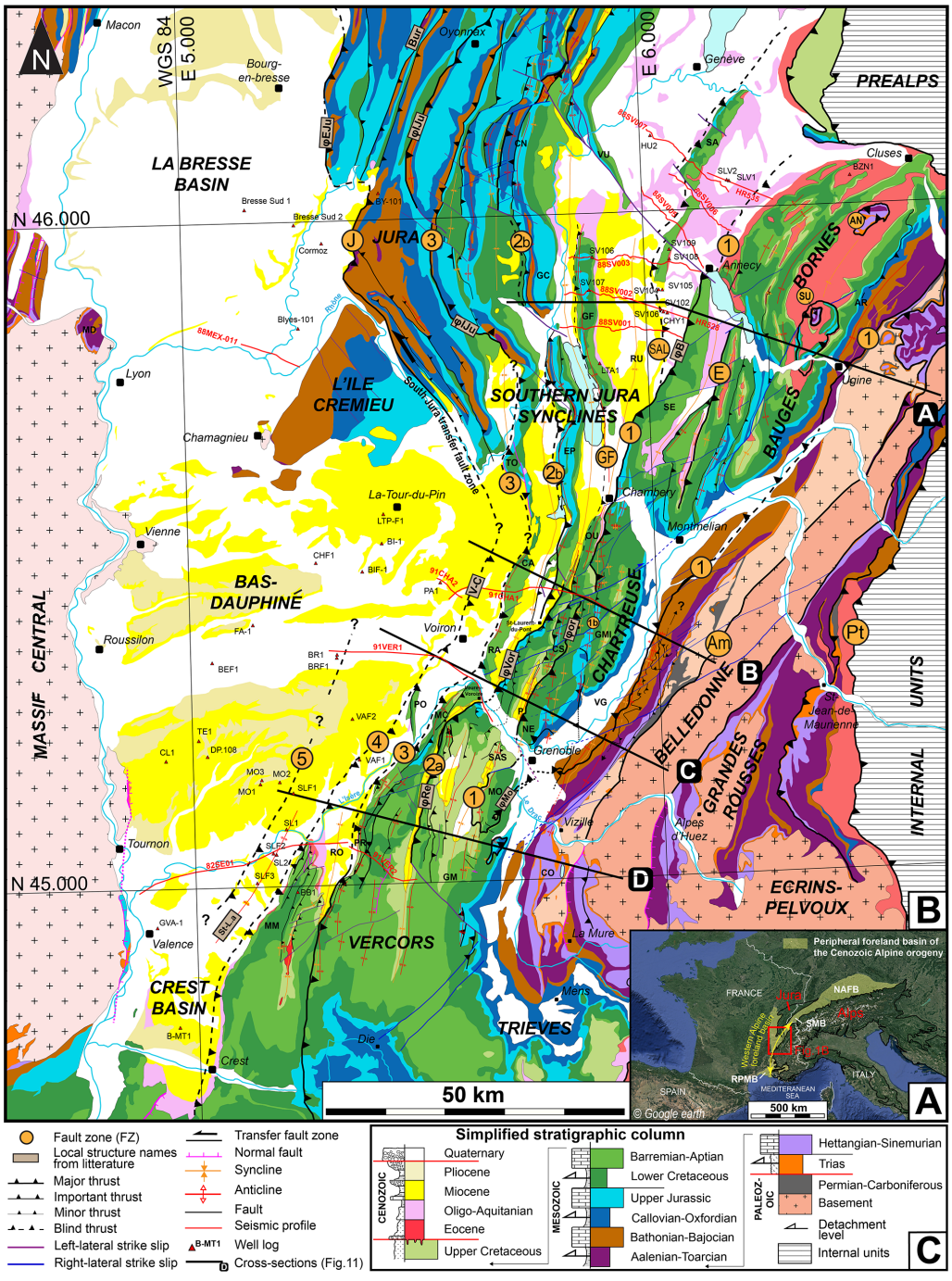

Figure 1. **(A)** Location of the western Alpine foreland basin and the study area. NAFB: North Alpine Foreland Basin. SMB: Swiss molasse basin. RPMB: Rhodano–Provencal molasse basin. **(B)** Structural map of the subalpine massifs, the southern Jura, and adjacent basins (Bas-Dauphiné, Crest, La Bresse). Names of the main faults are indicated within orange circles: 1 to 5 are fault zones (FZs) defined in this study. PT: Penninic thrust; Am: internal Belledonne thrust; E: Entrevernes thrust; SAL: Salève thrust; J: Jura thrust; SU: Sulens klippe; AN: Annes klippe. Local fault names from the literature are as follows. φB: Bauges thrust; φEJu: external Jura thrust; φIJu: internal Jura thrust; φMo: Moucherotte thrust; φor: oriental Chartreuse thrust; φvor: Voreppe thrust; φRe: Rencurel thrust; Bur: Buron thrust; St-L.a: Saint Lattier anticline; V-C: Voiron–Chirens fault. Local ranges and structures names are as follows. AR: Aravis; CA: Chailles; CN: Crêt du Nu; CO: Conest; EP: Epine; GC: Grand Colombier; GM: Grande Moucherolle; GMI: Grand Manti; GF: Gros Foug anticline; MC: Montaud col; MD: Monts-d'or; MM: Monts-du-Matin; MO: Moucherotte; NE: Néron; P: Proveyzieux anticline; PO: Poliénas; PR: Pont-en-Royans anticline; OU: Outherans; RA: Ratz; RO: Royans; RU: Rumilly syncline; SA: Salève; SAS: Sassenage; SE: Semnoz; TO: Tournier; VG: Grésivaudan valley; VU: Vuache. Seismic profiles appear as red lines and wells as red triangles. **(C)** Simplified synthetic stratigraphic column of the area stressing the main unconformities (red lines) and potential detachment levels (arrows). Same colors as for Figs. 3, 7, 8, 9, 10, 11, 14, and S1.

and constitute the infill of the foreland basin. These deposits generally lie unconformably on the thick Mesozoic substratum or conformably on Oligocene continental deposits (Bass, 1991; Butler, 1992b; Kalifi et al., 2020; Allen and Bass, 1993; Gidon and Arnaud, 1978) and result from the second shallowing-upward cycle of the western Alpine foreland basin overfilled phase (Sinclair and Allen, 1992). During this cycle, the regional paleogeography corresponded to a narrow and shallow seaway that connected the Mediterranean Sea (ex-Tethys) to the NAFB (ex-ParaTethys, Allen and Bass, 1993; Bass, 1991; Demarcq, 1970; Rubino et al., 1990).

In the study area, the Cenozoic chronostratigraphical framework is still poorly constrained and relies mainly on lithostratigraphical subdivisions (Giot, 1943; Pelin, 1965; Bocquet, 1966; Latreille, 1969; Lamiraux, 1977; Mortaz-Djalili, 1977; Mortaz-Djalili and Perriaux, 1979; Nicolet, 1979; Mujito, 1981; Bass, 1991; Allen and Bass, 1993; Berger, 1985, 1992), since biostratigraphical data are scarce. The main compressive phase has been commonly dated to the end of the Miocene (i.e., Tortonian to Messinian; ∼ 11–5 Ma) (Butler, 1989b, 1992b; Gidon et al., 1978). However, seismic data from the southern Jura synclines (Deville et al., 1994; Beck et al., 1998), as well as field observations (Blanc, 1991; Kalifi et al., 2020), suggest that deformation started much earlier with syntectonic sedimentation of the earliest marine deposits (Burdigalian–Langhian; 20–14 Ma).

$^{87}Sr/^{86}Sr$ and sedimentological analyses (Kalifi et al., 2020) defined a new and well-constrained sequence stratigraphy for the lower Miocene (with depositional sequences S1, S2, and S3 deposited from the late Aquitanian at ∼ 21.3 Ma to the early Langhian at ∼ 16 Ma) in piggyback basins (e.g., the subalpine massifs and the southern Jura area). The upper Burdigalian onset of the deformation is evidenced by the sedimentary transition of flexural subsiding distal deposits to syntectonic proximal deposits (Kalifi et al., 2020). This transition corresponds to the westward progressive migration of the orogenic wedge towards the foreland basin and is materialized by (i) a shallowing-upward sedimentation defined by shallow marine successions capped by gravel-rich fan delta (marine to continental) and continental (fluvial) deposits, (ii) growth strata relationships, and (iii) abnormally thick sediment accumulations induced by an increased subsidence due to the migration of the depocenter located in front of the adjacent thrust belt and their piggyback basins.

In the study area, the principal structures correspond to cover folds and thrusts striking NNE–SSW. The thrusts juxtapose Mesozoic units over Cenozoic or Upper Cretaceous units and accommodate the last ∼ WNW–ESE shortening phase of the Alpine collision wedge (Mugnier et al., 1990; Doudoux et al., 1982; Bellahsen et al., 2014; Menard and Thouvenot, 1987). On one hand, based on geophysical data, most authors propose that the thrusts are rooted in basement thrust(s) below the Belledonne massif (Guellec et al., 1990; Deville et al., 1994; Deville and Chauvière, 2000; Bellahsen et al., 2014). On the other hand, Gidon (2001) stresses that there is no clear field evidence for such thrust below Belledonne, but rather argues for shortening and thrusting affecting the Mesozoic grabens within Belledonne. Balanced sections of the sedimentary cover document horizontal shortening increasing from the Vercors (∼ 6 km) to the Chartreuse (∼ 22 km) (Mugnier et al., 1987; Bellahsen et al., 2014; Philippe et al., 1996, 1998).

The easternmost major thrust has large, up to 10 km offsets (Deville and Chauvière, 2000). To the north, at the front of the Bauges and Bornes massifs (Fig. 1B), this thrust corresponds to the"chevauchement des nappes inférieures" of Doudoux et al. (1982) and the "chevauchement frontal des Bauges" (φB, Fig. 1B) of Gidon (1999). The thrust extends southwards in the Chartreuse massif and was named differently by various authors (Gidon, 1964; Butler and Bowler, 1995; Gidon and Arnaud, 1978; Gidon et al., 1978; Deville and Chauvière, 2000; Philippe et al., 1998). The southern prolongation of this fault beyond the Isère valley is contentious but possibly corresponds to the Moucherotte thrust (φMo, Fig. 1B) (Debelmas, 1965; Gidon, 1981; Donzeau et al., 1993), whose geometry and structural interpretation are still debated (Gignoux and Moret, 1952; Debelmas, 1953, 1966; Gidon, 1981). We discuss that point in more detail below (Sect. 4.3).

West of this thrust zone, other major thrusts involve Miocene molasse deposits. In the Vercors massif, from east to west, these thrusts include (i) the Rencurel thrust (φRe, Fig. 1B) or the thrust zone 3 (Watkins et al., 2017). In the south, the thrust originates at the tip of a NW–SE left-lateral ramp (Barféty et al., 1967; Gidon, 1964) and can be followed to the north until the Montaud col (MC, Fig. 1B). Its northward prolongation is still disputed: the thrust is connected either to the northern part of the thrust zone 2 (Watkins et al., 2017) (see below) or to the Voreppe thrust in the Chartreuse massif (φVor, Fig. 1B) (Gidon, 2018; Gidon and Arnaud, 1978). Also included are (ii) the tectonic front of the Vercors massif, which partly corresponds to the thrust zone 2 of Watkins et al. (2017), (iii) the thrust zone 1 (Watkins et al., 2017) at the western border of the Monts-du-Matin massif (MM, Fig. 1B) and (iv) the Saint Lattier anticline (St-L.a, Fig. 1B) (Deville et al., 1992).

In the Chartreuse massif, at least three thrust zones exist west of the "chevauchement de la Chartreuse orientale" (φOr, Fig. 1B). From east to west they include (i) the Voreppe thrust zone (φVor, Fig. 1B) (Butler and Bowler, 1995; Gidon, 1994), also named the Voreppe fault (Gidon et al., 1978; Gidon and Arnaud, 1978) or the "chevauchement ϕ 1 de la Chartreuse occidentale" (Gidon, 1988; or F1, Gidon, 1964). From Saint-Laurent-du-Pont northwards, the prolongation of this accident becomes unclear (Butler, 1992a). Also included are (ii) the Ratz anticline (RA, Fig. 1B) corresponding to the tectonic front of the Chartreuse massif and (iii) the Voiron–Chirens fault (V-C, Fig. 1B) indirectly deduced from a 100 m vertical offset of middle Miocene deposits (Nicolet, 1979).

Further north, west of the Bauges and Bornes massifs, the southern Jura synclines widen progressively northwards. The synclines are separated by anticlines that develop in the hanging walls of blind thrust (Beck et al., 1998; Doudoux et al., 1982; Lickorish et al., 2002). From west to east, these anticlines are (i) the Salève mountain (SA, Fig. 1B) (Gorin et al., 1993; Mastrangelo and Charollais, 2018) and (ii) the Gros Foug mountain (GF, Fig. 1B). Further west, in the Jura massifs, three main thrust systems exist from east to west: (i) the thrust involving the Grand Colombier anticline (GC, Fig. 1B); (ii) the "chevauchement interne du Jura" (φIJu, Fig. 1B) (Philippe, 1995), which corresponds to the northern prolongation of the thrust involving the Tournier anticline (TO, Fig. 1B); and (iii) the "chevauchement externe du Jura" (φEJu, Fig. 1B) (Philippe, 1995).

At the latitude of Chambéry, the transition between widely spaced and more closely spaced thrusts and folds (Fig. 1B) has been attributed to the presence of a more efficient décollement level in the Triassic layers in the north (Philippe, 1995; Philippe et al., 1996).

As mentioned above, the detailed chronology of these thrusts is poorly constrained. Moreover, Miocene deposits were poorly investigated in the Vercors and Chartreuse massifs. As a result, the main compressive phase could have started during the late Miocene (http://www.geol-alp.com, last access: 18 September 2021; Gidon et al., 1978; Butler, 1989a, b, 1992a, b). However, this is off-phase with the observations to the north in the southern Jura, where detailed investigation of lower Miocene deposits in seismic profiles and field observations revealed seismites and growth strata relationships, which suggests that a compressive phase started during the early Miocene (Deville et al., 1994; Beck et al., 1998; Blanc, 1991; Rangheard et al., 1990).

3 Material and methods

Sedimentological and stratigraphical analyses were conducted from 35 well-outcropping sections of the Miocene molasse deposits (sections 4, 5, 13, 16, 22 are detailed in Kalifi et al., 2020) and from partially preserved sections (< 40 m) outcropping in adjacent localities. Sedimentary successions up to 1050 m thick were logged at the decimeter (dm) to meter (m) scale resolution in the field. Using the combined analyses of textural characteristics, clastic and biogenic components, bed thickness, bed organization and geometry, sedimentary structures, and paleocurrent measurements, 25 facies grouped into 11 facies associations (FAs) were previously defined by Kalifi et al. (2020). Building on these results and using the same methodology, depositional sequences were identified based on facies association evolution and the main stratigraphical surfaces (Embry, 1993, 1995). Depositional sequences were identified using the Posamentier and Allen (1999) methodology on spontaneous potential (SP) and gamma ray (GR) log data from 28 well logs located in the Bas-Dauphiné basin.

Three dating approaches have been combined in order to constrain the ages of the depositional sequences. The results have been calibrated on the GTS2016 chronostratigraphic chart (Ogg et al., 2016).

Biostratigraphical dating was conducted on field and well-log samples using calcareous nannofossils (calibrated using Young et al., 2017), dinoflagellate cysts (using Hardenbol et al., 1998, biozonation and calibrated using TimeScale Creator 7.4), and foraminifera (calibrated using BouDagher-Fadel, 2015; Lirer et al., 2019; and Wade et al., 2011, biozonations; see Kalifi, 2020, for details). Calcareous nannofossils, foraminifera, and mammal dating available in the literature were also implemented (21 mammal localities were calibrated on the GTS 2016 using TimeScale Creator 7.4; see Kalifi, 2020, for details).

Strontium (Sr) isotope dating was performed on samples collected in the field, as well as on a few well-log samples. To the 57 samples published by Kalifi et al. (2020) we add 72 new samples (Table S1 in the Supplement). The Sr isotope ratios were measured on marine carbonate skeletons (oysters and pectens) at CRPG (Centre de Recherches Pétrographiques et Géochimiques) in Nancy. A thorough inspection of shells was preliminarily conducted at TOTAL using (i) cathodoluminescence in order to select shells yielding a pristine structure and to avoid recrystallized structures as well as (ii) stable isotope ratios (δ^{13}C and δ^{18}O) in order to evaluate possible diagenetic disturbance (Hudson, 1977; Nelson and Smith, 1996; Hudson, 1975). The maximum confidence zone corresponds to δ^{13}C values between -1 ‰ and $+3.5$ ‰, as the global ocean δ^{13}C during Miocene was between 0 and $+2.5$ ‰ (Hayes et al., 1999) and an additional margin of about ± 1 ‰ must be applied for epicontinental seas (Saltzman and Thomas, 2012). Samples with δ^{13}C values lower than -5 ‰ are excluded as they are considered diagenetized (Kalifi, 2020). Corresponding ages are derived from measured $^{87}Sr/^{86}Sr$ ratios using the LOWESS nonparametric regression curve of McArthur et al. (2012). A mean value was calculated when more than one sample was available for one stratigraphic level. The average of the $^{87}Sr/^{86}Sr$ ratios was converted to ages using the LOWESS 5 table (McArthur et al., 2012). The average uncertainty corresponds to the largest value between the values defined by 2 standard errors ($2\times$ the standard deviation of isotopic ratios divided by the square root of the number of data involved) and the individual minimum error of the sample (taking into account the measurement error and the standard error). More details about the geochemical analyses used in this study are given in Kalifi (2020) and Kalifi et al. (2020).

Paleomagnetic results were obtained for 84 samples. A total of 33 and 51 oriented cores or blocks were retrieved from the Forezan (24 layers) and Grésy-sur-Aix (48 layers) sedimentary sections 4 and 5. Samples were subjected to stepwise alternating field (AF) demagnetization, thermal demag-

netization, or a composite procedure (thermal up to 350 °C and then AF) of the natural remanent magnetization (NRM). All remanent magnetizations were measured using the superconducting rock magnetometer (SRM) 760R (2G Enterprises) of the CEREGE (Aix-en-Provence, France). AF online and thermal experiments were performed using the magnetically shielded oven MMTD80 (Magnetic Measurements Ltd.). All paleomagnetic results (directions, treatment, and statistics) are archived in Table S1. According to the moderate quality of the paleomagnetic results (especially for the Grésy-sur-Aix section) and the rather low values of bedding dips, no fold test could be calculated. The magnetic component most resistant to the demagnetization protocols was considered to be (or be close to) the directional geomagnetic signal acquired during or just after deposition of magnetic particles.

The structural study was carried out by a systematic reappraisal of published structural maps and cross sections in light of new field data. Published geological maps at 1 : 50 000 scale (BRGM), as well as local structural observations and cross sections (i.e., http://www.geol-alp.com, and references therein), were used together with new field observations (stratification and fault measurements, observation of panoramas, study of stratigraphic successions) in key areas at 821 locations (Fig. S1 in the Supplement) to determine the geometry of the structures and their continuity. Bedding measurements are listed in Table S6. Seismic profiles (Fig. 1b) that partially penetrate the front of the subalpine chains are located on the western edge of the Vercors and Chartreuse massifs (91CHA1-2, 91VER1, 82SE01-91VER2; published in Deville, 2021) and on the western edge of the Bauges and Bornes massifs (88SV01, 88SV02-HR528, 88SV03, 88SV05, 88SV06, 88SV07-HR535; Gorin et al., 1993; Signer and Gorin, 1995; Beck et al., 1998; available at BRGM) and were reinterpreted by using the stratigraphic column presented in Fig. 1 and by integrating new field data. Interpretations may differ from those of Deville (2021) published after the realization of this study. Further information has been obtained from well logs in the southern Jura synclines, as well as the La Bresse and Bas-Dauphiné basins (Fig. 1B). The combined analysis of these data allows for proposing a new structural map of the area (Fig. 1B) along with four regional cross sections (A to D). The cross sections B and C in the Chartreuse massif were balanced and restored backward taking into consideration the timing of deformation provided by this study using the "flexural slip algorithm" of the MOVE software. In order to ensure realistic fault geometries, the restoration was performed using the top of the most laterally continuous pre-thrusting unit (i.e., Barremian–Aptian limestones).

4 Results and interpretations

4.1 Dating

4.1.1 Chemostratigraphy

At total of 129 Sr dating results are compiled in this study (Table S2); 12 samples display evidence for diagenetic alteration with $\delta^{13}C$ values $< -5‰$ (Table S2) and cathodoluminescence imagery exhibiting recrystallization patterns. Since their stable isotope data exhibit no evidence of diagenetic bias ($\delta^{13}C > -5‰$) but the obtained ages are older than the age of the stratigraphic level, four samples were further interpreted as reworked samples and considered to be outliers (Table S2). Excluding those 16 recrystallized or outlier samples, the $^{87}Sr/^{86}Sr$ ratios range between 0.708338 and 0.708914, corresponding to stratigraphic ages between 21.45 ± 0.30 Ma (late Aquitanian) and 8.58 ± 1.78 Ma (Tortonian), thereby allowing for the dating of 113 stratigraphic levels.

4.1.2 Magnetostratigraphy

For the Forezan and Grésy-sur-Aix sections (sections 5 and 4, respectively; Fig. 2 – locations in Fig. 3), the NRM intensity ranges between 1.53×10^{-5} and 8.43×10^{-3} Am^{-1} with an average of 1.12×10^{-3} Am^{-1} and between 3.19×10^{-5} and 3.95×10^{-3} Am^{-1} with an average of 8.83×10^{-4} Am^{-4}. The Forezan section (enriched in clayey facies) presents slightly higher NRM intensities and better paleomagnetic results, probably due to finer and more abundant ferromagnetic grains. Orthogonal projection of paleomagnetic results exhibits different patterns: (i) a stable reverse polarity slightly overprinted by a normal polarity (Fig. S2A) in many samples of the Forezan sedimentary section, (ii) a large normal overprint with a path toward reverse polarity (Fig. S2B) for many samples of the Grésy sedimentary section, (iii) rarely stable normal polarity (Fig. S2C) attributed to full normal remagnetization or eventually a subchron, and (iv) in the 868–870 m interval of the Grésy section (for two neighboring samples), a stable normal polarity affected by a post-lock tilting (Fig. S2D). Declination and inclination of the stable magnetization, or the direction displayed in the very last steps of demagnetization, were plotted together with the reversal angle (Fig. S3A, B). Due to large normal magnetic overprints, the reversal angle, which is the angle between the calculated direction and the expected direction for the normal geomagnetic polarity, helps to determine geomagnetic polarity scale, especially in carbonates affected by partial but intense remagnetizations (e.g., Demory et al., 2011). The entire Forezan sedimentary section displays very high reversal angles (Fig. S3A) attributed to the record of the reverse geomagnetic Chron C5Cr according to the age frame inferred from Sr dating (Fig. 2). Most of the Grésy-sur-Aix section is characterized by reverse polarities except the normal polar-

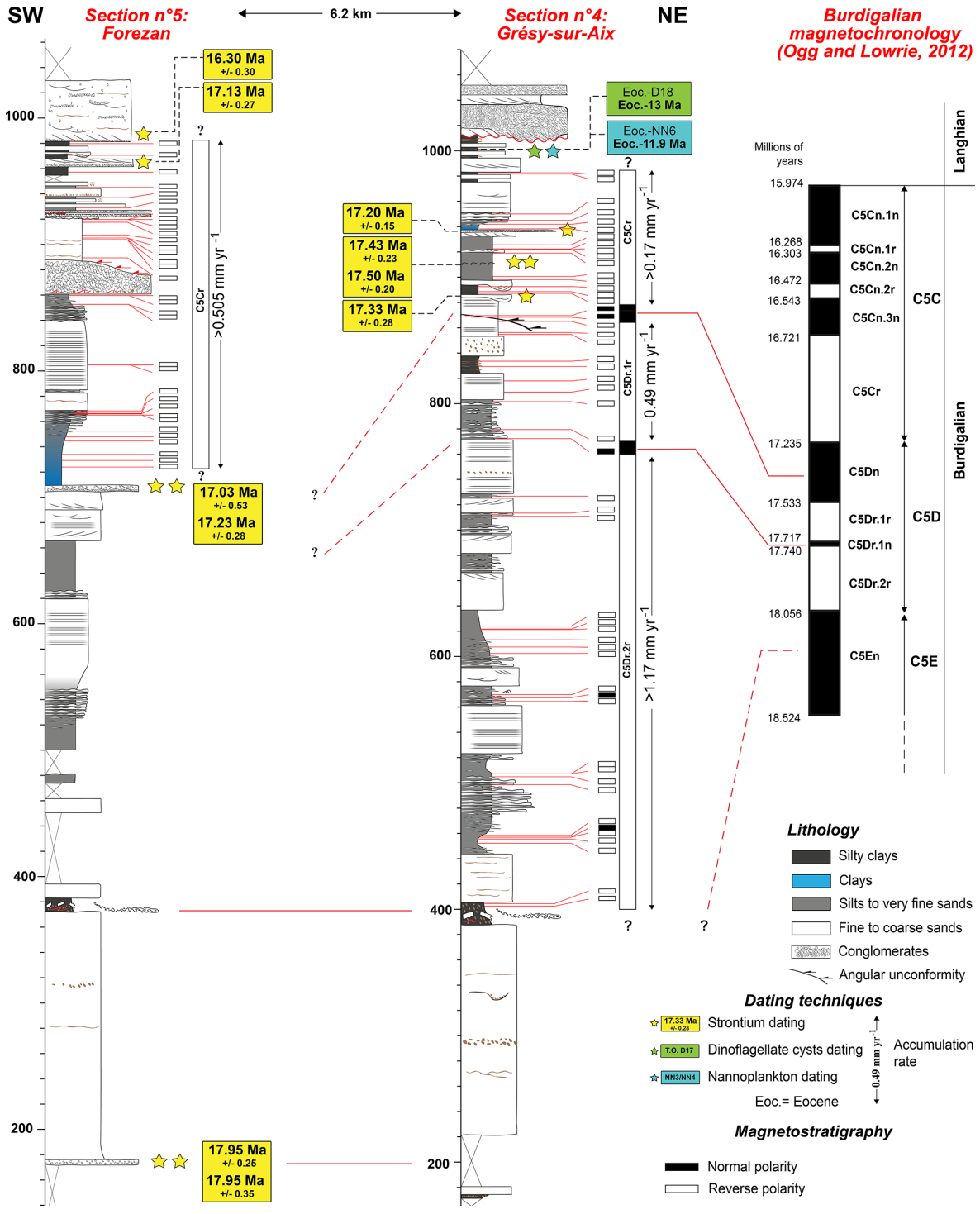

Figure 2. Magnetostratigraphy of the Forézan and Grésy-sur-Aix sections, integrated with strontium and biostratigraphic dating.

ity recorded at 772 m, which may be attributed to Subchron C5Dr.1n., and tilted normal polarities (Figs. S2D and S3B) located at 868 m – just below a major unconformity – that may be related to the record of Chron C5Dn (Fig. 2). In the case of post-lock tilting, the reversal angle is higher than expected for normal polarity.

4.1.3 Biostratigraphy

A total of 34 out of 74 analyzed samples enabled the biostratigraphical dating of sedimentary sections based on nannofossil assemblages (Table S3). Species that allowed precise stratigraphical calibrations are *Coccolithus miopelagicus* (NN5–NN8; 14.91–10.55 Ma), *Helicosphaera ampliaperta* (middle part of NN2–top NN4; 20.4–14.91 Ma), *Helicosphaera scissura* (upper NN2–NN5; 20.1–14.91 Ma), *Helicosphaera stalis* (NN6–NN11; 13.53–5.59 Ma), *Sphenolithus belemnos* (base NN3–top NN3; 19–18 Ma), and *Sphenolithus heteromorphus* (base NN4–top NN5; 18–13.5 Ma).

A total of 21 out of 34 analyzed samples allowed biostratigraphical constraints from dinoflagellate cyst assemblages (Table S4). Species that allowed precise stratigraphic calibrations are *Cousteaudinium* sp. (upper D16–top D17; 20.5–14.8 Ma), *Ectosphaeropsis burdigalensis* (lower D16–lower D18; 23.2–13.8 Ma), *Hystrichosphaeropsis obscura* (lower D17–top D19; 18.65–7.5 Ma), and *Systematophora placacantha* (Eocene–D18; Eocene–13 Ma).

Only 2 out of 40 analyzed samples provided a biostratigraphical dating of sedimentary sections based on foraminiferal assemblages (Table S5). In addition, 13 foraminiferal assemblages were already available from the literature (Lamiraux, 1977; Latreille, 1969; Mein, 1985; Aguilar et al., 2004) and were implemented in this study using recent biostratigraphical charts (Table S5). The species allowing firm stratigraphical constraints are *Globigerinoides sicanus* (MMi4a–MMi4c; 16.1–14.87 Ma, sensu Lirer et al., 2019), *Paragloborotalia bella*, and *Praeorbulina circularis* (N5b–N9, respectively, 20.4–14.0 Ma; N8b–N9a, 15.9–14.5 Ma; sensu BouDagher-Fadel, 2015).

Also, 21 mammal assemblages available from the literature (Fig. S4; see also Kalifi, 2020, and references therein for more details) were revealed to be useful to constrain the age of the sea retreat (Figs. S5 to S17) between zones MN6 and MN9 (15.2–9.5 Ma).

Figure S4 compiles a synthesis of the Miocene biostratigraphy chart of the study area.

4.2 Sequence stratigraphy

Absolute and relative dating calibrations were crucial to constrain the timing of the sequence stratigraphy interpretations arising from the 35 sedimentological sections and 28 well-log data records (Fig. 3 for location; see also Kalifi, 2020, for sedimentological and stratigraphical details) integrated in this study. To add more timing constraints on these sections and well logs, 84 dating calibrations obtained from partially preserved successions outcropping in adjacent localities complete the previously published data (Kalifi et al., 2020; Figs. 3, S5 to S17). These additional points derive from new field observations and data from the literature (Kalifi, 2020, and references therein). Taken together, the whole dataset allowed the establishment of 11 marine depositional sequences between the late Aquitanian (S1a) and the early Tortonian (S7), capped by a continental upper Tortonian sequence (S8) (Fig. 4A). The Sr-based ages obtained in the basal transgressive deposits coincide with eustatic sea level rises (Fig. 4B, C), suggesting that the depositional sequences are eustatically driven (see also Kalifi et al., 2020), except for sequence S8 (Fig. 4A, B). A total of 12 paleogeographical zones (A to L, Fig. 3) with distinct infill histories were identified based on their specific sedimentological and chronostratigraphical records (Figs. S5 to S17). The error bars of the Sr-based ages obtained in the basal transgressive deposits do not allow the identification of diachronic transgressions from one paleogeographic zone to the other (Fig. 4C). Therefore, we assume that each transgression occurred sub-synchronously at the scale of the study area and that the eustatic sea level rise age (Fig. 4B) will be used to (i) constrain depositional sequences in time without dating controls and/or (ii) homogenize the age of the sequence at the basin scale.

The 12 Miocene paleogeographical zones can be grouped into four domains based on our chronostratigraphy (Fig. 5).

i. Oriental domain: this depositional area corresponds to the Rumilly–Chambéry synclines (zone A) and the Proveyzieux–Lans synclines (zone B). Located in the easternmost part of the subalpine chains, they are characterized by the occurrence of the lower marine Burdigalian sequences (S1a and S1b). The upper Burdigalian (S2a and S2b sequences) is also very thick ($\sim$ 800 m in the zone A) and is characterized by distal marine deposits in the north (zone A) and coarse-grained deltaic deposits in the south (zone B) (Fig. 5). The S3 (+S4?) sequence, on the other hand, is very poorly developed ($<$ 50 m) and corresponds to coarse-grained deltaic to continental deposits. The middle Miocene and younger deposits are absent in this domain.

ii. Median domain: from north to south, this depositional domain encompasses the Novalaise (zone C), Voreppe (zone D), and Rencurel–Méaudre synclines (zone E). The lower Burdigalian (S1a and S1b sequences) is absent in this domain set in the westernmost position of the subalpine chains (Fig. 5). The first deposit corresponds to the marine upper Burdigalian (S2a and S2b sequences), which is about 100 to 200 m thick. Sequence 3, on the other hand, is much thicker in this domain ($\sim$ 400 m in zone C). The S4 and S5 depositional sequences of the middle Miocene do not exceed 150 m in thickness and are characterized by coarse-

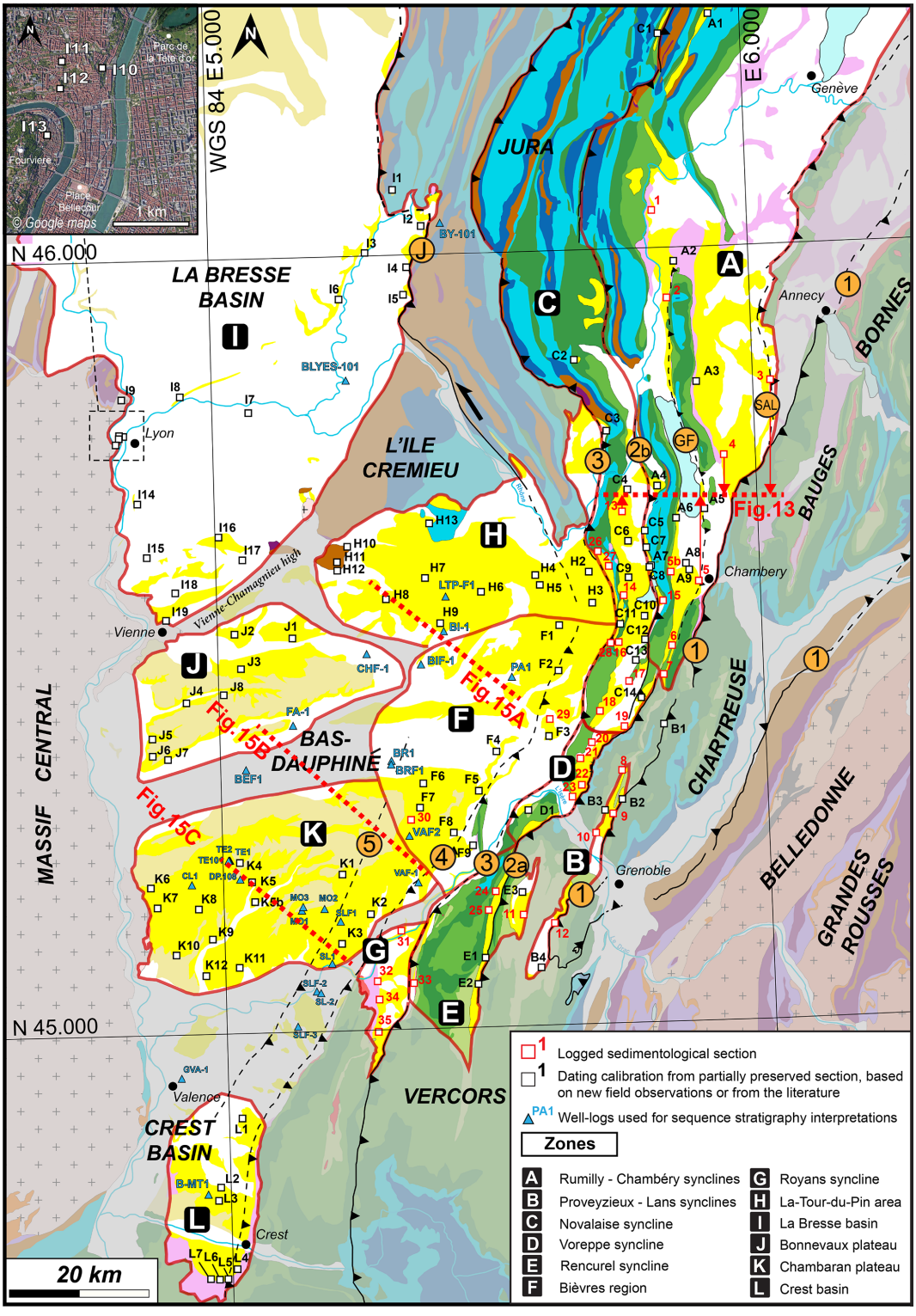

Figure 3. The 12 paleogeographical zones of the Miocene basin of the subalpine massifs, southern Jura, and adjacent basins (Bas-Dauphiné, La Bresse, Crest). Sedimentological and chronostratigraphical records of each zone are provided in Figs. S5 to S17.

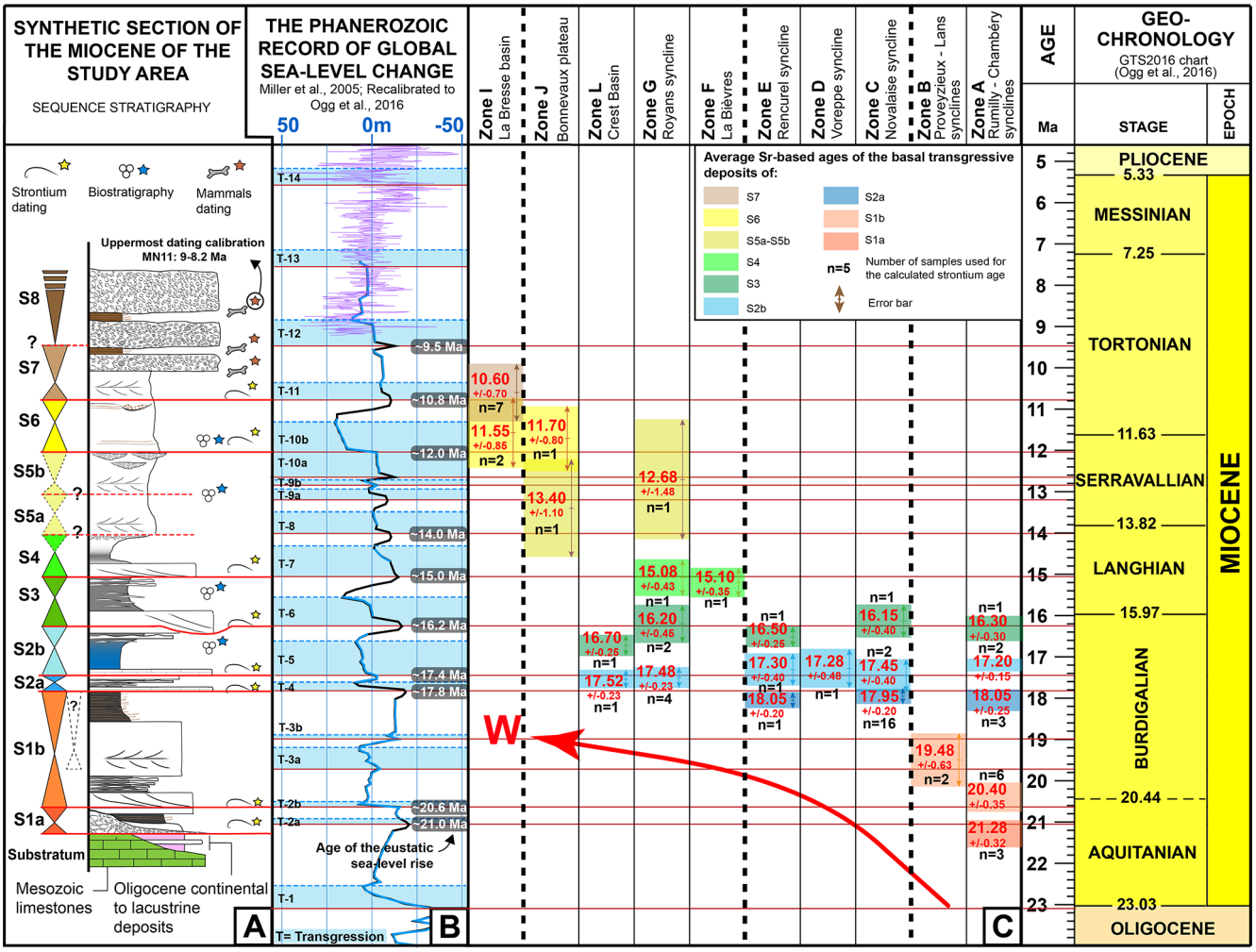

Figure 4. The Miocene chronostratigraphy of the subalpine massifs, southern Jura, and adjacent basins (Bas-Dauphiné, La Bresse, Crest). **(A)** Synthetic section of the Miocene of the study area and the 11 Miocene depositional sequences. Legend in Fig. 5. **(B)** The eustatic curve of Miller et al. (2005) recalibrated with the global timescale (GTS) of Ogg et al. (2016); **(C)** average Sr-based ages of the transgressions in the paleogeographical zones. n: number of age values. Only ages of samples with $\delta^{13}C$ values > -1 ‰ (Table S2) are considered here (maximum confidence zone). Red curved arrow: westward migration of the marine deposits during the lower Miocene.

grained deltaic to continental deposits (Fig. 5). The upper Miocene (above S5) is in turn rarely recorded, thin, or not expressed at all.

iii. Occidental domain: this domain concerns the Tour-du-Pin area (H), Bièvres region (F), Bonnevaux plateau (J), Chambaran plateau (K), Royans syncline (G), and Crest basin (L). These areas are characterized by the absence of the lower Burdigalian (S1a, S1b) and the discontinuous occurrence of the upper Burdigalian (S2a and S2b sequences). The Langhian and Serravalian depositional sequences (S3 to S6 sequences), however, are remarkably well developed (Fig. 5). The thickest upper Miocene deposits (S7 and S8 sequences), mainly containing continental sediments, are also found in this domain (Fig. 5).

iv. "Bressan" domain: this domain concerns solely the Bresse basin (I), where lower and middle Miocene (S1 to S5 sequences) marine sediments are absent (Fig. 5). This zone was only flooded during the major eustatic transgression of the S6 sequence. Upper Miocene deposits (S7 and S8 sequences) are particularly thick in this domain and mainly made of continental products.

4.3 Overall structure and main thrust zones

Structural maps and cross sections have been reappraised with the aim to produce a new regional structural map (Fig. 1B). West of the Belledonne external crystalline range, the Mesozoic cover is affected by numerous thrusts, nearly all dipping to the east. The uppermost thrust sheet is the Penninic thrust outcropping at the base of the Sulens and

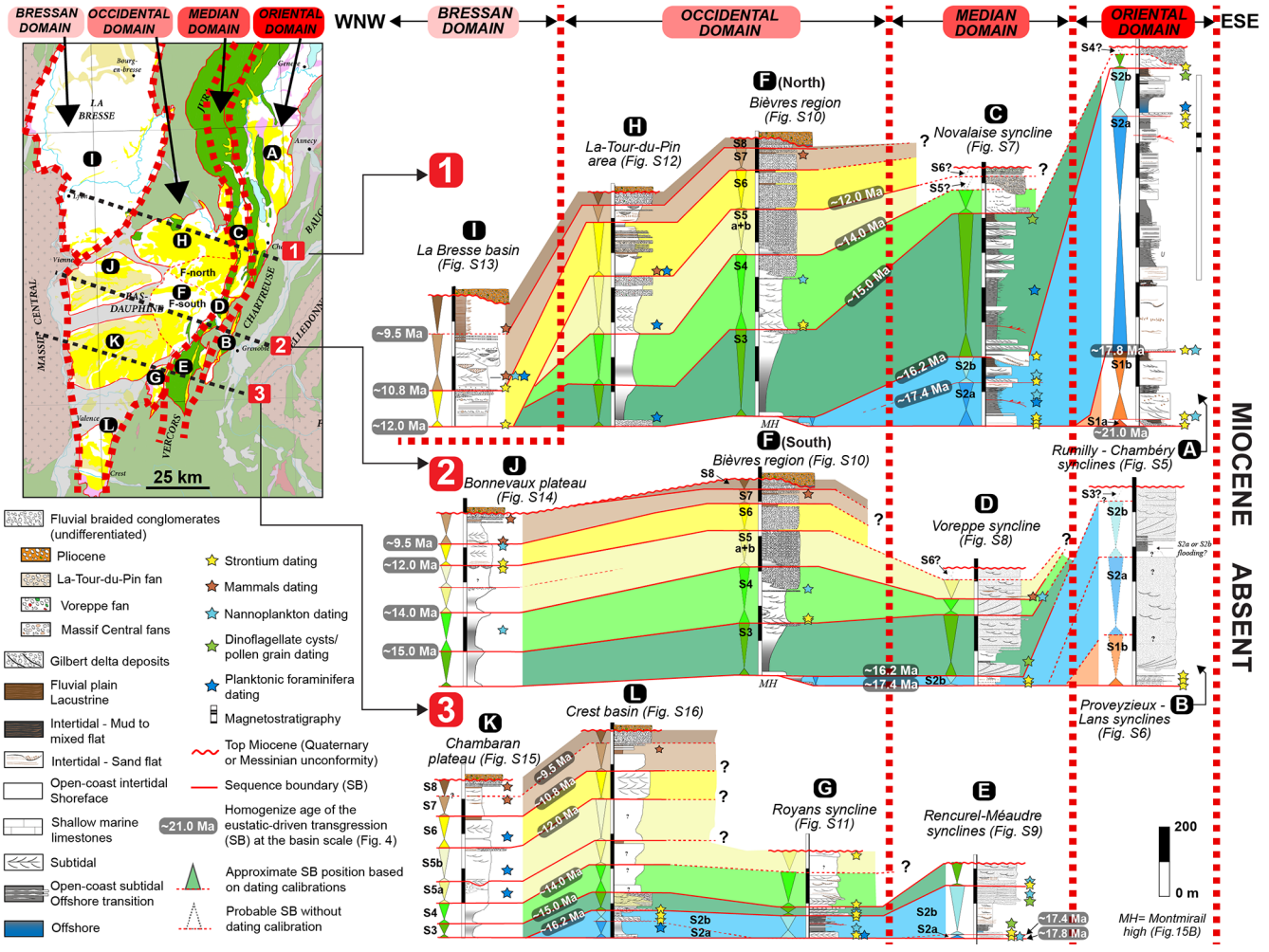

Figure 5. Spatiotemporal distribution of the Miocene depositional sequences of the subalpine massifs, southern Jura synclines, Bas-Dauphiné, Crest, and La Bresse, which highlight the four depositional domains resulting from the sequence stratigraphical interpretation of the 12 paleogeographical zones (presented in detail in Figs. S5 to S17).

Les Annes klippe (Fig. 1B). This thrust roots east of Belledonne and was active during the Oligocene (Simon-Labric et al., 2009; Dumont et al., 2008, 2011, 2012; Doudoux et al., 1982). To the west, in the footwall of the Penninic thrust, five main NNE–SSW-striking faults zones, locally offset by NE–SW right-lateral faults, straddle the Vercors and Chartreuse massifs. We describe these fault zones in more detail below, from east to west. We also evaluate the continuity of the fault zones between the southern area (Vercors and Chartreuse massifs) where folds and thrusts are closely spaced and the northern area where folds and thrusts are more widely spaced.

4.3.1 Chartreuse oriental thrust or fault zone 1 (FZ1)

Within the Chartreuse massif, a major thrust bringing Lower Cretaceous units on top of younger Cretaceous units has long been distinguished in the literature. It runs from Chambéry to the west of Grenoble and was successively referred to as the "chevauchement de la Chartreuse orientale" (Gidon, 1964, 1995) (φOr, Fig. 1B), the central Chartreuse thrust zone (Butler and Bowler, 1995), the "chevauchement subalpin principal" (Gidon and Arnaud, 1978; Gidon et al., 1978), the subalpine front (Deville and Chauvière, 2000), and the Chartreuse oriental thrust (Philippe et al., 1998). Here we refer to this thrust as the Chartreuse oriental thrust (φOr, Fig. 1B). It shows a large offset of about 10 km (Deville and Chauvière, 2000) at the latitude of Chambéry. Along its southern portion this thrust brings the Néron syncline affecting "Urgonian" (Barremian–Aptian) limestones on top of the Proveyzieux syncline filled with Miocene deposits. In its central part, it brings Mesozoic sediments on top of the Charmant Som anticline (CS, Fig. 1B), while further north Cretaceous strata are found over Oligocene deposits (Doudoux et al., 1992a, b; Gidon and Barféty, 1969). The Chartreuse oriental thrust is affected by numerous right-lateral NE–SW

faults (Fig. 1B). North of Chambéry, the thrust connects with the western front of the Bornes and Bauges massifs characterized by Mesozoic units thrust over Oligocene and Miocene deposits (φB, Fig. 1B).

The prolongation of this thrust towards the south across the Isère valley is more contentious. The valley has sometimes been interpreted as the location of either a fold saddle (e.g., Gignoux and Moret, 1952) or possibly a fault (Gidon and Arnaud, 1978) that would offset the structures outcropping on both sides. The most recent detailed study concluded that there is no offset in the downstream part of the valley, but possibly a tear fault in the upstream (Gidon, 1995). South of the valley, the Moucherotte thrust that brings Cretaceous sediments atop Miocene of the Villard-de-Lans syncline has a complex 3D geometry, connecting with the poorly exposed Perrières Fault through the Bruzier right-lateral fault (Debelmas, 1965; Gidon, 2020b) (Fig. 7A). We combine new field observations with the published geological maps and other publications to produce a new structural map, with corresponding cross sections (Fig. 7) and interpretation. North of the Isère valley, the Proveyzieux syncline is a complex structure since it corresponds in fact to two synclines separated by a pinched anticline (the Proveyzieux anticline in Figs. 6A and 7A). South of the Isère valley, the Sassenage fold is also an anticline conformably capped by Miocene deposits (Fig. 6B). On each side of the Isère valley, the two anticlines have close axis direction: N198°, 03° for Proveyzieux and N181°, 06° for Sassenage (Fig. 7A). In both cases, the eastern limb of the anticline is overthrusted by Cretaceous sediments including Urgonian limestones (Moucherotte thrust in the south, Néron thrust in the north), strongly suggesting that the thrust system is continuous across the Isère valley (Gidon, 1995) (Figs. 7A and S18B). Therefore, we propose that the Proveyzieux and Sassenage anticlines correspond to the same structure. The precise trace of the thrust is unclear and hidden by Quaternary sediments, but the Moucherotte–Bruzier–Perrières thrust appears to be offset from the Neron thrust by $\sim$ 2km along a left-lateral NW–SE strike-slip fault along the Isère valley (Figs. 7A and S18B). Such a fault is compatible with the general direction of shortening ($\sim$ E–W). A major thrust thus appears to be continuous from the western front of the Bauges massif to the western front of the Moucherotte range (from north to south φB, φOr, φMo) and is referred to here as fault zone 1 (FZ1) (Fig. 1B).

Although the westward Moucherotte thrust has long been described, its detailed geometry is still discussed. We conducted a detailed mapping based on field observations at 210 stations (Table S6) combined with a detailed analysis of previous maps and publications as well as one aircraft flight in order to constrain the 3D geometry of the Moucherotte range geology.

On the western flank of the Moucherotte range, the Cretaceous beds of the Moucherotte anticline are thrusted on top of the Miocene of the Villard de Lans syncline, above the Sassenage anticline (Figs. 6B and 7D) (Gidon, 1981). In the Comboire range, at the foot of the eastern flank of the Moucherotte massif (locality 1, Fig. 7A), gently dipping to the west Upper Jurassic strata rest above marls. These marls, previously mapped as Jurassic (Vif geological map; Barféty et al., 1967), are rather Early Cretaceous in age based on the occurrence of *Berriasella* (Gidon, 2020a). This implies a duplication of the Mesozoic series and thus the emergence of a westward-dipping thrust. This thrust most probably connects in depth with the Moucherotte thrust, making the Moucherotte range a klippe (Fig. 7D).

A few kilometers further south, near the Col de l'Arc (locality 2, Fig. 7A), the Cretaceous series are also duplicated. To the west, Urgonian beds of the Moucherotte anticline rest on top of the Upper Cretaceous (Figs. 6C and 7E). The hanging wall structure is complex with a syncline of Upper Cretaceous sediments in the footwall and a boxed anticline overlain by a monocline in the hanging wall (Fig. 6D). To the east of the Col de l'Arc, below the Crête des Crocs (locality 3, Fig. 7A), the Lower Cretaceous dips steeply to the east ($\sim$ 70°, Fig. 6C) and is allochthonous above more gently dipping Urgonian limestones. Further to the north the Urgonian limestones and Upper Cretaceous are seen below the Lower Cretaceous through the St. Ange window (locality 4, Fig. 7A) (Fig. 6E) (Barféty et al., 1967). The top of the Moucherotte range is thus a klippe that can be traced $\sim$ 1 km farther to the south to the Pierre Vivari (locality 5, Fig. 7A).

Further south, the Moucherotte klippe has been completely eroded, and the Cornafion summit (locality 6, Fig. 7A) corresponds to the inverted eastern limb of a N10°-trending syncline in the footwall of the thrust (Figs. 6E and 7F), while further east the Upper Jurassic and Lower Cretaceous series are duplicated, constituting the Pieu klippe (Figs. 6G and 7F) (Barféty et al., 1967). At the western edge of this klippe, Upper Jurassic limestone allochthonous strata form a bent-fault anticline above the autochthonous Jurassic and Cretaceous strata (Fig. 6H) suggesting thrusting toward the west. We interpret this klippe as the southern and lower extension of the Moucherotte one (Fig. 7F).

The Moucherotte klippe probably did not extend south of the Double Brêche fault (locality 7, Fig. 7A), south of which the footwall syncline is no longer observed (Fig. 7A). Further south, the Mesozoic formations are weakly deformed, locally exhibiting westward-verging anticlines such as the Grande Moucherolle (Figs. 6I and 7G).

No evidence of the westward-verging Moucherotte thrust is found east of the Pieu klippe, implying that it roots east of the Conest range, which is the southwestern prolongation of the external Belledonne cover (Figs. 1B; 7A, D, E, F; 11D). Such geometry, resulting in apparent normal motion along the westward-dipping portions of the thrust (i.e., east of the Pieu klippe and Comboire range), strongly suggests that the thrust was folded after its activity.

Apparent offsets measured along NW–SE cross sections increase from south to north: 1.1 km along the Pieu sec-

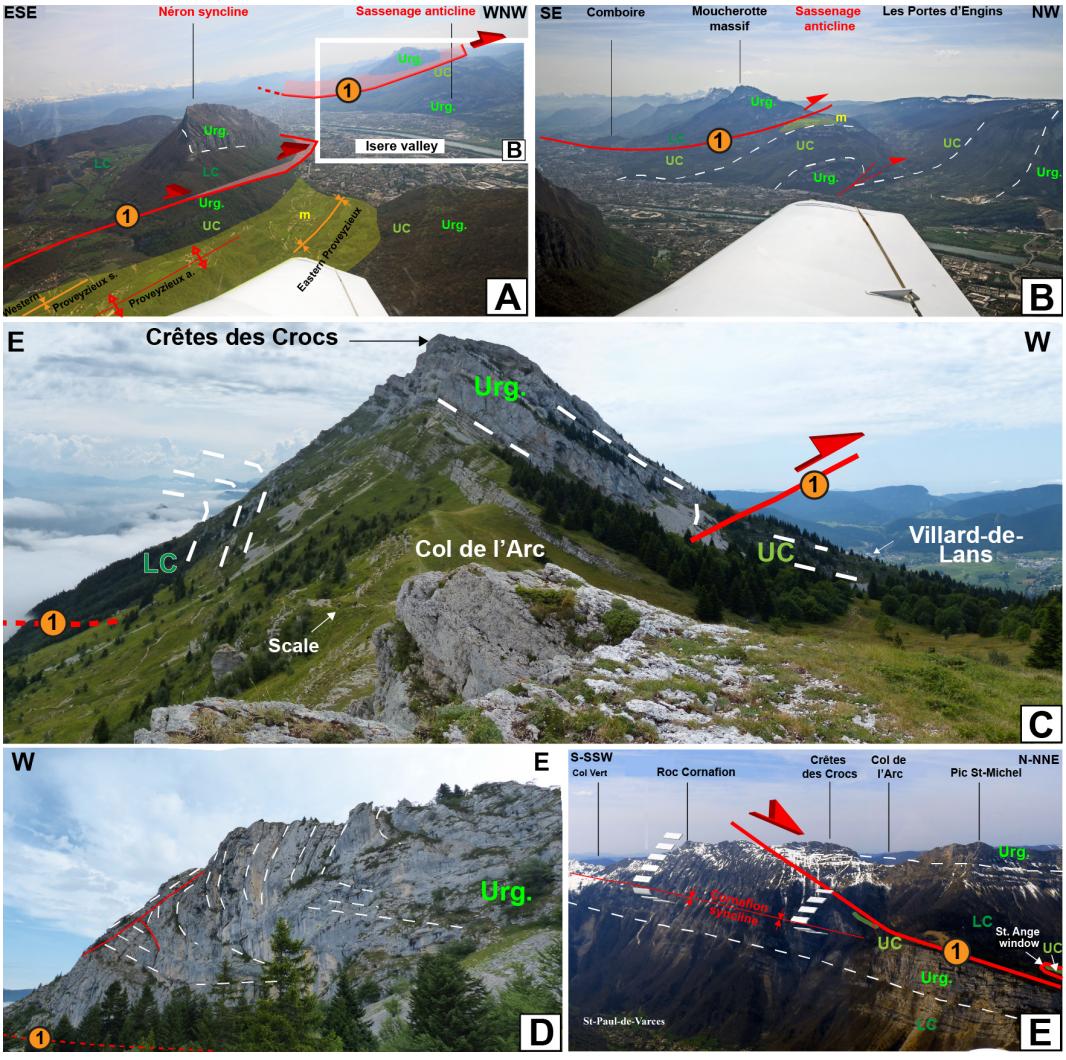

Figure 6.

tion (Fig. 7F) and 3.3 km along the Pic St. Michel and Moucherotte sections (Fig. 7E, D).

As discussed above, we interpret the Moucherotte thrust as the prolongation of the Chartreuse oriental thrust, or FZ1, locally call the Néron thrust, across the Isère valley. In the same way, the Corenc–Jalla folded-thrust system (locality 8, Fig. 7A) (Blanchet and Chagny, 1923; Gignoux and Moret, 1952), also termed φc in the geological map of Grenoble (Gidon and Arnaud, 1978), probably corresponds to the northern prolongation of the eastern flank of the Moucherotte thrust outcropping in Comboire south of the Isère valley (Gidon, 1981) (Fig. 7A, B). This thrust system has been affected by the Ecoutoux anticline, a late eastward-verging fold that also affects the autochthonous units (Blanchet and Chagny, 1923; Gidon, 1981) (Fig. 7A, B). Apparent offset of the base of the Lower Cretaceous across the Neron–Corenc thrust (FZ1) measured along a NW–SE cross section amounts to 2.8 km (Fig. 7B).

Barféty and Gidon (1996) further consider FZ1, which they termed $\varphi 1$, to be a major thrust which re-emerges to the east of the Isère valley on the western edge of the Belledonne massif (Fig. S19A, D). There, along the Grésivaudan valley on top of the Belledonne basement, $\varphi 1$ dips 20–40° to the west, being sub-parallel to the Mesozoic series it affects, and duplicates the Dogger (Barféty and Gidon, 1996) (Fig. S19A, D). $\varphi 1$ thus appears as a top to the west fault with an apparent normal motion, but that is an additive contact and thus more probably a tilted thrust (Deville et al., 1994; Barféty and Gidon, 1996). Further to the north, at the eastern edge of the Bornes massif, the Dogger and Lias are tightly folded in a top-to-the-west ∼ 4 km thick shear zone (Barféty and Barbier, 1983; Barféty and Gidon, 1996; Doudoux et al., 1982, 1999) that also possibly corresponds to a thrust tilted by the later uplift of the Belledonne range (Doudoux et al., 1999) (Fig. S19A, B, C).

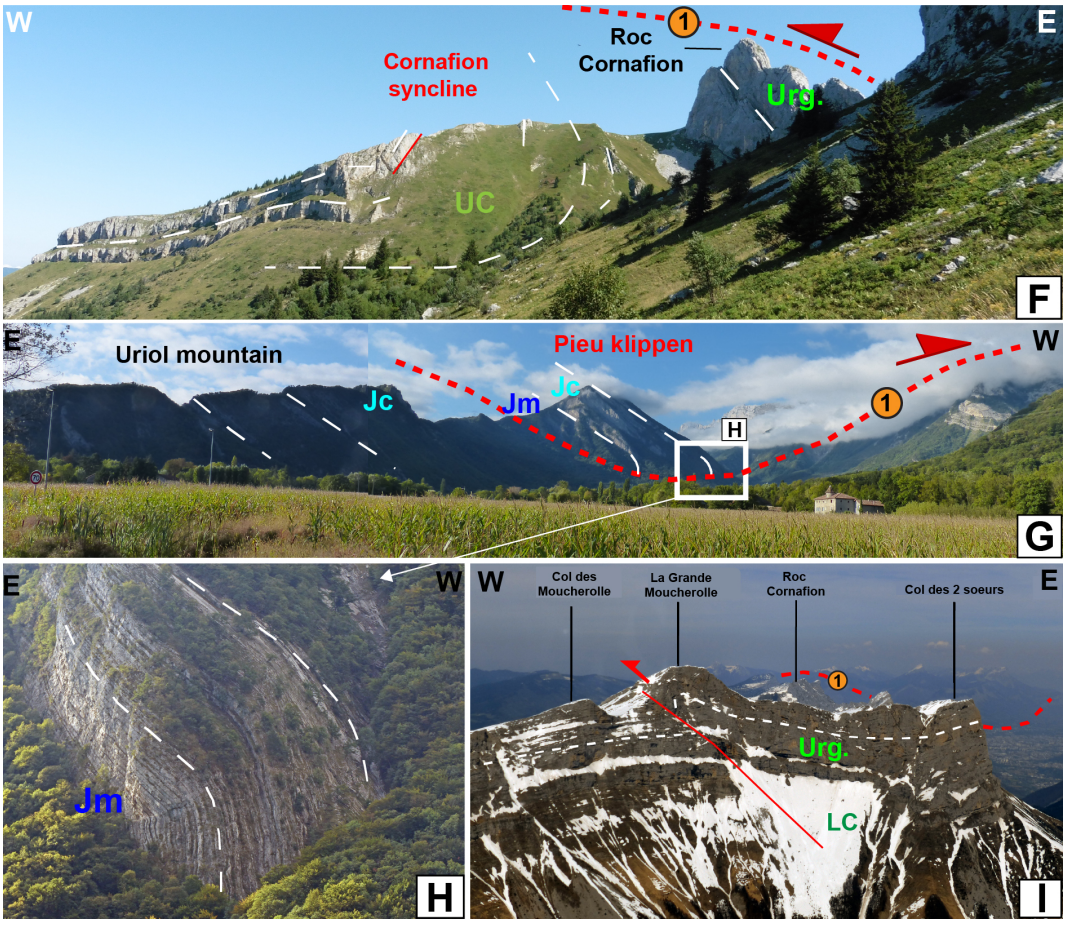

Figure 6. Field and aircraft pictures of the Chartreuse oriental and Moucherotte thrusts (FZ1) in southern Chartreuse and northern Vercors. See viewpoints A to I and locations in Fig. 7A. M: Miocene; UC: Upper Cretaceous; Urg.: Urgonian (Barremian–Aptian limestones); LC: Lower Cretaceous; Jc: Upper Jurassic limestones; Jm: Upper Jurassic marls. Dashed white lines underline the stratifications. Thrust faults are in red. Orange circle: fault zone (FZ). **(A, B)** Néron and Moucherotte thrusts, aerial views from the N. The Proveyzieux Miocene deposits are underthrusted below the Néron syncline. Beyond the Isère valley, the Sassenage fold capped with Miocene deposits is underthrusted below the Moucherotte massif. Note that the Proveyzieux syncline corresponds to two synclines separated by an anticline. **(C)** View towards the south of the Col de l'Arc and the Crête des Crocs: the folded Urgonian is thrusted above the Upper Cretaceous. **(D)** Urgonian limestones of the Moucherotte anticline in the FZ1 hanging wall. **(E)** View towards the west of the eastern flank of the Moucherotte massif with the FZ1 geometry. **(F)** View towards the north of the Cornafion syncline. The Urgonian is overturned in the FZ1 footwall. **(G)** Duplication of the Jurassic series in the Pieu klippe; view from the north. **(H)** Zoomed-in view of the anticline on the hanging wall of FZ1 in the Pieu klippe. **(I)** View towards the north of the Grande Moucherolle, where autochthonous series are weakly deformed.

Whilst further field study would be necessary to support this interpretation, we propose that the Chartreuse oriental thrust (FZ1) runs continuously from the western front of the Bornes to the western Moucherotte thrust in the south and from the east of Moucherotte to east of the Bornes, defining a $\sim$ 120 km long thrust nappe (Fig. 1B). This thrust sheet was termed the Aravis–Mt. Granier unit (Bellahsen et al., 2014) or the subalpine nappe (Pfiffner, 2014). These authors further suggested that this thrust roots in the basement east to the Belledonne massif, which would have been uplifted after motion along the thrust ended (also see Doudoux et al., 1982; Lacassin et al., 1990; Menard and Thouvenot, 1987).

4.3.2 Voreppe thrust or fault zone 2 (FZ2)

In the Vercors massif, the main thrust west of FZ1 is the Rencurel thrust (φRe, Figs. 1B and 7A) which outcrops near La Balme de Rencurel (Fig. 8A). There, the thrust exhibits Barremian–Aptian limestones thrusted above overturned Miocene molasse deposits (Fig. 8B). The apparent offset for the top of the Urgonian is of 1.5 km along this section (Fig. 8C). Miocene strata are limestones bearing *Chlamys praescabriusculus*, which are upper Burdigalian in age (Fig. S9). At this location, the fault strikes N3°, 40° E with slickensides having a pitch of 80° S (Fig. 8B), indicating an almost pure reverse faulting. Analysis of the dips in

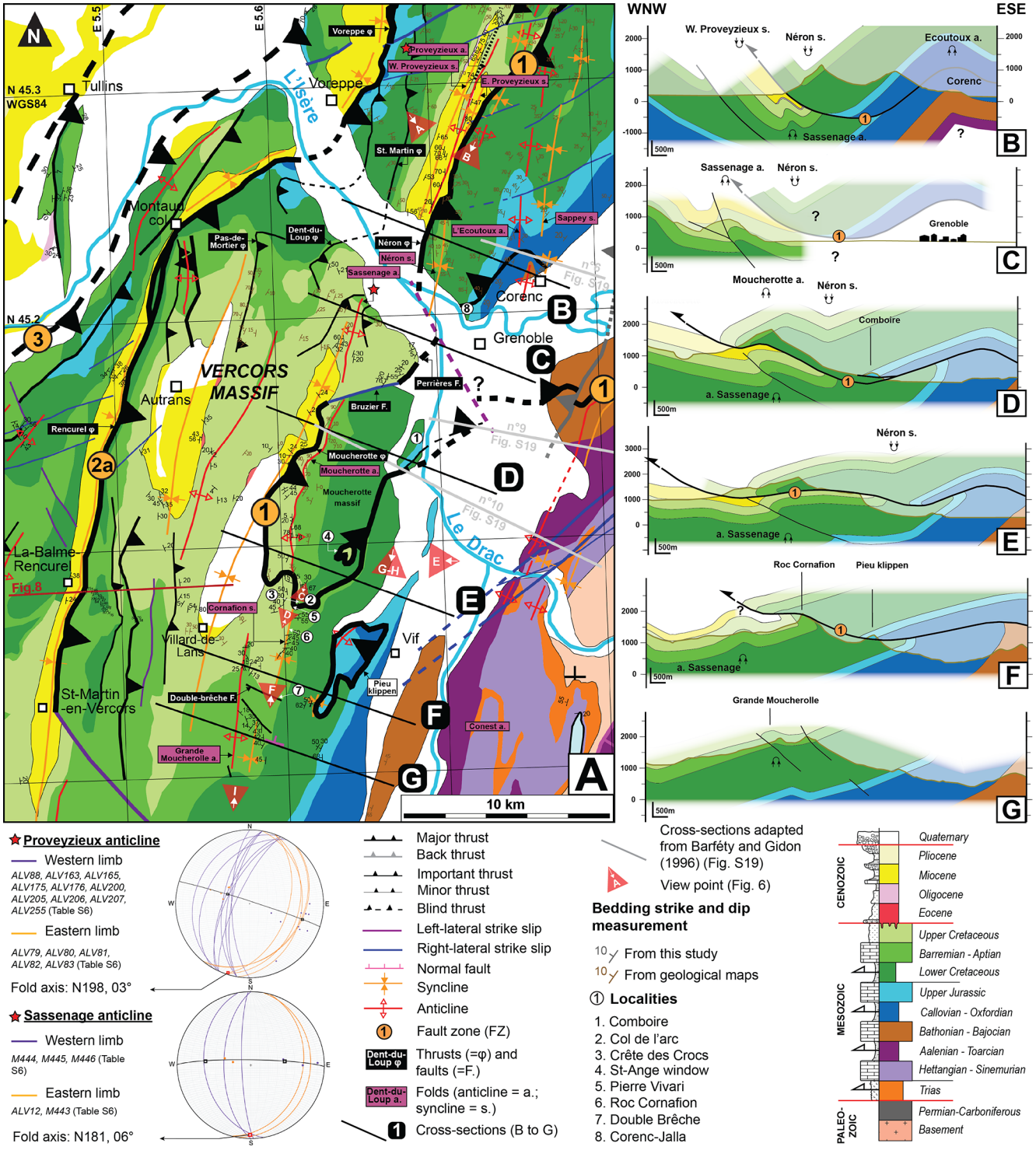

Figure 7. Structure of the Chartreuse oriental thrust (FZ1) in northern Vercors and southern Chartreuse. See Fig. 1 for the legend of the stratigraphy. **(A)** Structural map. Figure 6 viewpoints (A) to (I) are located. **(B–G)** Geological cross sections (see location in **A**). The two stereo diagrams (Stereonet software; Cardozo and Allmendinger, 2013) at the lower left are plots of the stratifications and their poles in order to calculate the anticline axis.

the Lower Cretaceous marls indicates that the hanging wall of the fault is characterized by two anticlinal structures separated by a syncline (Fig. 8C). Further east, two other thrusts with smaller offsets (0.8 and 0.9 km) are observed parallel to the Rencurel thrust (Fig. 8C). According to the published geological map (Barféty et al., 1967), the thrust extends southwards for 6 km until it branches at the tip of a NW–SE left-lateral fault (Fig. 1B). Towards the north, the thrust is continuous until the Col de Montaud (MC, Fig. 7A), with Miocene deposits observed in the footwall. At this location, it was proposed that the thrust connects with the thrust at the western front of the Vercors (Watkins et al., 2017). However, the fault does not cut across the footwall Miocene deposits (Gidon and Arnaud, 1978) but more likely turns from N–S to NNE–SSW to reach Veurey–Voroize where Upper Jurassic sediments are found thrusting atop the Miocene (Fig. 1B; Fig. 7A). We suggest that the Rencurel thrust prolongates toward the NE to the Voreppe thrust across the Isère valley (Fig. 7A). Indeed, the seismic profile 91VER1 that follows the Isère valley (Fig. 9A) reveals a major thrust at this location (Fig. 9C) with a 1.5 km apparent offset of the basal Lower Cretaceous reflector. Hence, we interpret the Rencurel and Voreppe thrusts as the same tectonic structure as previously proposed by Gidon et al. (1978) and Dumont and SPIA (2020).

Further north, the Voreppe thrust is mapped as a continuous structure bringing Jurassic sediments on top of Miocene deposits of the Voreppe syncline (Fig. 1B) (Gidon and Arnaud, 1978). North of Saint-Laurent-du-Pont, this thrust terminates, but other thrusts continue further to the north: to the west two faults merge together before bounding the western limb of the l'Epine anticline (EP, Fig. 1B), while to the east Miocene and Cretaceous deposits are vertical in the western flank of the Outherans (OU) anticline (Fig. 1B). The seismic profile 91CHA1 stands across the four faults (Fig. 9A, B). Its interpretation suggests that the two western faults (2b and 2c) merge at depth just above the basement and that they could also merge with the Voreppe thrust (2a) just east of the eastern limit of the seismic profile (Fig. 8B). We thus interpret the western faults (2b and 2c) as the northern prolongation of the Voreppe thrust (2a), with an 8 km long left-lateral step-over (Fig. 1B). Within the step-over, short NW–SE left-lateral faults are reported on the 1 : 50 000 map (M. Gidon, 1970) (Fig. 1B) that may concur with the westward shift of the shortening from the Voreppe thrust to the l'Epine thrust. Based on the basal Lower Cretaceous reflector, the apparent offsets are 2.2 km for the Voreppe thrust (2a), 2.3 km for the fault (2b), and 1.1 km for the fault (2c) (Fig. 9B). Following this interpretation, the FZ2 thrust system would be shifted westwards and continue northward as the (2b) thrust bordering the western flank of the Epine (EP), Grand Colombier (GC), and Crêt du Nu anticlines (Fig. 1B).

The seismic profile 91CHA1 shows that the western flank of the Outherans anticline is bounded by the Outherans blind thrust (OU), which is almost parallel to the three other ones and has a 1.3 km apparent offset (Fig. 9B). To the south, the Outherans (OU) anticline corresponds to the Chartreuse median anticline of Gidon (1964, 1990) (CS, Figs. 1B and 10A), while to the north it most likely connects with the Gros Foug (GF) anticline across the Chambéry valley (Fig. 1B). The geometry of the Gros Foug anticline can be observed on seismic profiles 88SV01 and 88SV03 (Fig. 10C, D) and supports an eastward-dipping Gros Foug thrust with an apparent offset between 2 and 2.5 km of the basal Upper Jurassic limestone reflector. This thrust appears to root in the Triassic detachment level above the basement (Fig. 10C, D) and is probably the northern extent of the Outherans thrust between the Chartreuse oriental (FZ1) and the Voreppe thrust (FZ2) (Fig. 10A).

The seismic profiles also reveal another thrust fault between FZ1 and FZ2: the Salève (SAL) thrust bounding the Salève (SA) anticline (Figs. 1B and 10A, B) that also roots above the basement in the Triassic. The apparent offset of the SAL fault is evaluated to be 2.5 km based on the basal Barremian–Aptian limestone reflector in seismic profile 88SV01 (Fig. 10D) and on the basal Upper Jurassic limestone reflector in seismic profile SV03 (Fig. 10C). The seismic profiles do not allow for the visualization of the connection between FZ1 and the SAL faults, and two hypotheses have been proposed: (i) FZ1 and the SAL faults are connected at depth (Deville and Sassi, 2006; Beck et al., 1998); (ii) FZ1 and the SAL faults are distinct (Guellec et al., 1990; Doudoux et al., 1982).

4.3.3 The Royans–Ratz thrust or fault zone 3 (FZ3)

The western edge of the Vercors and Chartreuse massifs corresponds to open anticlines characterized by steep westward-dipping forelimbs and gently dipping back-limbs. Such anticlines are continuous from Pont-en-Royans in the Vercors massif (PR) to the Chailles anticline in the Chartreuse massif (CA), with the Ratz (RA) anticline in an intermediate position (Fig. 1B). Seismic profiles crossing these structures (Fig. 9A) reveal that these anticlines formed in the hanging wall of a major thrust zone: the Royans–Ratz thrust (FZ3). This thrust zone corresponds to a single fault bringing Barremian–Aptian to Upper Jurassic limestones above Miocene strata. According to the basal Upper Jurassic limestone reflector, the apparent offset is estimated to be 1.5 km along the 91CHA1-2 and 91VER1 seismic profiles (Fig. 9B, C). Alternatively, the seismic profile 82SE01 (Fig. 9D) shows that the main fault (FZ3) has an apparent offset of 4.5 km but that other minor faults also occur. FZ3 roots in the Triassic detachment level above the basement (Fig. 9B, C). According to the published geological maps the Chailles anticline appears to connect in the north with the Tournier anticline (TO) (Fig. 1B), suggesting that FZ3 could connect with the Jura internal thrust (φIJu) (Fig. 1B).

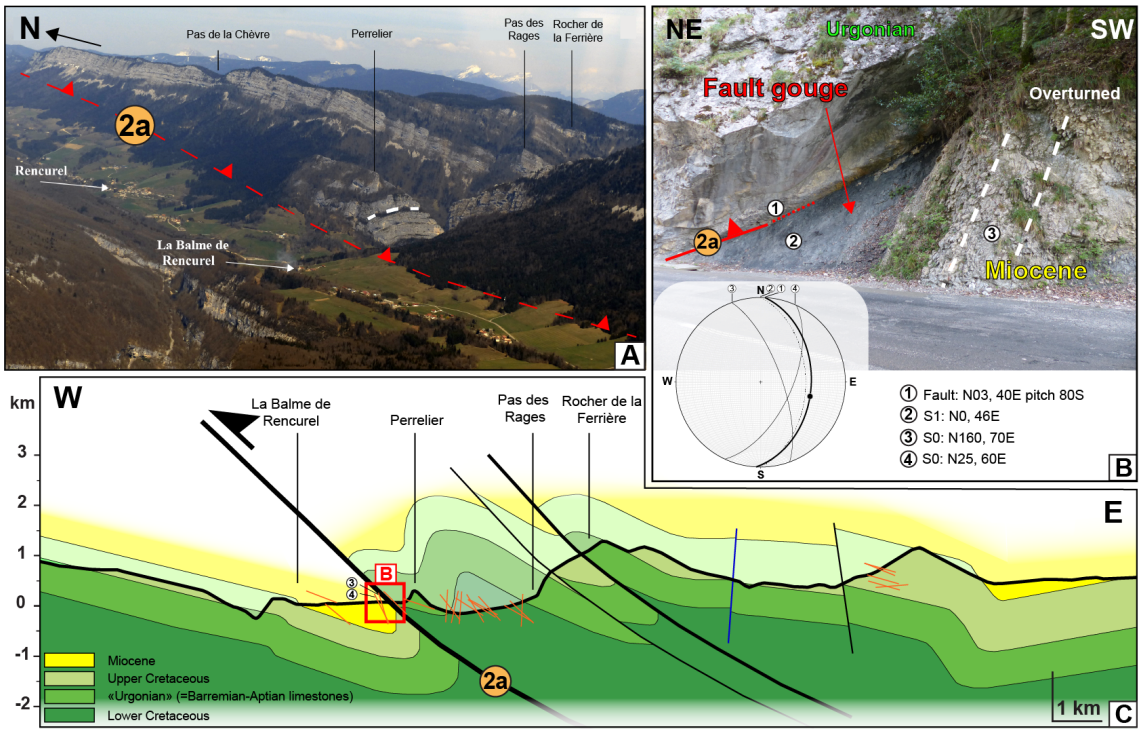

Figure 8. The Rencurel thrust in the Vercors massif. **(A)** The N–S Rencurel thrust that juxtaposes Cretaceous units on top of Miocene molasse deposits. View from the southwest. **(B)** Outcrop of the Rencurel thrust along the D103 road, SE to the La Balme–Rencurel village, exhibiting Barremian–Aptian limestones thrust on top of overturned Miocene deposits. Corresponding sterographic diagram (lower hemisphere) at the bottom. **(C)** E–W cross section along the "gorges de la Bourne". Orange lines: projected dip measurements. Blue line: right-lateral strike-slip fault. Black line: thrust. See Fig. 7A for the location of the cross section and dip measures in map view.

4.3.4 The Monts du matin–Voiron thrust or fault zone 4 (FZ4)

To the west of FZ3, seismic profiles reveal a blind thrust system with two thrusts likely connected at depth, referred to as FZ4 here, with a total apparent offset of the basal Upper Jurassic limestone reflector of ∼ 100–300 m in the north (91CHA1-2; 91VER1, Fig. 9B, C) and ∼ 1.24 km in the south (82SE01, Fig. 9D). To the south, this thrust system bounds the Monts-du-Matin anticline (MM, Fig. 9A). The thrusts crosscut inherited normal faults (i.e., the Saint-Nazaire fault – SN, Fig. 9D) as already reported by Deville et al. (1992) and root in the Triassic detachment level (Fig. 9).

4.3.5 The St. Lattier thrust or fault zone 5 (FZ5)

West of FZ4, the seismic profile 82SE01 (Fig. 9D) highlights the presence of an additional blind thrust system that corresponds to the St. Lattier anticline (St-La, Fig. 1B) (Deville et al., 1992), referred to as FZ5 here. The extension of FZ5 to the north is not well constrained but may coincide with thrusts exhibiting small offsets (< 100 m) that are rooted on an inherited normal fault seen along profile 91VER1 ∼ 40 km further north (Fig. 9C). FZ5 is not observed on the seismic profile 91CHA1-2 in the north (Fig. 9B).

4.3.6 Summary of the structure of the subalpine and southern Jura domains and regional cross sections

Five main westward-verging thrust zones have been identified that all mostly trend NNE–SSW on an updated structural map of the subalpine ranges (Fig. 1B) and are presented on four regional cross sections (Fig. 11). Folds between the thrusts have the same general trend, and the cross sections have been drawn in a WNW–ESE direction.

More specifically, subsurface data and surface data (field observations and geological maps at 1 : 50 000) were used to build cross section A west of FZ1, while east of FZ1, the construction of the cross section relies on the analysis of 1 : 50 000 scale geological maps and the ECORS-CROP profile (Guellec et al., 1990; Roure et al., 1990; Mugnier and Marthelot, 1991) recently revised by Pfiffner (2014). The Cenozoic filling consists of Oligocene and Eocene deposits and is involved in superposed nappes (Doudoux et al., 1982). In the northern part of the zone, west of Cluses, the Upper Jurassic limestones are found three times vertically along the BZN1 borehole (Fig. 1B for location) (Charollais and Jamet, 1990). Seismic imaging suggests the presence of a thrust uplifting the Brizon basement high (Guellec et al., 1990). To the east, we have also integrated the Montjoie valley syn-

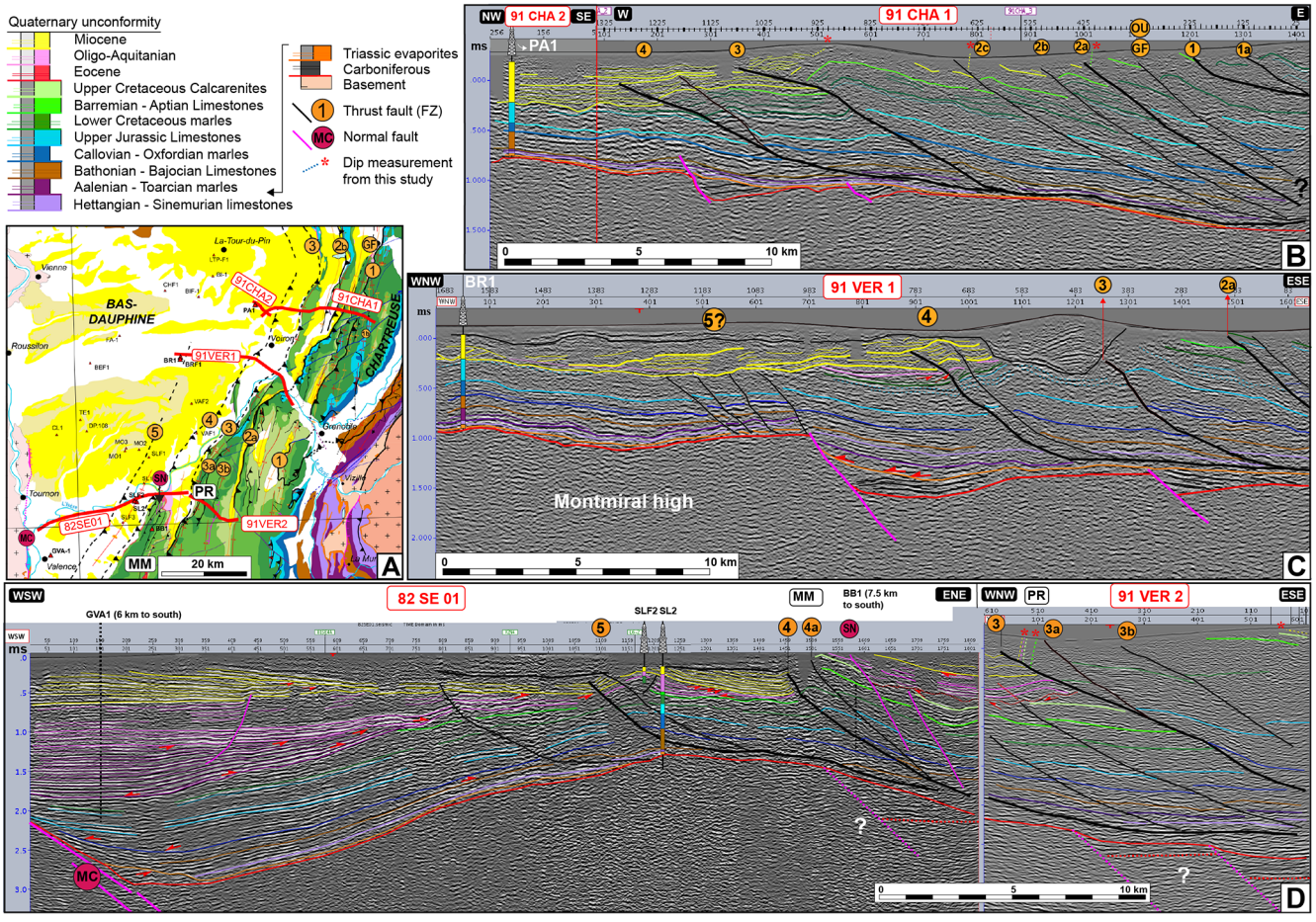

Figure 9. Seismic profiles along the Vercors and Chartreuse massifs (seismic lines published by Deville, 2021, and reinterpreted). **(A)** Geographical and geological locations of the interpreted seismic lines. **(B)** Seismic profiles 91CHA1 and 91CHA2. Interpretation is proposed using PA-1 well data and fieldwork data. Note that the Outherans blind thrust (OU) corresponds further north to the GF thrust. **(C)** Seismic profile 91VER1. Interpretation is proposed using BR-1 well data and fieldwork data. **(D)** Seismic profiles 82SE01–91VER2. Interpretation is proposed using SLF-2, SL-2, and extrapolated BB1 and GVA-1 well data and fieldwork data.

thetic section of Gidon (2019) (Fig. S19A, B, C) for the Aravis and Belledonne chain relationships. In order to build the westernmost part of section B up to FZ1, subsurface data and surface data (field observations and geological maps at 1 : 50 000) were used. Between FZ1 and the summit of the Grand Manti (Fig. 11B), the construction of the cross section relies on detailed analyses of 1 : 50 000 geological maps. To the east of the Grand Manti, the data originate from the northernmost section available in Barféty and Gidon (1996). The results presented in Figs. 6 and 7 and in Barféty and Gidon (1996) (Fig. S19A, D) were used to build sections C and D (Fig. 10C, D) east of FZ2, while subsurface data (Fig. 9C, D) and results presented in Fig. 7 (for section D) were used to the west of FZ2. Sections B and C have been balanced and restored using the MOVE software (Fig. 18).

In this interpretation, FZ1 has been refolded and roots east of the external Belledonne with large parts of the subalpine ranges (Moucherotte, eastern Chartreuse, Beauges, Bornes) being a klippe. West of FZ1, FZ2 (2a, 2b, 2c) runs from south to north from the Vercors to the l'Epine and the Grand Colombier–Crêt du Nu. Seismic profiles (Fig. 9B) and structural mapping (Fig. 1B) highlight the fact that FZ2 has not been refolded as FZ1, but most probably branches at the top of the basement on a flat décollement in the Triassic evaporites that root further east below the external Belledonne massif in the Belledonne basal thrust (Doudoux et al., 1982; Bellahsen et al., 2014, 2012; Butler, 2017; Deville and Chauvière, 2000; Deville et al., 1992, 1994). FZ1 and FZ2 are only 4 to 9 km apart in the Vercors–Chartreuse but 39 km apart in the Jura–Bauges (Fig. 1B). Such widening is the combination of a fan-like map shape of the folds and offsets by left-lateral NW–SE faults. The greater distance between the thrust and the inner part of the belt in the Jura is likely to represent a more efficient décollement in the north, where Triassic evaporitic series are thicker (Philippe et al., 1996; Lickorish et al., 2002; Deville, 2021). Anticlines are found in

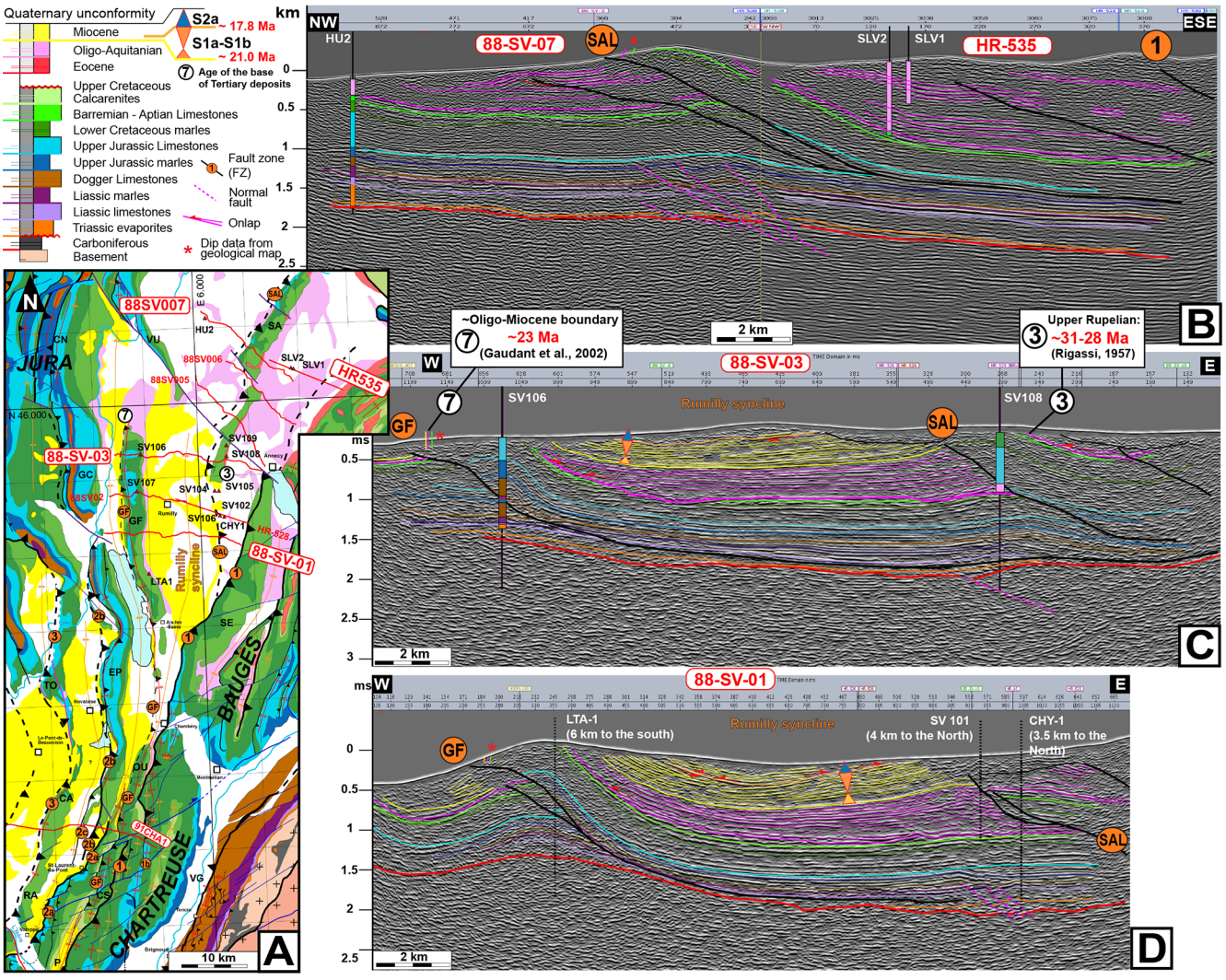

Figure 10. The Salève (SAL) and Gros Foug (GF) faults between the Chartreuse massif and the Jura synclines (**A**, legend in Fig. 1) as based on seismic profiles 88SV07+HR-535 **(B)**, 88SV03 **(C)**, and 88SV01 **(D)**.

the FZ2 hanging wall and thus in the FZ1 footwall (Figs. 1B and 11), but these are related to the activity of FZ2 according to Guellec et al. (1990) and Doudoux et al. (1982). FZ3 is continuous from the Vercors to the western Chartreuse. Further north, according to published geological maps, it appears to turn to the west and merge with the "chevauchement majeur du Jura interne" (φIJu, Fig. 1B) (Philippe, 1995). The map pattern is similar to that of FZ2 and interpreted in the same way. As there is no significant basement culmination between FZ2 and FZ3, FZ3 is interpreted to follow the same décollement level and to root underneath the Belledonne external massif as FZ2. FZ4 is only documented from seismic profiles, and its apparent offset decreases toward the north. The general fault pattern might suggest that FZ4 could connect with the "chevauchement majeur du Jura externe" (φEJu, Fig. 1B) through the NW–SE Jura transfer zone followed by the Rhône river (J, Fig. 1B) (Philippe, 1995). FZ5 is only documented west of the Vercors. As there is no significant basement culmination between FZ5 and FZ2, FZ5 and FZ4 are interpreted to follow the same décollement level and to root underneath the Belledonne external massif. Eastward-verging thrusts are locally described. East of the Royans (RO, Fig. 1B) in the Vercors and in the crêt du Nu in the Jura (CN, Fig. 1B), they appear to be linked with the underlying westward-verging décollement (Philippe, 1995). In Grenoble (Ecoutoux anticline, Figs. 7A, B and 11C), they appear to be related to a late deformation phase (Barféty and Gidon, 1996).

As described above, the NW–SE (N145°) left-lateral southern Jura transfer zone appears to offset FZ3 and possibly FZ4 (Fig. 1B). The step-over between the Voreppe (2a) and the Epine (2b) thrusts stands in the prolongation of this zone and shows small NW–SE left-lateral faults (Fig. 1B), suggesting that it is linked to the same process. Other simi-

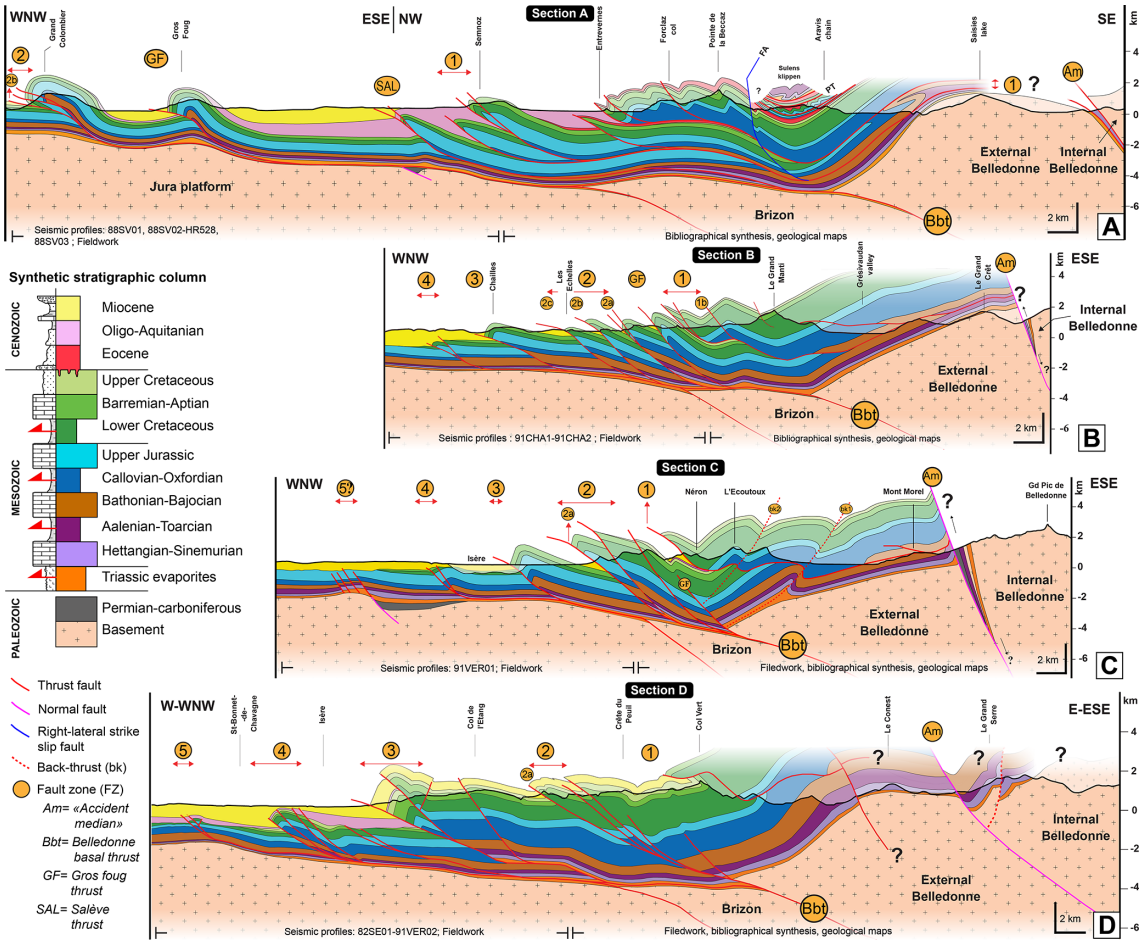

Figure 11. Regional cross sections of the study area. Cross section location in Fig. 1. **(A)** Cross section A through the eastern Jura and the Bornes. PT: Penninic thrust. AF: Arcalod fault. **(B)** Cross section B through central Chartreuse and Belledonne. **(C)** Cross section C through southern Chartreuse and Belledonne. **(D)** Cross section D through Vercors and southern Belledonne.

lar faults are only found at the southern tip of the Rencurel thrust (2a, N140°) and possibly along part of the Isère valley near Grenoble offsetting FZ1 (Fig. 1B). Numerous NE–SW (∼ N65°) right-lateral faults affect the southern Bauges, the Chartreuse, and the northern Vercors (Fig. 1B). These faults offset FZ1 and possibly FZ2 but not FZ3 (Fig. 1B). Both the left-lateral and the right-lateral faults are compatible with an ∼ WNW–ESE compression as the main trusts and folds.

4.4 Relationships between sedimentation and tectonics

4.4.1 The Rumilly syncline

In the footwall of FZ1, in the Rumilly syncline located to the north of the oriental domain (zone A, Fig. 5), the Oligo-Miocene succession starts with sub-concordant onlaps on the Mesozoic substratum, according to seismic profiles (Fig. 10). The thickness of the Oligo-Aquitanian continental deposits decreases westward (Fig. 10C, D). Indeed, these deposits are ∼ 200 m thick west of the Rumilly syncline (Fig. 9C, D) (Enay et al., 1970; P. Gidon, 1970), while to the east, they reach 1838 m between the footwall of FZ1 and the hanging wall of the SAL fault (SLV2 well data, Fig. 10A, B), and 1716 m at the footwall of the SAL fault (SV-101 well data, Fig. 10A, D). Thus, on both sides of the SAL fault, which appears west of FZ1 (Fig. 10B), the thickness of Oligocene deposits is relatively similar (Fig. 10B, D), suggesting that the Oligo-Aquitanian depocenter was located in the footwall of FZ1. This, along with sub-concordant Oligocene strata on the Mesozoic substratum, suggests that the SAL fault likely activated after the deposition of both Oligocene and early Miocene sediments (21–18 Ma). This is further consistent with field analyses revealing that the basal Miocene molasse deposits (upper Aquitanian–lower Burdigalian) are conformably lying on continental Aquitanian deposits dipping vertically in the eastern flank of the Rumilly syncline (Alby-sur-Chéran, 3, Fig. 3). Altogether, this implies that both Oligocene and Miocene sediments were deformed by the SAL fault after deposition, then after the early Burdigalian.

4.4.2 Grésy-sur-Aix section

To the south of the Rumilly syncline in the Grésy-sur-Aix sedimentological section (4, Figs. 3 and 12), the sequence S2a basal boundary (dated to 18.05 ± 0.3 Ma based on correlation with the Forezan section 5; see Figs. 2 and 3 for location) was extrapolated along-strike to the north. In the 88SV01 and 88SV03 seismic profiles (Fig. 9D, C), this major stratigraphic surface coincides with a high-amplitude reflector. This reflector is characterized by low-angle toplaps and onlaps that either suggest (i) an angular unconformity, which would materialize the onset of a tectonic phase, or (ii) an erosive surface above the underlying deposits, which corresponds to a classic feature for sequence boundaries.

The Grésy-sur-Aix section outlines three examples of syntectonic sedimentation within sequence S2a (Fig. 12). First, sequence S2a is abnormally thick and has a very high sedimentation rate of $0.72 \pm 0.32\,\mathrm{mm\,yr^{-1}}$ (~ 750 m of sediments deposited over ~ 0.85 Myr between 18.05 ± 0.25 at the base to 17.2 ± 0.15 Ma at the top. For the top of the S2a sequence, which was recorded during the Chron C5Cr, the calculation excludes an age older than the Chron C5Cr starting at 17.23 Ma) compared to the underlying sequences S1a–S1b that are only 200 m thick have an average sedimentation rate of $0.06 \pm 0.01\,\mathrm{mm\,yr^{-1}}$ (deposited over ~ 3.5 Myr between 21.45 ± 0.3 and 18.05 ± 0.25 Ma) (Fig. 12A). This suggests a significant increase in accommodation space at the initiation of sequence S2a, likely related to a regional tectonic event. Second, a 15 m thick interval (390–405 m, Fig. 12A) with a regional-scale continuity (also described 18 km to the south in section 5 at ~ 380 m, Fig. 2) containing disorganized monogenic clasts of various sizes (centimeters to pluri-meters; Fig. 12C) and "ball and pillow" structures (Fig. 12D) suggests an earthquake-disturbed layer (i.e., seismites, F25; sensu Kalifi et al., 2020). Third, the occurrence of an angular unconformity observed in tidal flat deposits (Fig. 12A, B) is characterized by a decrease in bedding dip from 18 to 7° up-section and an erosive surface exhibiting westward-directed onlaps above it. This angular unconformity argues for a compressive tectonic event.

The timing of the angular unconformity is further well constrained by magnetostratigraphy and has been associated with Chron C5Dn at 17.35 ± 0.15 Ma (Fig. 2). Thus, sequence S2a most probably records the onset of a compressive phase. In this interpretation, in the 88SV01 and 88SV03 seismic profiles (Fig. 9D, C), the S2a sequence boundary characterized by low-angle toplaps and onlaps is a tectonically driven angular unconformity and thus dates the initiation of compression at 18.05 ± 0.25 Ma.

4.4.3 Southern Jura synclines

Strontium, biostratigraphical, and magnetostratigraphical dating were applied to sedimentological sections 3, 4, 5 (oriental domain, zone A), and 13 (median domain, zone C) from the southern Jura synclines immediately north of Chambéry (Fig. 3). Sequence stratigraphy interpretations enable E–W correlations in lower Miocene deposits between sections 3 and 13 (Fig. 13) by using sequence boundaries and maximum flooding surfaces. The thicknesses of sequences S1a–S1b do not exceed 200 m in sections 3, 4, and 5 (Fig. 13) and are even absent to the west in section 13 (Fig. 13). During sequence S2a, the maximum thickness is ~ 750 m and is recorded in section 4 (Fig. 13), while to the west, in section 13 (Fig. 13), sequence S2a is 145 m thick. Furthermore, in section 4 (Fig. 13), the average sedimentation rate increases sharply from $0.06 \pm 0.01\,\mathrm{mm\,yr^{-1}}$ during sequences S1a–S1b to $0.72 \pm 0.32\,\mathrm{mm\,yr^{-1}}$ during sequence S2a (Fig. 12A). This firmly demonstrates that a depocenter localized close to section 4 (Fig. 13) appeared during sequence S2a. Subsequently, the thickest accumulation of the following sequence (S2b) lies further west at the Forezan locality (275 m, section 5, Fig. 13). This lateral variation of the thickness is associated with significant lateral facies variation characterized by a dominance of proximal marine deposits to the east (950–1015 m, section 4, Fig. 13), while to the west, sequence S2b is mainly represented by distal marine deposits (700–920 m, section 5, Fig. 13), thereby suggesting a westward migration of the depocenter between sequences S2a and S2b. This is also consistent with a progressive decrease in accommodation rates from ca. 1.17 to $0.17\,\mathrm{mm\,yr^{-1}}$ between sequences S2a and S2b in section 4 to the east (Fig. 13). Finally, the maximum thickness of sequence S3 is recorded west of section 5 (Fig. 13) at section 13 (Fig. 13). There, the sequence S3 is 390 m thick, while in the Rumilly–Chambéry syncline area (Fig. 13), the sequence S3 was probably much thinner. Furthermore, during deposition of sequence S3, lateral variation of the thickness is associated with significant lateral facies variation. At Loisieux (section 13, Figs. 13 and S7), sequence S3 is mainly characterized by distal marine deposits, while it exhibits coarse-grained deltaic deposits to the east (sections 4, 5, Figs. 13 and S5). These proximal deposits suggest that the Rumilly–Chambéry syncline area was progressively exhumed, which is also suggested by the continuation of the progressive decrease in accumulation rates recorded between sequences S2a and S2b. Thus, the S3 depocenter is most probably located in the Loisieux locality (section 13, Fig. 13), further highlighting the westward migration of the depocenter (Fig. 13).

4.4.4 Western Chartreuse

In the 91CHA1-2 seismic profile (Fig. 14A), the Miocene sequences were calibrated using the PA-1 well log (Fig. 14B, C). The thicknesses of sequences S4 and S5 increase from the hanging wall to the footwall of FZ4, which is likely associated with a decrease in bedding dip up-section (Fig. 14A), suggesting growth strata in response to FZ4 activity. On the other hand, the underlying S3 deposits are isopachous both in the footwall and the hanging wall of FZ4, giving an ini-

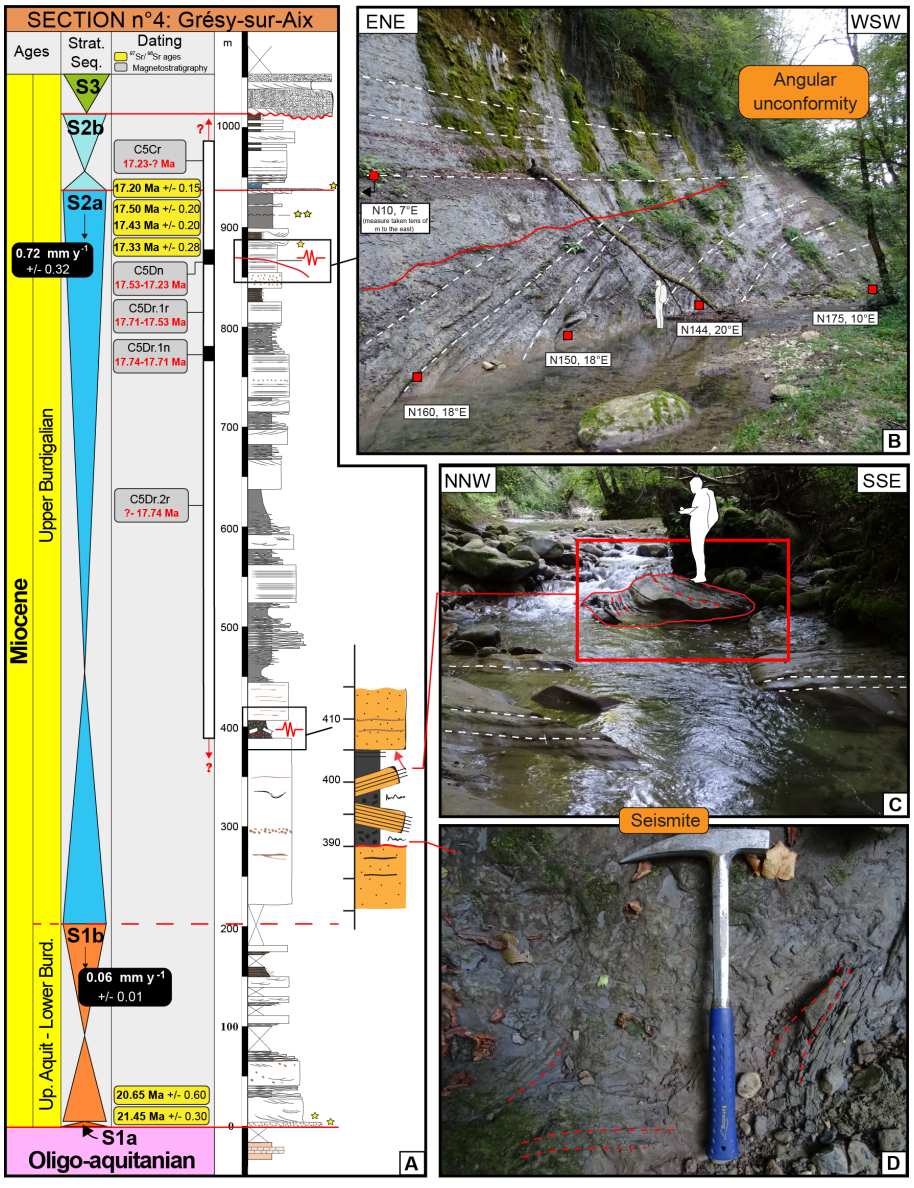

Figure 12. **(A)** Grésy-sur-Aix sedimentological section with sequence S2a syntectonic deposits indicated: seismite near the bottom (see also **C** and **D**) and angular unconformity near the top (see also **B**). The S2a sequence boundary was observed and dated in the Forezan section (5, Fig. 2). Legend in Fig. 5. Black box: average sedimentation rate of the sequence. **(B)** The angular unconformity has established between 17.53 and 17.23 Ma within Chron C5Dn. White dashed lines: bedding. Red line: erosive surface. Red square: dip measure. **(C)** Seismite disturbing 15 m of sediments in S2a, with plurimetric blocks tilted in situ and slump balls. **(D)** Detail of an intensively disturbed sedimentary level.

tiation of FZ4 after the deposition of sequence S3. The end of tectonic activity on FZ4 is not so well constrained since seismic data do not allow a detailed observation of S6 deposits, although sequence S6 apparently seals (conformably) the underlying deposits, which might suggest the end of tectonic activity. This could be in accordance with the fact that FZ4 offsets solely S4 deposits, while S5 deposits are simply folded, which probably indicates a progressive decrease in the tectonic activity from sequences S4 to S5. All together, these observations suggest that FZ4 activity was recorded by the sequences S4 and S5 ($\sim$ 15.0 to $\sim$ 12.0 Ma).

Further east, beyond the artifact located at the emergence of FZ3 (Massieu, Fig. 14A), the identification of sequence S4 is proposed based on similar seismic facies (Fig. 14D). In the hanging wall of FZ3, the basal Miocene deposits are conformably lying on the Mesozoic bedrock (on top of the Chailles anticline). This is consistent with fieldwork observations made 5 km to the north in the Chailles gorges (Fig. 14A,

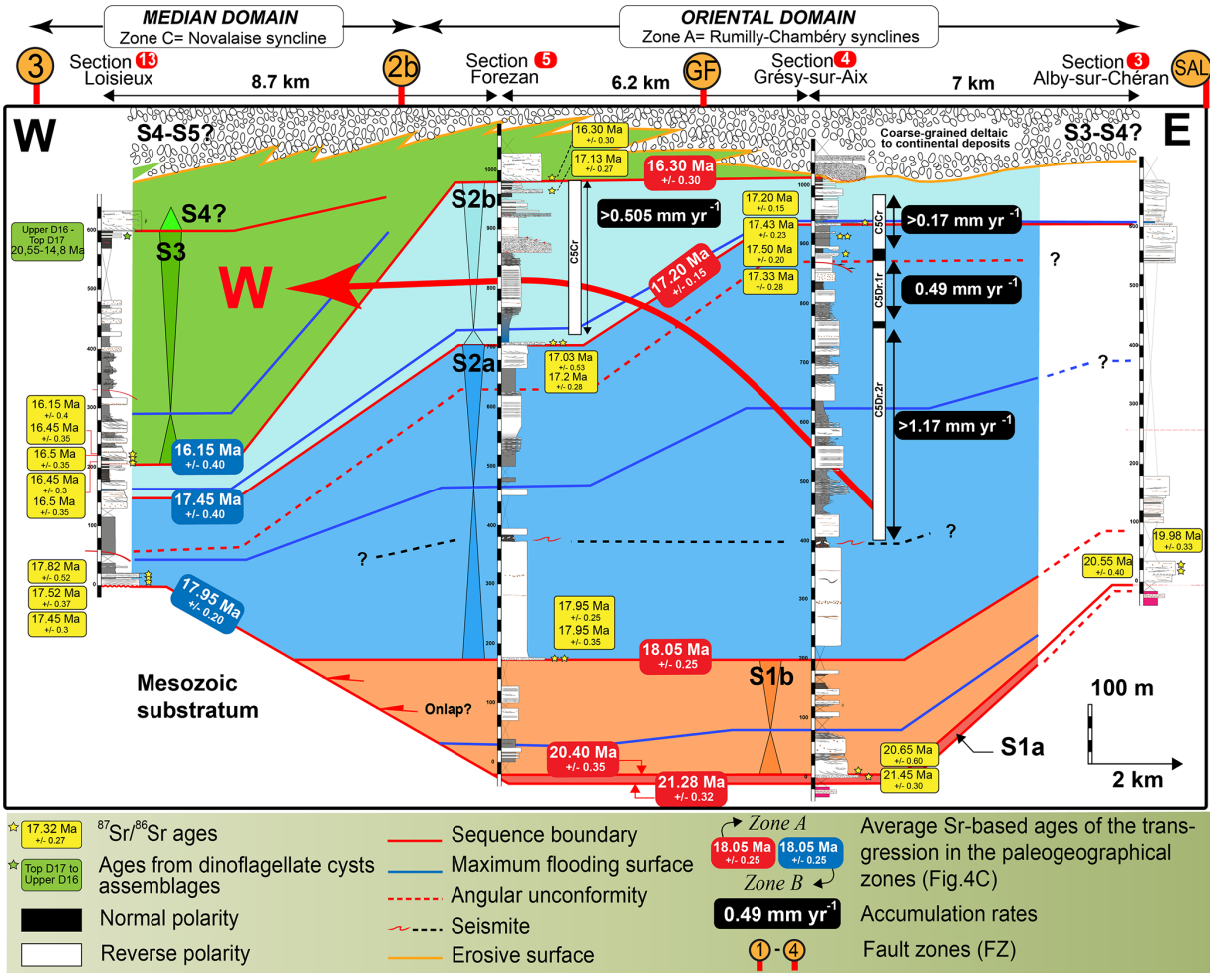

Figure 13. Westward migration of the depocenter during the lower Miocene (red curved arrow). The sedimentological sections were projected on an E–W axis, which corresponds to a direction orthogonal to the thrusts. See Fig. 3 for the location of the transect and sedimentological sections. Red squares: sedimentological sections quoted in the text and used for correlations. The dashed red line corresponds to the angular unconformity presented in Fig. 12B.

C), where the basal Miocene molasse deposits have been attributed to sequence S2a (Fig. 14E), suggesting that FZ3 was inactive during deposition of the sequence S2a. On the FZ3 hanging wall, the overlying sequence (S2b?–S3) geometries are observed on the 91CHA1-2 seismic profile (Fig. 14A), and their thicknesses decrease gradually when approaching the Chailles anticline together with a decrease in bedding dip. In the up-section, S2b(?), S3, and S4 sequences are also characterized by eastward-directed onlaps on the folded S2a deposits (Fig. 14A), thus suggesting growth strata related to FZ3 activity between these sequences. Downstream to the Chailles valley (Fig. 14C), above the S2a sequence, high in the cliff, growth strata (Fig. 14F) are again suggested based on apparent eastward-directed onlaps onto S2a deposits, in agreement with the interpretation of the seismic profile. However, these outcropping onlaps does not allow for the identification of the timing of the growth strata more precisely.

4.4.5 Bas-Dauphiné basin

In the Bas-Dauphiné basin (Fig. 1B), the Miocene molasse deposits are poorly deformed and only the upper part of the Miocene succession crops out. So, the three SE–NW transects (Fig. 3) presented here are proposed using the interpretation of borehole data using sequence stratigraphy (Fig. 15) and our updated chronostratigraphy. Correlations are proposed by using the elevation of the main sequence boundaries (in m a.s.l. – meters above sea level).

The Bas-Dauphiné basin is separated into two tectonic zones. West of the Montmiral high (Fig. 15B, C), no compressive structures were found (Kalifi, 2020; Couëffé and Tourlière, 2008). On the other hand, FZ4 and FZ5 blind thrusts are found to the east of the Montmiral and L'île Cremieu highs (Fig. 15A, B, C). In this area, the S2a, S2b, and S3 sequences exhibit very few thickness variations (∼ 100 m for S2a–b sequences between VAF-1 and VAF-2

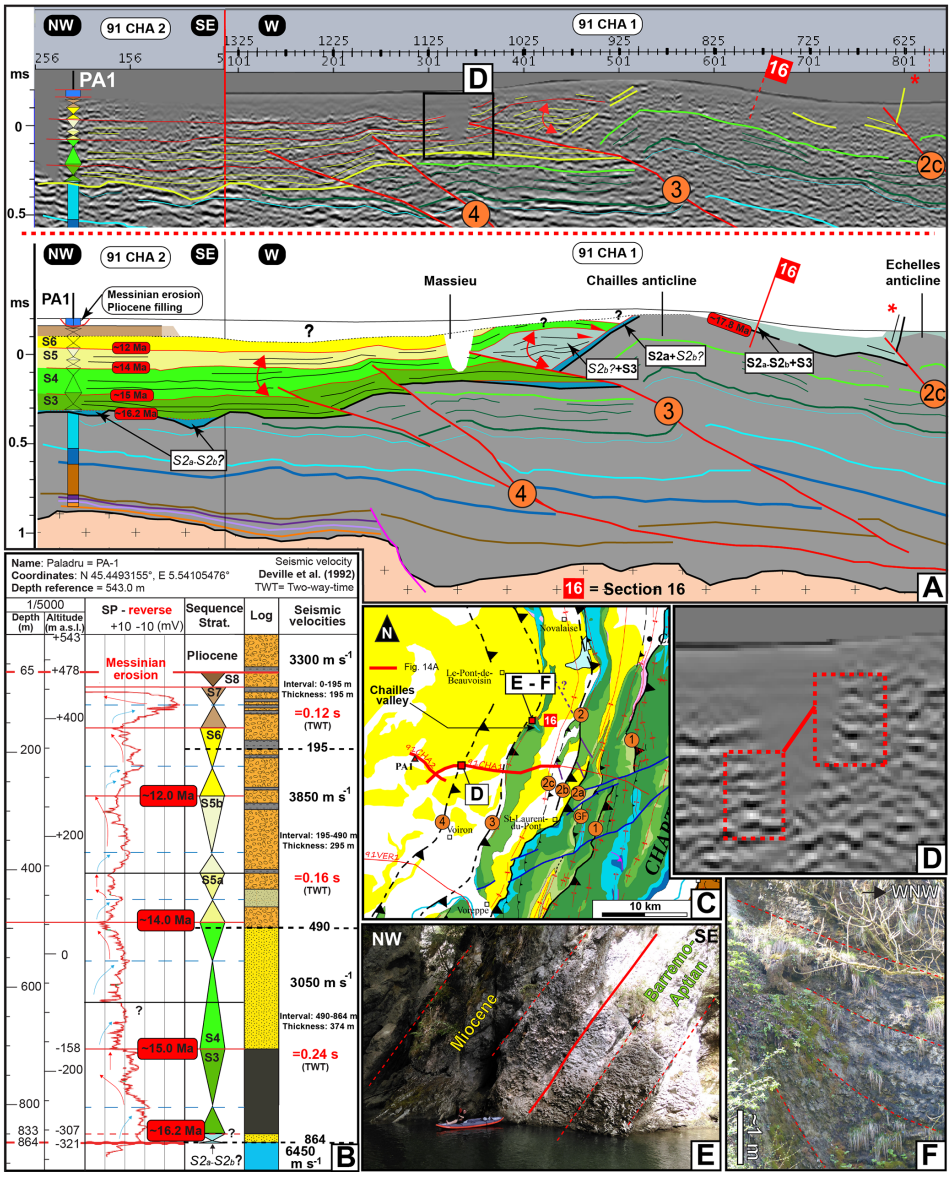

Figure 14. Growth strata relationships inferred for FZ3 and FZ4 based on the 91CHA1 and 91CHA2 seismic profiles, sequential interpretation of the PA-1 well, and fieldwork observations. The ages in red boxes correspond to the homogenized ages of the eustatically driven transgressions (Fig. 4B). Orange circle: fault zone (FZ). **(A)** Seismic profiles 91CHA1 and 91CHA2 depicting the Miocene reflectors and geometrical relationships associated with FZ3 and FZ4. The red double-curved arrows point to the growth strata. Legend in Fig. 9. **(B)** Sequential interpretation of the PA-1 well and conversions of sedimentary thicknesses into seismic velocities (Deville et al., 1992). Legend in Fig. 15. SP-reverse: reversed spontaneous potential curve (in response to water saturation) in millivolts (mV). **(C)** Geographical and geological locations. Legend in Fig. 1. **(D)** Zoomed-in view of the Massieu area (see location in **A**) showing similar seismic facies on both sides of the Massieu artifact and suggesting east side up offset across FZ3. **(E)** Tilted concordant Urgonian–Miocene basal conglomeratic contact (S2a). **(F)** Growth strata relationships at approximately 20 and 30 m above the river level, corresponding to S2b or S3 deposits according to regional correlation lines.

wells, Fig. 15B, and ∼50–70 m for S3 sequence between SLF-1, MO-1, MO-2, and MO-3 wells, Fig. 15C), despite the presence of the FZ5 thrusts within transect C and possibly B. On the western edge of the Bas-Dauphiné basin, the absence of S2a–S2b deposits (to the northwest of PA-1, VAF-2, and MO-3 wells, Fig. 15A, B, C) and the thickness variations of the S3 sequence to the west of the Montmiral high (Fig. 15B, C) are attributed to a complex inherited paleotopography (Kalifi, 2020) along the Oligocene western European Rift (Debelmas, 1974; Curial, 1986; Bergerat, 1987; Ziegler, 1988, 1990, 1994; Bergerat et al., 1990; Sissingh, 2003).

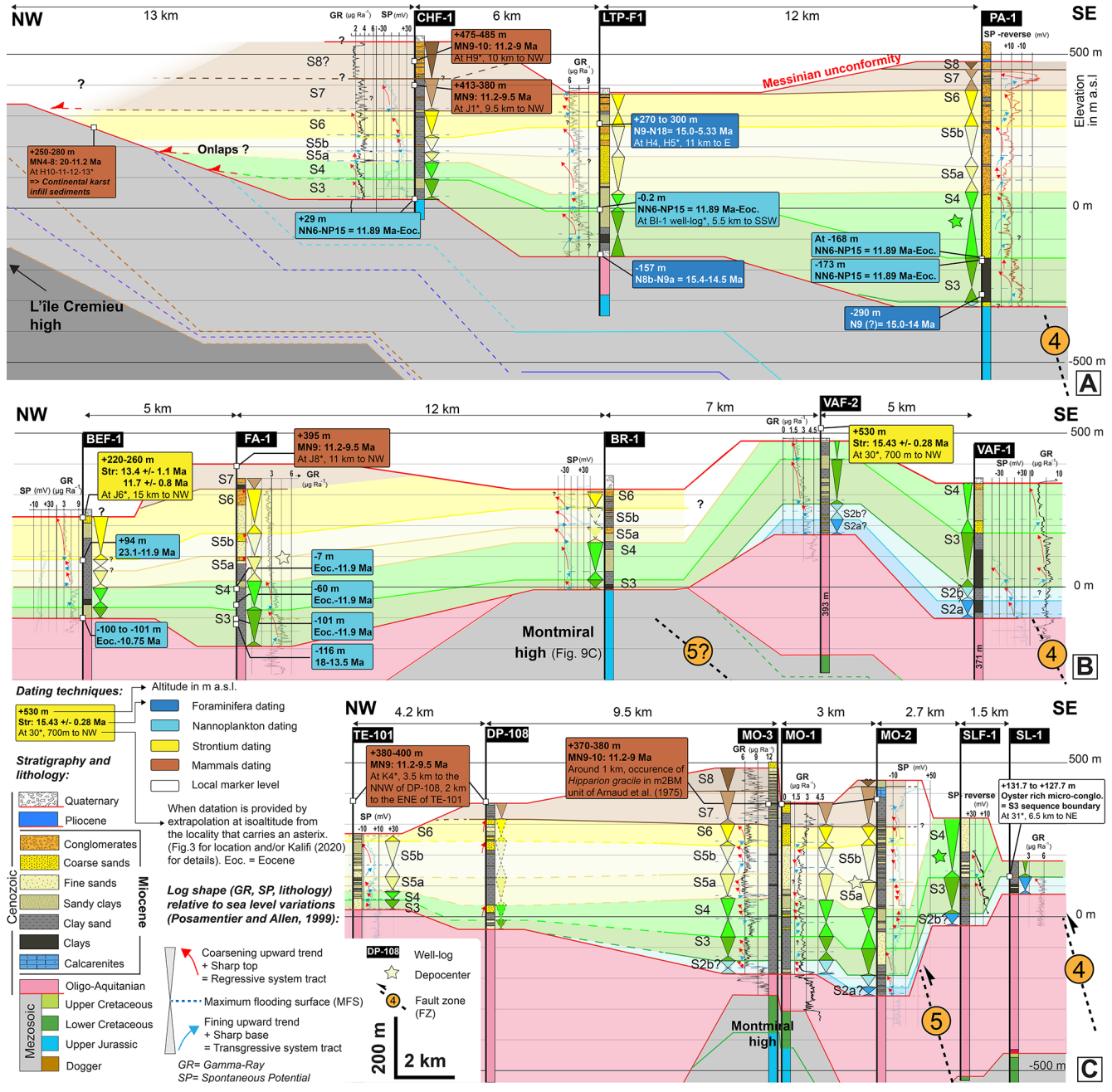

Figure 15. Spatiotemporal distribution of Miocene molasse deposits along SE–NW transects of the Bas-Dauphiné basin. Correlations are proposed based on sequence stratigraphy interpretations using stacking pattern methodology on SP (spontaneous potential), GR (gamma ray), and lithological data from well logs. See Fig. 3 for the location of transects.

East of the Montmiral high, significant variations in depositional thickness are observed for the S4 sequence with a maximum located in the footwall of FZ4. In transect A (Fig. 15A), S4 sequence maximum thickness of 215 m is recorded in the PA-1 well, while to the west, the sequence S4 thickness decreases progressively, reaching 53 m in the CH-1 well. In transect B, sequence S4 maximum thickness is recorded in the VAF-1 well, with a thickness of at least 161 m (since its top is eroded), while to the west, sequence S4 is 118 m thick in the BRI-1 well above the Montmiral high (Fig. 15B). In transect C, sequence S4 maximum thickness is recorded in the SLF-1 well, with a minimum of 190 m (eroded top), while to the west, sequence S4 is 129 and 116 m, respectively, in the MO-2 and MO-3 wells (Fig. 15C).

The sequences S5a–S5b also exhibit variation in thickness. In transect A, S5a–S5b maximum thickness of 210 m

is recorded in the PA-1 well, while it decreases progressively to the west, reaching 82 m in the CH-1 well (Fig. 15A). In transect B, S5a–S5b maximum thickness is difficult to estimate because the top of the VAF-1 and VAF-2 successions is eroded to the east of the Montmiral high (Fig. 15B). However, a probable depocenter is located to the west of FZ5 in the FA-1 well, with a thickness of 153 m (Fig. 15B). In transect C, the S5a–S5b depocenter can be located between the Montmiral high and FZ5 in the MO-2 well (Fig. 15C). There, the sequences S5a–S5b are 204 m thick, while to the west, they are ∼ 165 m thick above the Montmiral high (MO-2 and MO-3 wells, Fig. 15C). To the west, the interpretation of the DP-108 well is difficult as only lithological data are available but might suggest another depocenter with a thickness of 205 m (Fig. 15C).

No significant thickness variations are observed for the S6 sequence, which is ∼ 105 m thick along transect A (Fig. 15A), ∼ 145 m thick along transect B (Fig. 15B), and ∼ 70 m thick along transect C (Fig. 15C). The variation in thickness for S7 and S8 sequences cannot be estimated as they are rarely present in well logs (Fig. 15).

4.4.6 Bresse basin

To the east, the La Bresse basin is bordered by the l'île Cremieu high in the south and by the N–S-striking Jura thrusts in the north (Fig. 1B). In the La Bresse basin, the lower Miocene is absent, and the area is finally flooded at ∼ 12.0 Ma only during the S6 sequence (Fig. S13). The S6 sequence (∼ 12.0 to ∼ 10.8 Ma, Fig. 4B) and the transgressive deposits of the S7 sequence (∼ 10.8 to ∼ 10 Ma, Fig. 4B) are characterized by marine deposits, while the regressive system tract of sequences S7 and S8 exhibits purely continental deposits, implying a major regression starting during sequence S7.

At the Jura front, the BY-101 well log (Fig. 3) shows Mesozoic units thrusted atop Miocene deposits (Dumont, 1983). The same Miocene succession outcrops at the eastern border of the La Bresse basin, at Jujurieux (Dumont, 1983; I2, Fig. 3), and corresponds to marine deposits of sequences S6 and S7 based on Sr ages (Table S2), which are consistent with the magneto-biostratigraphical results of Aguilar et al. (2004). Therefore, sequences S6 and S7 are thrusted by the Jura thrust at the BY-101 locality. Thus, the onset of the Jura thrust is either synchronous or younger than the deposition of S6–S7 marine deposits (∼ 12 to ∼ 10 Ma).

At the Jura front, the continental deposits belonging to the S8 sequence according to mammal-based datings (I4, I5, I6 localities; Fig. 3) could also be partly deposited during the S7 regressive tract and are characterized by a 200 m thick continental clay and marl succession (Demarcq, 1970). This important thickness may suggest the existence of a tectonically controlled depocenter in the footwall of the Jura thrust.

5 Discussion

5.1 Genetic relationships between the stratigraphical domains and the fault zones (FZs)

The different depositional sequences depict a conspicuous spatial organization at the regional scale defining four depositional domains (Fig. 5). The oriental and median domains correspond to narrow longitudinal north–south bands, which are orthogonal to the general ∼ WNW–ESE direction of shortening linked to the Alpine compression. The age of the basal sequence becomes younger toward the west, indicating a westward migration of the depocenters (Fig. 4C). A similar migration can be deduced from the thickness variation of the sequences (e.g., S2a–S2b, S3, and S4) (Fig. 5). The oriental, median, and occidental domains are respectively bounded to the east by FZ1, FZ2, and FZ3 (Fig. 16). Such correspondence between the localization of the sedimentologic and structural boundaries suggests a genetic relationship between thrusting, accommodation space creation, and sediment infill.

The presence of angular unconformities and seismites within Burdigalian deposits of the southern Jura synclines (Fig. 1B) was already mentioned by Beck et al. (1998), Blanc (1991), and Deville et al. (1994), although the chronostratigraphic framework was still sketchy at that time. The present study, integrating evidence for syntectonic deposits, growth strata geometries, and depocenter migration at the basin scale within a well-constrained chronostratigraphy, allows for the depiction of the Miocene tectono-sedimentary evolution as follows.

5.1.1 The FZ1 activity (Phase 1)

The westward thinning of the Oligocene and Miocene S1a–S1b succession (∼ 21.0 to ∼ 18 Ma) observed in the Rumilly syncline implies a regular subsiding area between ∼ 29 ± 2 Ma (Rigassi, 1957; base of the Oligocene deposits dated by palynostratigraphy westwards of Annecy, locality 3; Fig. 10A, C) and 18.05 ± 0.15 Ma (S2a sequence boundary, Fig. 10A, C). Moreover, the westward-directed onlaps on the Mesozoic substratum, as well as the younger age of the base of the Oligocene sediments at the west of the Rumilly syncline (∼ 23 Ma based on mammals, Gaudant et al., 2002, locality 7; Fig. 10A, C), suggest a regular and slow westward migration of the depocenter. In a foreland basin, this geometry is consistent with a foredeep depozone located between the poorly subsiding proximal flank of the forebulge and the footwall of the active (tectonic) orogenic front, where the maximum of subsidence is recorded in response to the interplay between topographic loads and long-wavelength lithospheric deflection in relation with subduction process (DeCelles and Giles, 1996; Schlunegger and Kissling, 2015). The progressive decrease in depositional thicknesses towards the west might imply proximity to the forebulge, whereas

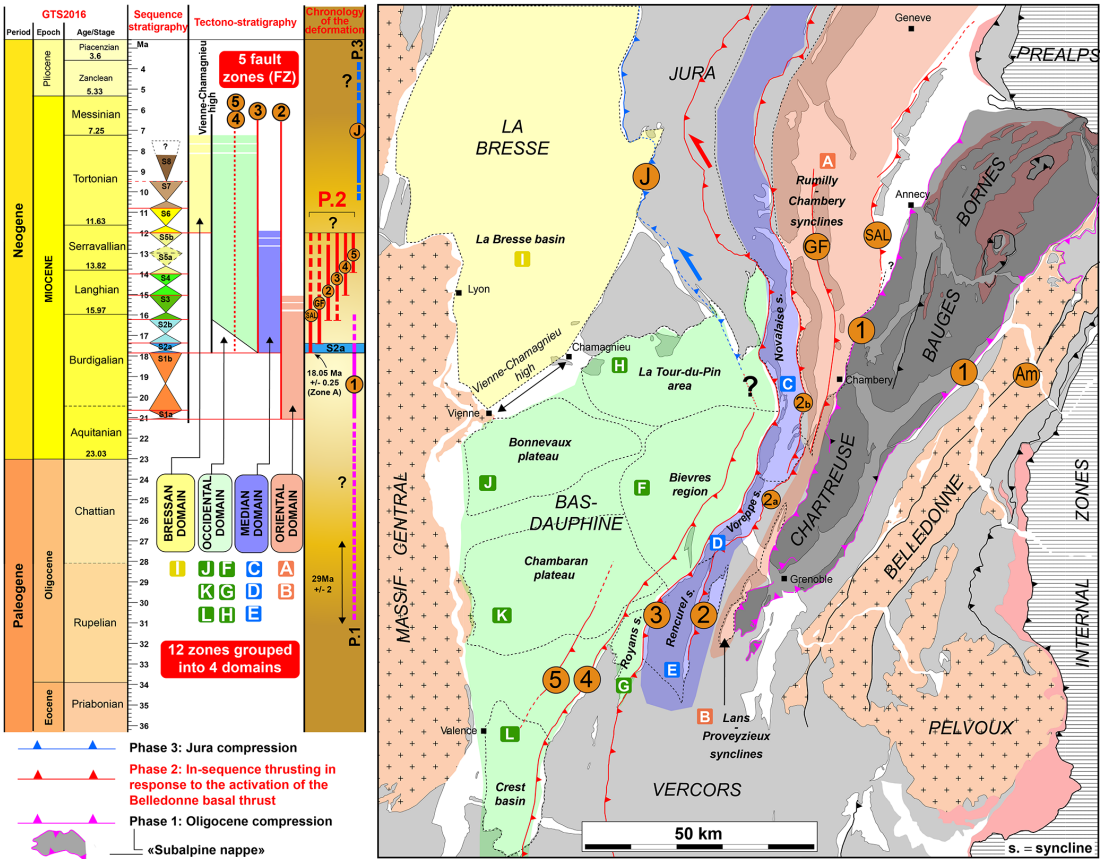

Figure 16. Summary of the structural, chronostratigraphical, and tectono-stratigraphic results of this study. The 11 sedimentary sequences revealed 12 paleogeographical zones, themselves grouped into four paleogeographical domains. Five fault zones (FZ1-5) were identified. Based on the established tectono-sedimentary evolution, three compressive phases were identified. The main phase corresponds to Phase 2, which involved the progressive onset, from east to west, of the SAL fault to FZ5 in response to the onset of the Belledonne basal thrust.

the maximum depositional thickness recorded to the east of the Rumilly syncline suggests proximity to the orogenic front. This interpretation is consistent with that of Deville et al. (1994), who previously interpreted the Oligocene sedimentary succession in this area as deposited in a passive foreland flexural basin. The upper Oligocene–lower Miocene tectonic front is therefore located east of the Rumilly syncline. Since marine Miocene deposits have never been described east of FZ1, we believe that it already formed a morphostructural barrier during the first marine sequences (S1a–S1b; 21.0 to ∼ 18 Ma, Fig. 4B, C) and was thus active prior to ∼ 21.0, possibly as early as 29 ± 2 Ma. However, in the early stage, the active front could also have been located east of FZ1, for example along the Entrevernes thrust (E) (Fig. 1B) or even further east, and other arguments are still needed to decipher the ante-21.0 Ma structural history.

5.1.2 Onset of the SAL, GF, and FZ2 faults (beginning of Phase 2)

Southwest of the Rumilly syncline, the E–W correlation between sedimentological sections 3, 4, 5, and 13 (Fig. 3) highlights important thickness variations (Fig. 13), leading us to propose the following chronology. At 18.05 ± 0.25 Ma, sequence S2a exhibits a prominent acceleration in accumulation rates, especially at the Grésy sur Aix locality (section 4, Fig. 13), suggesting the rapid production of accommodation space probably linked to a regional tectonic event. Interestingly, the occurrence of seismites involving a major earthquake is observed within the S2a transgressive tract (Fig. 12). Seismic profiles from the Rumilly syncline (Fig. 10) outline the S2a basal sequence boundary as corresponding to high-amplitude reflectors characterized by low-angle S1 toplaps and S2 onlaps, thereby advocating for an angular unconformity. Together, this suggests a tectonic event associated with the activation of the SAL thrust at 18.05 ± 0.25 Ma, since the sequence S2a depocenter is located at the footwall of this fault (Fig. 17). Subsequently, the angular unconformity highlighted in tidal flat deposits and associated with Chron C5Dn (17.53–17.23 Ma, Fig. 12A, B) recovered at the top of the S2a regressive tract, most probably reflects another regional tectonic event with the depocenter abruptly migrating westwards at that time at the footwall of the GF fault (section 5,

Fig. 13). These two lines of evidence therefore support the hypothesis of the onset of the GF fault during Chron C5Dn (Fig. 17). At ∼ 16.2 Ma (S3 transgression), the depocenter migrated westwards again and lies at the footwall of FZ2 (section 13, Fig. 13). There, during deposition of sequence S3, thick distal marine deposits were sedimented, whereas coarse-grained deltaic deposits prevailed to the east of FZ2 (sections 4, 5, Fig. 13), suggesting a more proximal and uplifted area. Thus, FZ2 was activated during deposition of sequence S3 (Fig. 17).

5.1.3 Onset of FZ3, FZ4, and FZ5

At the hanging wall of FZ3, the base of sequence S2a is concordant on the folded Urgonian, suggesting that folding did not start before the deposition of the S2a sequence. Sequences S2b(?)–S3 exhibit growth strata geometries suggesting a westward thickening of sedimentary deposits (Fig. 14C, D), which can be attributed to an anticline formation in the hanging wall of FZ3. Without further stratigraphic constraints, however, we can only speculate that FZ3 was active at least since deposition of sequence S3 (∼ 16.2 Ma, Fig. 17). On the eastern edge of the Bas-Dauphiné basin at the footwall of FZ4, the presence of growth strata geometries between sequences S4 and S5 (Fig. 14A), as well as the occurrence of a sequence S4 depocenter between FZ4 and FZ5 (Fig. 15), implies a flexural subsidence at the footwall of the active FZ4, therefore constraining the activity of FZ4 between the onset of sequence S4 and the end of sequence S5, so between ∼ 15.0 and ∼ 12.0 Ma (Figs. 4A, B and 17). This is also in agreement with the underlying S2 and S3 deposits, as well as the overlying S6 deposits, which all appear isopachous (Figs. 14 and 15), and thus suggests the absence of tectonic activity during deposition of these sequences. In the FZ5 footwall the presence of a sequence S5a–S5b depocenter (∼ 14.0 to ∼ 12.0 Ma) (Fig. 15C) suggests a continuous westward migration of the depocenters (Fig. 17) that could have been controlled by FZ5 activity at that time. This hypothesis is consistent with the general trend observed since the base of S2a at zone A 18.05 ± 0.3 Myr ago, which shows the successive activation of the fault zones from east to west (SAL fault, GF fault, FZ2, FZ3, FZ4, and finally FZ5). Thus, the thrusts that are interpreted to root below the Belledonne massif in the Belledonne basal thrust were activated in-sequence (Fig. 17).

5.1.4 Timing of the end of deformation

In the Rumilly–Chambéry synclines the thick S2a and S2b sequence (18.05 ± 0.15 to 16.3 ± 0.3) marine deposits of the depocenter that developed in the footwall of the SAL and GF (sections 4, 5, Figs. 13 and S5) are capped by a rapid shallowing-upward succession, followed by S3 gravel-rich braided-river deposits (Fig. S8). This evolution suggests a final immersion linked with the fold-and-thrust propagation (Heller et al., 1988; DeCelles and Giles, 1996; Sinclair, 1997) and thus that the SAL and GF faults were active during the S2 and S3 sequences (until ∼ 15 Ma). However, the lack of timing control within the S3 and overlying sequences at this location precludes any precise constraint on the timing of the end of motion on SAL and GF (Figs. 13 and S8).

In the footwall of FZ2 near Grenoble (zone D, 20, 22, Fig. 3), the sedimentary succession of the S4–S5 sequences of the Voreppe syncline is characterized by three stacked Gilbert deltas (GDs). GD1a and GD1b are 25 and 40 m thick, respectively, belong to the S4 (∼ 15.0 to ∼ 14.0 Ma), and GD2 belongs to the S5 (∼ 14.0 to ∼ 12.0 Ma) (Fig. S8). As these stacked Gilbert deltas attest a continuous creation of slope and accommodation space (Ricketts and Evenchick, 2007) we interpret them as reflecting continuous activity of FZ2, thus until at least ∼ 12 Ma (Kalifi et al., 2021). GD2 is much thinner than GD1b (20 m against 40 m, respectively) and shows an abrupt transition between foresets and ∼ 10 m thick topsets themselves overlain by ∼ 5 m high foresets interpreted as a mouth bar in a distal deltaic position, suggesting a final transgression corresponding to S5b (Kalifi et al., 2021) (Fig. S8). This unit is finally overlain by 50 m of planar-stratified conglomerates interpreted as braided fluvial deposits likely evolving from deltaic to fluvial hydrodynamics. This transition could correspond to the final shallowing-up succession of the Gilbert deltas' stacking pattern, thus suggesting a progressive decrease in FZ2 activity until the end of the S5 sequence (∼ 12.0 Ma) (Kalifi et al., 2021).

To the west, in the footwall of FZ3 and FZ4, the sequence S6 deposits have a constant thickness in the Bas-Dauphiné basin (Fig. 15) and the sequence S6 seals the underlying S4 and S5 growth strata (Fig. 14A). This suggests an end of FZ3 and FZ4 activity in the Vercors and Chartreuse massifs at ∼ 12.0 Ma (top S5 sequence).

5.2 Sequence of shortening of the southern Jura and subalpine massifs

To further quantify the amount and history of shortening, cross sections B and C (northern and southern Chartreuse, respectively; Fig. 11B, C) were balanced and restored to the initial geometry before the Alpine shortening. Such reconstruction takes into account the relative timing of the various faults and yields a reconstruction of the deformation through time as well as an initial state. The cross sections have been drawn perpendicular to the main thrusts and fold axis (Fig. 1B): N118° for cross section B and N114° for cross section C. Total horizontal shortening along cross section B is 22.24 km (33.9 %) and 13.72 km (22.5 %) along cross section C (Fig. 18). These values are somehow approximate since they result from the hypothesis of a planar strain along a single and uniform direction of deformation for each section. They are in agreement with the previous finding of an increase in the shortening toward the north (Menard and Thouvenot, 1987; Sinclair, 1997; Philippe et al., 1998) that

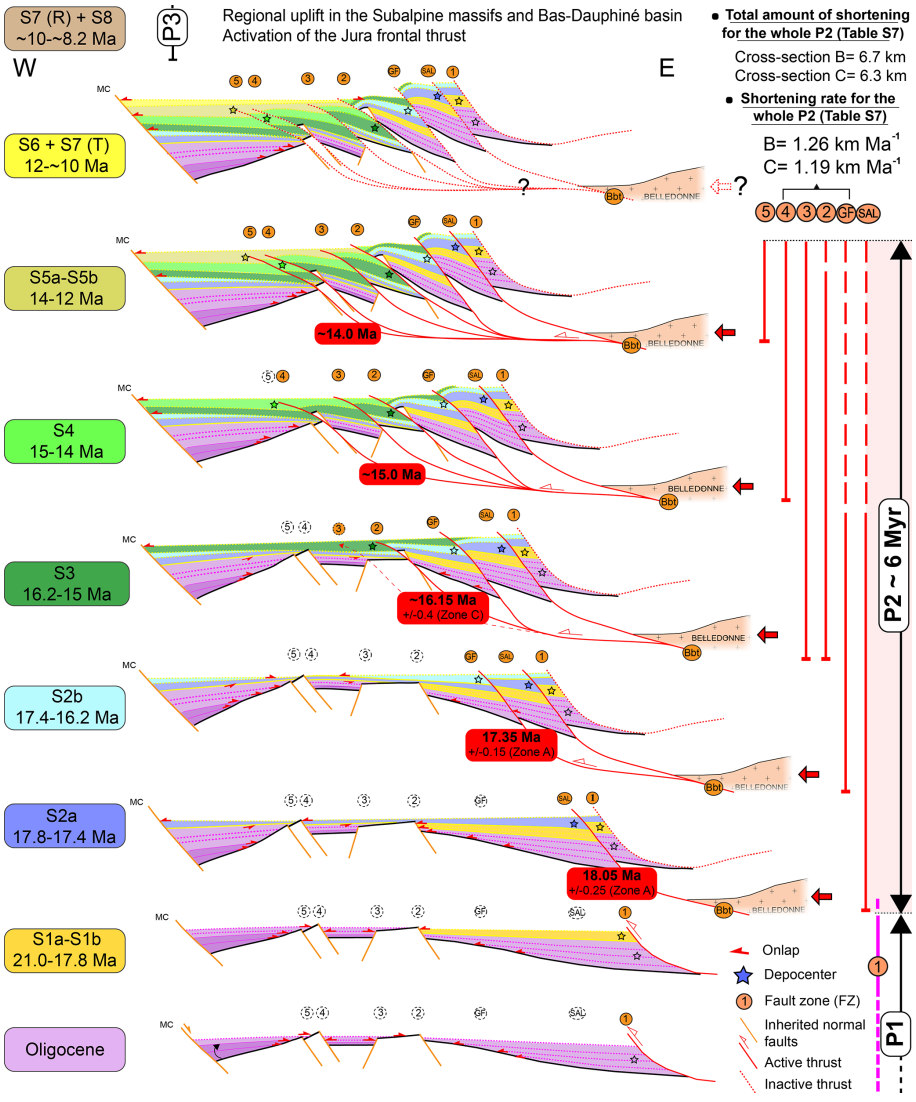

Figure 17. Schematic framework summarizing the main phases of thrust propagation at the western Alpine front and their chronology based on a thorough revision of the regional chronostratigraphy between the Oligocene and the late Miocene. The horizontal and vertical scales are not respected. MC: Massif Central; P: tectonic phase; T: transgressive deposits; R: regressive deposits. The colored boxes on the left side correspond to the homogenized ages of the eustatically driven depositional sequences (Fig. 4A, B). Red boxes highlight the timing of fault initiation deduced from depocenter migration (Fig. 13). Vertical lines on the right represent the proposed timing of activity for each fault.

is interpreted as reflecting a larger amount of convergence (Bellahsen et al., 2014).

The sequential reconstruction allows for the calculation of the shortening related to each fault and fold, and our chronological constraints on the thrusts bounds the quantification of some deformation rates. The amount of horizontal shortening for the whole of Phase 1 (i.e., FZ1 horizontal shortening) is 14.1 km along cross section B and 5.8 km along cross section C (Fig. 18A, B, Table S7). Note that the backthrusts visible in the east of section C corresponding to ~ 1.6 km of shortening (bk1 and bk2, Figs. 11C and 18B) are excluded from that calculation as they are only seen along that section and interpreted as related to a later tectonic phase. The amount of horizontal shortening for the whole of Phase 2 (i.e., GF thrust, FZ2, FZ3, and FZ4 horizontal shortening) is 6.7 km in cross section B and 6.3 km in cross section C (Fig. 18A, B, Table S7). In the Chartreuse massif, the SAL fault is not present along section B (Fig. 1B), and Phase 2 is assumed to last from the onset of the GF (17.35 ± 0.15 Ma) to the end of deformation on FZ4 and FZ5 (~ 12 Ma), thus for ~ 5.3 Myr. This implies a migration of the deformation toward the external parts (west) at a rate of ~ 2.9 km Myr^{-1} along sections B and C. This also corresponds to average shortening rates of 1.26 km Myr^{-1} for cross section B and 1.19 km Myr^{-1} for cross section C.

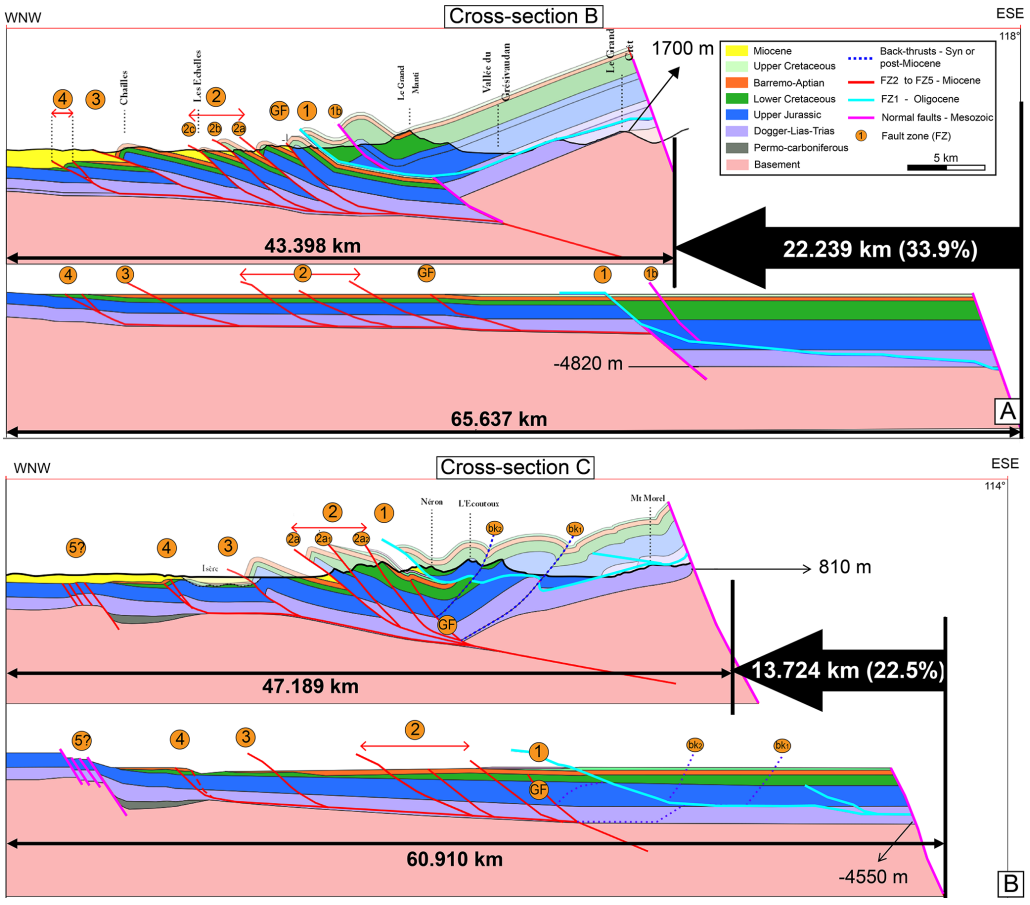

Figure 18. Balanced cross sections throughout the Chartreuse massif using the MOVE software, assuming that ZF2 to ZF4 are rooted below a single Belledonne basal thrust. **(A)** Cross section B (Fig. 11B). **(B)** Cross section C (Fig. 11C). See Fig. 1B for locations. Note that the backthrusts visible in the east of section C (bk1 and bk2, Fig. 11C and panel **B** of this figure) are interpreted as related to a late tectonic phase; see text for details. Corresponding shortening amounts and rates are listed in Table S7.

5.3 Comparison of deformation phases affecting the Miocene molasse in the western Alps

In Chartreuse and Vercors we thus document the phase of ∼WNW–ESE shortening shaping the subalpine ranges (Phase 2) as starting at 18.05 ± 0.25 Ma (SAL fault) or 17.35 ± 0.15 Ma further south (GF fault). Then, surface thrusting propagated to the west at a rate of $\sim 1.2\,\mathrm{km\,Myr^{-1}}$, with the successive onset of FZ2, FZ3, FZ4, and FZ5, FZ5 initiation occurring at ∼14 Ma, and the deformation ending at ∼12 Ma (Figs. 16 and 17).

In the southern Jura, east of the La Bresse basin in drill hole BY-101 (Fig. 1B), the sequence S6 and S7 marine deposits (∼12 to ∼10 Ma, Fig. S13) are overthrusted by Mesozoic sediments along the external Jura thrust (J and φEJuE, Fig. 1B), indicating that the onset of the Jura thrust is either synchronous or younger than sequences S6–S7. Due to the occurrence of abnormally thick Tortonian S7 and S8 continental deposits (∼10 to ∼8.2 Ma) at the footwall of the Jura thrust that suggest a tectonically controlled depocenter, we propose that the Jura frontal thrust (J, Fig. 1B) was active during sequence S8 (∼9.5 Ma; Fig. 4A) and perhaps even coeval with the deposition of sequence S7 continental sediments (∼10 Ma). This hypothesis is supported by earlier chronostratigraphical studies based on mammals, suggesting that the activity of the Jura frontal thrust (J, Fig. 1B) started between the Serravalien (∼11 Ma) and the Pliocene (Bolliger et al., 1993; Steininger et al., 1996; Kälin, 1997). U–Pb ages of syntectonic calcite mineralizations sampled from the nearby Buron thrust (Bur, Fig. 1B) give an age of 10.6 ± 0.5 Ma (Smeraglia et al., 2021). Paleontological evidence combined with tectonic evidence suggest a termination of Jura thin-skinned foreland tectonics between 9 and 4 Ma (Becker, 2000).

To the northeast, the whole Swiss molasse basin (SMB, Fig. 1A) lies in the prolongation of the southern Jura synclines between the subalpine sediments of the Aar External Crystalline Massif (ECM) and the folded Mesozoic series of the Jura. At the time of Phase 2 (18–12 Ma) the zone was affected by several transgression and regressions: con-

tinental deposits of the Lower Freshwater Molasse (USM) last until ∼ 20 Ma (Burdigalian), when a marine transgression yields to the deposition of the Upper Marine Molasse (OMM-I) until ∼ 18.3 Ma (Homewood, 1981; Allen, 1984; Kempf et al., 1999; Garefalakis and Schlunegger, 2019). After a sedimentation hiatus until ∼ 17.8 MA a new transgression yields to the deposition of the Upper Marine Molasse (OMM-II), until a final regression at ∼ 16.5 Ma yielding to deposition of the upper fresh marine molasse (OSM) until at least 14 Ma, after which time sediments have not been preserved (Kempf et al., 1999; Garefalakis and Schlunegger, 2019). Drainage directions in the USM and OMM-I are towards the northeast, while in the OSM they are towards the southwest (Berger et al., 2005; Garefalakis and Schlunegger, 2019). Based on apatite (U–Th–Sm) / He thermochronometry, Mock et al. (2020) infer exhumation of the molasse between 12 and 4 Ma. These oscillations result from the interplay of eustatism and surface and/or deep-seated tectonic processes, the details of which are still discussed. From apatite and fission-track data, exhumation of the Aar ECM started at ∼ 22 Ma at a rate of 1.3–1.6 km Myr^{-1} in the southeast and 0.1 km Myr^{-1} in the northwest, and it lasted until today in two phases with uniform exhumation rates of 0.5–0.9 km Myr^{-1} between 13 and 5 Ma and 0.6–0.8 km Myr^{-1} until then (Herwegh et al., 2020). From these data it has been proposed that thrusting toward the NW below the Aar started at ∼ 22 Ma and that it propagated from Aar to Jura at ∼ 13 Ma along a NW-verging flat décollement level (Mock et al., 2020, and references therein). Such timing fits well with the U–Pb calcite ages of calcite veins in the footwall of that décollement at the eastern tip of the Jura that suggest it was active at least between 14.3 and 13.2 Ma (Looser et al., 2021). Similar ages from calcite slickensides suggest that frontal thrusts of the Jura were active between 11.3 ± 0.9 and 4.5 ± 1.5 Ma (Looser et al., 2021). Similar ages are documented further west from the inner to the external Jura: 11.4 ± 1.1, 10.6 ± 0.5, and 7.5 ± 1.1 Ma for the Montlebon, Fuans, and Arguel thrusts, respectively (Smeraglia et al., 2021). Such ages are also in good condordance with those from the southwest Jura (see above). This NW-verging deformation is locally characterized by SE-verging backthrusts, including one close to the southern boundary of the Swiss molasse basin west of the Aar valley that was active between ca. 13 and 4 Ma and contributed to the exhumation of the molasse at that time (Looser et al., 2021, and references therein). In Vercors and Chartreuse we have interpreted the thrusts of Phase 2, starting at $\sim 18.05 \pm 0.25$ Ma (GF), to be rooted below the Belledonne external crystalline massif. This would imply a start of the exhumation of that range slightly before 18 Ma. Such an age is close to that proposed for the onset of the exhumation of the Aar range (∼ 22 Ma). In front of the Aar crystalline range the thrust front appears to have stayed stable between 22 and ∼ 13 Ma at ∼ 30 km from the edge of the range. In front of the central Belledonne the thrust front migrated from 20 to 40 km away from the crystalline range between ∼ 18 and ∼ 15 Ma. Both structural histories are quite similar, suggesting that similar mechanisms were active along-strike of that part of the Alpine belt, with a slight diachronism from north (22 Ma) to south (18 Ma): ∼ NW–SE shortening rooted below the ECM.

To the south, in the Rhodano–Provencal molasse basin (RPMB, Fig. 1A), middle Miocene syntectonic deposits (upper Burdigalian–Langhian; ∼ 18–14 Ma) are described in the Digne (Gigot et al., 1974; Beaudoin et al., 1975; Crumeyrolle et al., 1991), the Lubéron (Clauzon, 1974), the Alpilles (Colomb, 1982), and the Vaison-la-Romaine (Brasseur, 1962) areas. These syntectonic sediments were deposited in response to the first Miocene Alpine tectonic phase of the RPMB (Gigot et al., 1974), which is coeval to the onset of Phase 2 in our study area. Thus, the upper Burdigalian tectonic phase (Phase 2 in this paper) was recorded at the western Alpine foreland basin scale, suggesting a major tectonic event, as is highlighted by new Miocene paleogeographical reconstructions at the foreland basin scale (Kalifi et al., 2021).

The following structural history, however, strongly differs between the north and south: at ∼ 13 Ma in the Aar the deformation front appears to have quickly migrated more than 50 km to the NW to form the Jura, while it ended at ∼ 12 Ma in front of the central Belledonne. However, some observations suggest that the Bas-Dauphiné experienced uplift after 12 Ma. In the western and southern parts of the Bas-Dauphiné basin and the Crest basin (J, K, and L zones, respectively; Fig. 3) the Miocene final sea retreat is recorded during deposition of sequence S7 (∼ 10 Ma; Figs. S13, 14, 15, 16). The absence of marine deposits during S8 (∼ 9.5 to ∼ 8 Ma) is unexpected, as it corresponds to a eustatic transgression corresponding to a higher sea level (+40 m) than that of sequence S7 (+5 to 10 m, Miller et al., 2005, Fig. 4B). This implies that the ∼ 10 Ma Miocene sea retreat was induced by a basin-scale event. In the northeastern part of the Bas-Dauphiné basin (F, H zones, Fig. 5), the uppermost marine deposits (sequence S6 regressive deposits, ∼ 11 Ma, Figs. S10 and S12) outcrop today at an elevation of ∼ 350 m a.s.l. (Figs. 14B and 15A). The sequence S6 transgression involved a +25 m sea level rise, which suggests a post-sequence S6 (12 Ma) minimum uplift of ca. 325 m. This is in agreement with the Deville et al. (1994) observations implying a post-Langhian uplift. These authors interpreted this uplift as the result of a crustal thickening due to a crustal imbrication under the molasse basins, implying the activation of out-of-sequence thrusts in an internal position of the subalpine massifs. However, these thrusts have not been clearly identified and it is unclear how such thrusts could induce uplift of the Bas-Dauphiné. Other possible interpretations are that this uplift could be linked to the activation of late backthrusts such as those described along section C (bkt1 and bkt2, Fig. 11) or to a still unclear deeper process.

6 Conclusions

This study focused on the Miocene molasse of the western Alpine foreland basin (subalpine massifs, southern Jura, the Bas-Dauphiné, the la Bresse, and the Crest basins). The combination of chemostratigraphy, biostratigraphy, and magnetostratigraphy applied to sedimentological sections and well logs from the Miocene succession across the entire area allowed the establishment of a new chronostratigraphic framework. The Miocene is characterized by 11 depositional sequences dated between the late Aquitanian and the Tortonian. The spatial distribution of these sequences defines 12 depositional zones grouped into four domains. These domains are bounded by the main thrust fault zones, therefore implying a strong interplay between active tectonics and sedimentation during the Miocene, and lead us to propose three main tectonic phases (Fig. 17).

Phase 1 started prior to 21 Ma, possibly since the early Oligocene (29 ± 2 Ma), and lasted until the early Miocene (~ 17.8 Ma). During this phase, the southern Jura synclines were affected by flexural subsidence induced by the Alpine tectonic front to the east. The maximum depositional thickness recorded to the east of the Rumilly syncline, as well as the absence of early Miocene marine deposits to the east of FZ1, most probably indicates that the tectonic activity along FZ1 rooted east of the Belledonne external range.

Phase 2 took place between the late Burdigalian (18.05 ± 0.25 Ma) and the Serravalian (~ 12 Ma). In the Chartreuse massif, the shortening rate related to that phase averages $\sim 1.2\,\mathrm{km\,Myr^{-1}}$. At 18.05 ± 0.25 Ma, the development of a depocenter at the footwall of the SAL thrust along with the occurrence of seismites (of regional extent) together suggest the activation of the SAL fault. Subsequently, at 17.35 ± 0.15 Ma, an angular unconformity characterized by westward-directed onlaps is recorded. This angular unconformity discloses a rapid westward migration of the depocenter at the footwall of the GF fault and thereby points to its activation. At ~ 16.2 Ma, growth strata relationships in the S3 sequence (+S2b?) in the hanging wall of FZ3, combined with the occurrence of a sequence S3 depocenter in the footwall of FZ2, argue for the quasi-synchronous activation of FZ2 and FZ3 thrusts. Subsequently, at ~ 15.0 Ma, sequence S4 growth strata geometries and the development of a sequence S4 depocenter in the footwall of the FZ4 document the onset of FZ4. Finally, at ~ 14.0 Ma, the sequence S5 depocenter occurs in the footwall of FZ5 and probably dates the activation of the FZ5 thrust. The end of Phase 2 took place at ~ 12.0 Ma, as the S6 deposits have a constant thickness in the Bas-Dauphiné basin, and sequence S6 seals the underlying growth strata (S2 to S5 sequences). We interpret this phase as corresponding to the activation of the Belledonne basal thrust, rooted below the external Belledonne massif, and to the propagation at an average rate of $\sim 2.9\,\mathrm{km\,Myr^{-1}}$ of the surface deformation toward the west within the subalpine ranges (successively SAL fault, GF fault, FZ2, FZ3, FZ4, and FZ5 thrusts). This appears quite similar to the Serravallian and Langhian thrusting at the base of the Aar range and is coeval with the first Miocene Alpine tectonic phase of the Rhodano–Provencal molasse basin, implying a tectonic phase affecting the whole western Alps.

In the north of the study area, deformation migrated NW in the Jura after 13 Ma but stopped in Vercors and Chartreuse at ~ 12 Ma. Thick accumulation of continental S7 and S8 deposits at the footwall of the Jura frontal thrust is coeval with thrusting of Mesozoic series atop S6 and S7 marine deposits (~ 12 to ~ 10 Ma), indicating that the Jura front initiated during the Tortonian (~ 10 Ma, Phase 3). Synchronously, to the south in the Bas-Dauphiné zones and the Crest basin, no thrust activity is recorded after deposition of sequence S5 (~ 12 Ma). A mild uplift after ~ 12 Ma (≤ 325 m) is probably linked with the ~ 10 Ma (lower Tortonian) sea retreat and possibly to late backthrusts east of the Chartreuse.

Data availability. The research data are included in this paper and in the Supplement, and they can be freely accessed.

Supplement. The supplement related to this article is available online at: https://doi.org/10.5194/se-12-2735-2021-supplement.

Author contributions. This study was performed by AK in the framework of his PhD, co-supervised by TOTAL (CSTJF, Pau, France) and the LGL-TPE (University Lyon 1). JLR conceptualized the original research topic of this study, with the support of VS, in the EXPLO/EP/GTS/ISS entity of TOTAL. Fieldwork and interpretations related to the chronostratigraphical study were performed by AK under the supervision of PS, BP, and JLR, as well as by BH under the supervision of JLR and AK for the northern part of the Bas-Dauphiné basin. Fieldwork and interpretations related to the structural study were performed by AK under the supervision of PHL and the helpful support of VS. Restoration of the structural cross sections was conducted by KL supervised by PHL and AK. The sampling and the sample preparation for the chemostratigraphical study were achieved by AK, and the analysis and interpretations were conducted by AG. The sampling for the paleomagnetic study was carried out by FD, PS, RG, and AK. AK prepared the samples, and the interpretations were conducted by FD. The sampling for the biostratigraphical study was conducted by AK, BH, and RG, and the interpretations were performed by FQ for the planktonic foraminifera, by DM for the dinoflagellate cysts, and by FR for the calcareous nannofossils. AK wrote the paper, with major contributions from PHL, PS, and BP, as well as corrections from all other all co-authors.

Competing interests. The contact author has declared that neither they nor their co-authors have any competing interests.

Special issue statement. This article is part of the special issue "New insights into the tectonic evolution of the Alps and the adjacent orogens". It is not associated with a conference.

Acknowledgements. The authors would like to thank TOTAL for financing this PhD study. We would like to thank Andrea-Lopez Vega, Thomas Pichancourt, Hawoly Bass, Astrid Jonet, Antoine Mercier, Alessandro Menini, Pierre and Thomas Courrier, Daniel Fournier, Ludovic Mocochain, Sidonie Revillon, Hugues Fenies, Gilles Escarguel, Loïc Costeur, Jonathan Pelletier, Edouard Le-Garzic, Xavier Du-Bernard, Jean-Pierre Girard, and Francois Lafont for their precious help in the field and/or for fruitful discussions. Constructive reviews by Thierry Dumont and Fritz Schlunegger helped to clarify the paper. The authors would also like to pay special tribute to Bernard Pittet, who recently passed away and who contributed greatly to this study.

Financial support. This research has been supported by TOTAL (grant no. 2016/1180 (Cifre)).

Review statement. This paper was edited by Arjen Stroeven and reviewed by Fritz Schlunegger and Thierry Dumont.

References

Aguilar, J.-P., Berggren, W. A., Aubry, M.-P., Kent, D. V., Clauzon, G., Benammi, M., and Michaux, J.: Mid-Neogene Mediterranean marine–continental correlations: an alternative interpretation, Palaeogeogr. Palaeocl., 204, 165–186, 2004.

Allen, P. A.: Reconstruction of ancient sea conditions with an example from the Swiss Molasse, Mar. Geol., 60, 455–473, 1984.

Allen, P. A. and Bass, J. P.: Sedimentology of the upper marine molasse of the Rhône-Alp Region, Eastern France: implications of basin evolution, Eclogae Geol. Helv., 86, 121–172, 1993.

Arnaud, H., Combier, J., and Monjuvent, G.: Notice explicative, Carte géol. France (1 / 50 000), feuille Romans-sur-Isère (795), BRGM, Orléans, 30 pp., 1975.

Barféty, J.-C. and Barbier, R.: Carte géologique (1 / 50 000), feuille La Rochette (750), BRGM, Orléans, 1983.

Barféty, J.-C. and Gidon, M.: La structure des Collines bordières du Grésivaudan et des secteurs adjacents, à l'est de Grenoble (Isère, France), Géologie Alp., 72, 5–22, 1996.

Barféty, J.-C., Antoine, P., Girod, J.-P., Bellamy, J., Chabod, J.-C., Boullud, C., Bullière, J., Debelmas, J., Sarrot-Reynaud, J., and Goguel, J.: Carte géol. France (1 / 50 000), feuille Vif (796), BRGM, Orléans, 1967.

Bass, J. P.: The sedimentology and basin evolution of the upper marine molasse of the Rhône-Alp region, France, PhD Thesis, Department of Earth sciences, University of Oxford, 1991.

Beaudoin, B., Campredon, R., Cotillon, P., and Gigot, P.: Alpes Méridionales Françaises : Reconstitution du bassin de sédimentation, Excursion No. 7, IX Congrès International de Sédimentologie, Nice, IAS Publ., 1975.

Beaumont, C.: Foreland basins, Geophys. J. Int., 65, 291–329, 1981.

Beck, C., Deville, E., Blanc, E., Philippe, Y., and Tardy, M.: Horizontal shortening control of Middle Miocene marine siliciclastic accumulation (Upper Marine Molasse) in the southern termination of the Savoy Molasse Basin (northwestern Alps/southern Jura), Geol. Soc. Lond. Spec. Publ., 134, 263–278, 1998.

Becker, A.: The Jura Mountains – an active foreland fold-and-thrust belt?, Tectonophysics, 321, 381–406, 2000.

Bellahsen, N., Jolivet, L., Lacombe, O., Bellanger, M., Boutoux, A., Garcia, S., Mouthereau, F., Le Pourhiet, L., and Gumiaux, C.: Mechanisms of margin inversion in the external Western Alps: Implications for crustal rheology, Tectonophysics, 560, 62–83, 2012.

Bellahsen, N., Mouthereau, F., Boutoux, A., Bellanger, M., Lacombe, O., Jolivet, L., and Rolland, Y.: Collision kinematics in the western external Alps, 33, 1055–1088, 2014.

Berger, J.-P.: La transgression de la molasse marine supérieure (OMM) en Suisse occidentale, Munchn. geowiss. Abh. A5, 1–207, 1985.

Berger, J.-P.: Paléontologie de la Molasse de Suisse occidentale, Th. d'habilitation sci., University of Fribourg, 452 pp., 1992.

Berger, J. P., Reichenbacher, B., Becker, D., Grimm, M., Grimm, K., Picot, L., Storni, A., Pirkenseer, C., Derer, C., and Schaefer, A.: Eocene-Pliocene time scale and stratigraphy of the Upper Rhine Graben (URG) and the Swiss Molasse Basin (SMB), Int. J. Earth Sci., 94, 711–731, 2005.

Bergerat, F.: Paléo-champs de contrainte tertiaires dans la plateforme européenne au front de l'orogène alpin, Bull. la Société géologique Fr., 3, 611–620, 1987.

Bergerat, F., Mugnier, J.-L., Guellec, S., Truffert, C., and Cazes, M.: Extensional tectonics and subsidence of the Bresse basin: an interpretation from ECORS data, Mémoires la Société géologique Fr., 156, 145–156, 1990.

Blanc, E.: Evolution sédimentaire syntectonique au front d'une chaîne de collision en environnement littoral, Mem. DEA., Université de Savoie (Chambéry), 35 pp., 1991.

Blanchet, F. and Chagny, E.: Le promontoire de la Porte de France près de Grenoble: Analyse tectonique détaillée-Massif de la Chartreuse, Bull. Serv. Carte Geol. Fr., 149, 253–276, 1923.

Bocquet, J.: Le delta miocène de Voreppe. Etude des faciès conglomératiques du Miocène des environs de Grenoble, Trav. du Lab. Géologie l'Université Grenoble, 42, 53–75, 1966.

Bolliger, T., Engesser, B., and Weidmann, M.: Première découverte de mammifères pliocènes dans le Jura neuchâtelois, Eclogae Geol. Helv., 86, 1031–1068, 1993.

Bonnet, C., Malavieille, J., and Mosar, J.: Interactions between tectonics, erosion, and sedimentation during the recent evolution of the Alpine orogen: Analogue modeling insights, Tectonics, 26, TC6016, https://doi.org/10.1029/2006TC002048, 2007.

BouDagher-Fadel, M. K.: Biostratigraphic and Geological Significance of Planktonic Foraminifera, updated 2nd Edn., UCL Press, London, https://doi.org/10.14324/111.9781910634257, 2015.

Brasseur, R.: Etude Géologique du Massif de Suzette (Vaucluse), PhD Thesis, Université de Lyon, 195 pp., 1962.

Burkhard, M. and Sommaruga, A.: Evolution of the western Swiss Molasse basin: structural relations with the Alps and the Jura belt, Geol. Soc. Lond. Spec. Publ., 134, 279–298, 1998.

Butler, R. W. H.: The geometry of crustal shortening in the Western Alps, in: Tectonic evolution of the Tethyan region, Springer, Dordrecht, 43–76, 1989a.

Butler, R. W. H.: The influence of pre-existing basin structure on thrust system evolution in the Western Alps, Geol. Soc. Lond. Spec. Publ., 44, 105–122, 1989b.

Butler, R. W. H.: Structural evolution of the western Chartreuse fold and thrust system, NW French Subalpine chains, in: Thrust tectonics, edited by: McClay, K. R., Chapman and Hall, London, 287–298, 1992a.

Butler, R. W. H.: Thrusting patterns in the NW French Subalpine chains, Annales Tectonicae, 6, 150–172, 1992b.

Butler, R. W. H.: Basement-cover tectonics, structural inheritance, and deformation migration in the outer parts of orogenic belts: A view from the western Alps, Linkages Feed. Orog. Syst., 213, 55–74, 2017.

Butler, R. W. H. and Bowler, S.: Local displacement rate cycles in the life of a fold-thrust belt, Terra Nova, 7, 408–416, 1995.

Cardozo, N. and Allmendinger, R. W.: Spherical projections with OSXStereonet: Comput. Geosci., 51, 193–205, https://doi.org/10.1016/j.cageo.2012.07.021, 2013.

Charollais, J. and Jamet, M.: Principaux résultats géologiques du forage Brizon 1 (BZN 1) Haute-Savoie, France, Mémoires la Société géologique Fr., 156, 185–202, 1990.

Clauzon, G.: Quel âge le Lubéron a-t-il?, Etudes Vauclusiennes, XI, 1–6, 1974.

Colomb, E.: Relation plate-forme carbonatée – continent dans le cas de la transgression Miocène dans les Alpilles (Bouches-du-Rhône), Géologie Méditerranéenne, 9, 213–215, 1982.

Couëffé, R. and Tourlière, B.: Modélisation géologique multicouche Bresse, Dombes, Bas-Dauphiné, Couloir rhodanien – Méthodologie de réalisation, guide d'utilisation des produits numériques – Rapport final, REP-57712-, BRGM, Orléans, 62 pp., 2008.

Crumeyrolle, P., Rubino, J., and Clauzon, G.: Miocene depositional sequences within a tectonically controlled transgressive–regressive cycle, in: Sedimentation, Tectonics and Eustasy: Sea-Level Changes at Active Margins, edited by: MacDonald, D. I. M., Spec. Publ. Int. Ass. Sediment., 371–390, 1991.

Curial, A.: La sédimentation salifère et suprasalifère du Paléogène bressan (France): comparaison entre les données diagraphiques et lithologiques, Etude diagraphique du champ d'Etrez et synthèse du bassin, PhD Thesis, Université Lyon 1, 1986.

Debelmas, J.: Etude tectonique de la bordure orientale du Massif du Vercors entre Grenoble et le Mont-Aiguille, Thèse de 3e cycle, University of Grenoble, 44 pp., 1953.

Debelmas, J.: Quelques observations sur l'extrémité N-orientale du massif du Vercors, Trav. Lab. Géol. Fac. Sci. Grenoble., 41, 275–281, 1965.

Debelmas, J.: Structure géologique du massif du Moucherotte, Géol. Alp., 42, 109–116, 1966.

Debelmas, J.: Géologie de la France, Tome 2: Les Chaînes plissées du cycle alpin et leur avant-pays, Ed. Doin, Paris, 296–540, 1974.

DeCelles, P. G. and Giles, K. A.: Foreland basin systems, Basin Res., 8, 105–123, 1996.

De Graciansky, P. C., Roberts, D. G., and Tricart, P.: The Western Alps, from rift to passive margin to orogenic belt, an intergated overview, Developments in Earth Surface Processes, Vol. 14, Elsevier, Amsterdam, 398 pp., ISBN 9780444537249, 2011.

Demarcq, G.: Etude stratigraphique du Miocène rhodanien, Mém. BRGM, Orléans, Vol. 61 257 pp., 1970.

Demory, F., Conesa, G., Oudet, J., Mansouri, H., Münch, P., Borgomano, J., Thouveny, N., Lamarche, J., Gisquet, F., and Marié, L.: Magnetostratigraphy and paleoenvironments in shallow-water carbonates: the Oligocene-Miocene sediments of the northern margin of the Liguro-Provençal basin (West Marseille, southeastern France), Bull. la Société géologique Fr., 182, 37–55, 2011.

Deville, E.: Structure of the Tectonic Front of the Western Alps: Control of Fluid Pressure and Halite Occurrence on the Decollement Processes, Tectonics, 40, 4, https://doi.org/10.1029/2020TC006591, 2021.

Deville, É. and Chauvière, A.: Thrust tectonics at the front of the western Alps: constraints provided by the processing of seismic reflection data along the Chambéry transect, Comptes Rendus l'Académie des Sci. IIA-Earth Planet. Sci., 331, 725–732, 2000.

Deville, E. and Sassi, W.: Contrasting thermal evolution of thrust systems: An analytical and modeling approach in the front of the western Alps, Am. Assoc. Pet. Geol. Bull., 90, 887–907, 2006.

Deville, E., Mascle, A., and Deronzier, J. F.: Etude non exclusive Chartreuse-Vercors 91. Rapport d'interprétation (Atlas, 52 planches), IFP-CGG, Paris, 1992.

Deville, E., Blanc, E., Tardy, M., Beck, C., Cousin, M., and Ménard, G.: Thrust propagation and syntectonic sedimentation in the Savoy Tertiary Molasse Basin (Alpine foreland), in: Hydrocarbon and petroleum geology of France, Springer, Berlin, Heidelberg, 269–280, 1994.

Dickinson, R. W.: Plate tectonics and sedimentation, in: Tectonics and Sedimentation, Vol. 22, edited by: Dickinson, R. W., Special Publications of SEPM, Tulsa, Oklahoma, USA, 1–27, https://doi.org/10.2110/pec.74.22.0001, 1974.

Donzeau, M., Gamond, J.-F., and Mugnier, J.-L.: Evolution latérale et amortissement d'une structure chevauchante, un exemple du Nord Vercors, Comptes rendus l'Académie des Sci. Série 2, Mécanique, Phys. Chim. Sci. l'univers, Sci. la Terre, 317, 1675–1682, 1993.

Doudoux, B., de Lepinay, B. M., and Tardy, M.: Une interprétation nouvelle de la structure des massifs subalpins savoyards (Alpes occidentales): nappes de charriage oligocènes et déformations superposées, CR Acad. Sci., 295, 63–68, 1982.

Doudoux, B., Rosset, J., Barféty, J.-C., Carfantan, J.-C., and Pairis, J.-L.: Carte géologique (1/50 000), feuille Annecy-Ugine (702), BRGM, Orléans, 1992a.

Doudoux, B., Barféty, J. C., Carfantan, J. C., Tardy, M., and Nicoud, G.: Notice explicative, Carte géol. France (1 / 50 000), feuille Annecy-Ugine (702), BRGM, Orléans, 62 pp., 1992b.

Doudoux, B., Barféty, J.-C., Vivier, G., Carfantan, J.-C., Nicoud, G., Colletta, B., and Tardy, M.: Carte géologique (1 / 50 000), feuille Albertville (726), BRGM, Orléans, 1999.

Dumont, M.: Etude stratigraphique et sédimentologique du Miocène supérieur de la région de Jujurieux (Ain, France), PhD thesis, University Lyon 1, 155 pp., 1983.

Dumont, T. and SPIA: Échaillon stone from France: a Global Heritage Stone Resource proposal, Geol. Soc. Lond. Spec. Publ., 486, 115–128, 2020.

Dumont, T., Champagnac, J.-D., Crouzet, C., and Rochat, P.: Multistage shortening in the Dauphiné zone (French Alps): the record of Alpine collision and implications for pre-Alpine restoration, Swiss J. Geosci., 101, 89–110, 2008.

Dumont, T., Simon-Labric, T., Authemayou, C., and Heymes, T.: Lateral termination of the north-directed Alpine orogeny and onset of westward escape in the Western Alpine arc: Structural and sedimentary evidence from the external zone, Tectonics, 30, TC5006, https://doi.org/10.1029/2010TC002836, 2011.

Dumont, T., Schwartz, S., Guillot, S., Simon-Labric, T., Tricart, P., and Jourdan, S.: Structural and sedimentary records of the Oligocene revolution in the Western Alpine arc, J. Geodyn., 56, 18–38, 2012.

Embry, A. F.: Transgressive–regressive (T–R) sequence analysis of the Jurassic succession of the Sverdrup Basin, Canadian Arctic Archipelago, Can. J. Earth Sci., 30, 301–320, 1993.

Embry, A. F.: Sequence boundaries and sequence hierarchies: problems and proposals, Seq. Stratigr. Northwest Eur. Margin, 5, 1–11, 1995.

Enay, R., Gidon, P., Caillon, M., and Doudoux, B.: Carte géologique de la France à 1 / 50 000: Rumilly (701), BRGM, Orléans, 1970.

Ford, M. and Lickorish, W. H.: Foreland basin evolution around the western Alpine Arc, Geol. Soc. Lond. Spec. Publ., 221, 39–63, 2004.

Garefalakis, P. and Schlunegger, F.: Tectonic processes, variations in sediment flux, and eustatic sea level recorded by the 20 Myr old Burdigalian transgression in the Swiss Molasse basin, Solid Earth, 10, 2045–2072, https://doi.org/10.5194/se-10-2045-2019, 2019.

Gaudant, J., Weidmann, M., Berger, J.-P., Bolliger, T., Kalin, D., and Reichenbacher, B.: Recherches sur les dents pharyngiennes de Poissons Cyprinidae de la Molasse d'eau douce oligo-miocène de Suisse (USM, OSM) et de Haute-Savoie (France), Rev. Paléobiologie, 21, 371–389, 2002.

Gidon, M.: Nouvelle contribution à l'étude du massif de la Grande-Chartreuse et de ses relations avec les régions avoisinantes, Trav. du Lab. Géologie Alp., 40, 187–205, 1964.

Gidon, M.: Carte géologique (1 / 50 000), feuille Annecy-Ugine (748), BRGM, Orléans, 1970.

Gidon, M.: La structure de l'extrémité méridionale du massif de la Chartreuse aux abords de Grenoble et son prolongement en Vercors, Géologie Alp., 57, 93–107, 1981.

Gidon, M.: L'anatomie des zones de chevauchement du massif de la Chartreuse (Chaînes subalpines septentrionales, Isère, France), Géologie Alp., 64, 27–48, 1988.

Gidon, M.: Les décrochements et leur place dans la structuration du massif de la Chartreuse (Alpes occidentales françaises), Géologie Alp., 66, 39–55, 1990.

Gidon, M.: Quelques aspects des rapports entre l'histoire tectonique et la morphogenèse dans le massif de la Chartreuse, Géologie Alp., 70, 13–27, 1994.

Gidon, M.: Tectonique et origine de la cluse de Grenoble (France), Géologie Alp., 71, 175–192, 1995.

Gidon, M.: Tectoniques superposées dans le synclinal des Aillons et ses abords (massif des Bauges, Savoie, France), Géologie Alp., 75, 91–102, 1999.

Gidon, M.: Les massifs cristallins externes des Alpes occidentales françaises sont-ils charriés, Géologie Alp., 77, 23–38, 2001.

Gidon, M.: Voreppe, cours inférieur de la Roize, available at: http://www.geol-alp.com/chartreuse/6_localites_ch/voreppe.html, last access: 17 August 2018.

Gidon, M.: Ugine, gorges de l'Arly, available at: http://www.geol-alp.com/bornes/_lieux_aravis/Ugine_NE.html, last access: 23 November 2019.

Gidon, M.: Comboire, Claix, Rochefort, available at: http://www.geol-alp.com/drac/_draclieuxN/comboire.html, last access: 13 January 2020a.

Gidon, M.: Seyssins – Fontaine, available at: http://www.geol-alp.com/h_vercors/lieux_vercors/seyssins.html, last access: 13 January 2020b.

Gidon, M. and Arnaud, H.: Carte géologique détaillée de la France à 1 / 50.000, feuille Grenoble, 2nd Edn., BRGM, Orléans, 1978.

Gidon, M. and Barféty, J.-C.: Carte géologique (1 / 50 000), feuille Montmélian (749), BRGM, Orléans, 1969.

Gidon, M., Arnaud, H., and Montjuvent, A.: Notice explicative, Carte géol. France (1 / 50 000), feuille Grenoble (772), BRGM, Orléans, 37 pp., 1978.

Gidon, P.: Notice explicative, Carte géologique de France (1 / 50 000), feuille Vif (701), BRGM, Orléans, 11 pp., 1970.

Gignoux, M. and Moret, L.: Géologie dauphinoise: initiation à la géologie par l'étude des environs de Grenoble, 2nd Edn., Masson et Cie, Paris, 391 pp., 1952.

Gigot, P., Grandjacquet, C., and Haccard, D.: Evolution tectono-sédimentaire de la bordure septentrionale du bassin tertiaire de Digne depuis l'Eocène, Bull. Soc. Géol. Fr., Sér., 7, 128–139, 1974.

Giot, P. R.: Contribution à l'étude des terrains tertiaires du Royans (Isère et Drôme), Trav. Lab. Géol. Grenoble, 24, 49–68, 1943.

Gorin, G., Signer, C., and Amberger, G.: Structural configuration of the western Swiss Molasse Basin as defined by reflection seismic data, Eclogae Geol. Helv., 86, 693–716, 1993.

Guellec, S., Mugnier, J.-L., Tardy, M., and Roure, F.: Neogene evolution of the western Alpine foreland in the light of ECORS data and balanced cross-section, Mémoires la Société géologique Fr., 156, 165–184, 1990.

Heller, P. L., Angevine, C. L., Winslow, N. S., and Paola, C.: Two-phase stratigraphic model of foreland-basin sequences, Geology, 16, 501–504, 1988.

Herwegh, M., Berger, A., Glotzbach, C., Wangenheim, C., Mock, S., Wehrens, P., Baumberger, R., Egli, D., and Kissling, E.: Late stages of continent-continent collision: Timing, kinematic evolution, and exhumation of the Northern rim (Aar Massif) of the Alps, Earth-Sci. Rev., 200, 102959, https://doi.org/10.1016/j.earscirev.2019.102959, 2020.

Homewood, P.: Faciès et environnements de dépôt de la Molasse de Fribourg, Eclogae Geol. Helv., 74, 29–36, 1981.

Hardenbol, J. A. N., Jacquin, T., Farley, M. B., Jacquin, T., De Graciansky, P.-C., and Vail, P. R.: Mesozoic and Cenozoic Sequence Chronostratigraphic Framework of European Basins, in: Mesozoic and Cenozoic sequence chronostratigraphic framework of European basins, edited by: Graciansky, P.-C., Hardenbol, J. A. N., Jacquin, T., Vail, P. R., SEPM Society for Sedimentary Geology, Vol. 60, https://doi.org/10.2110/pec.98.02.0003, 1998.

Hayes, J. M., Strauss, H., and Kaufman, A. J.: The abundance of ^{13}C in marine organic matter and isotopic fractionation in the global biogeochemical cycle of carbon during the past 800 Ma, Chem. Geol., 161, 103–125, 1999.

Hudson, J. D.: Carbon isotopes and limestone cement, Geology, 3, 19–22, 1975.

Hudson, J. D.: Stable isotopes and limestone lithification, J. Geol. Soc. Lond., 133, 637–660, 1977.

Kalifi, A.: Caractérisation sédimentologique et distribution des dépôts syn-orogéniques Miocènes des chaines subalpines septentrionales (Royans-Vercors-Chartreuse-Bauges), du sud du Jura et du Bas-Dauphiné, Cadre chronostratigraphique et tectonostratigraphique, PhD thesis, University of Lyon 1, 578 pp., 2020.

Kalifi, A., Sorrel, P., Leloup, P.-H., Spina, V., Huet, B., Galy, A., Rubino, J.-L., and Pittet, B.: Changes in hydrodynamic process dominance (wave, tide or river) in foreland sequences: The subalpine Miocene Molasse revisited (France), Sedimentology, 63, 2455–2501, https://doi.org/10.1111/sed.12708, 2020.

Kalifi, A., Sorrel, P., Leloup, P.H., Galy, A., Spina, V., Huet, B., Russo, S., Pittet, B., and Rubino, J.-L.: Tectonic control on the paleogeographical evolution of the Miocene seaway along the Western Alpine foreland basin, Geol. Soc. Lond. Spec. Publ., in review, 2021.

Kälin, D.: Litho-und Biostratigraphie der mittel-bis obermiozänen Bois de Raube-Formation (Nordwestschweiz), Eclogae Geol. Helv., 90, 97–114, 1997.

Kempf, O., Matter, A., Burbank, D. W., and Mange, M.: Depositional and structural evolution of a foreland basin margin in a magnetostratigraphic framework: the eastern Swiss Molasse Basin, Int. J. Earth Sci., 88, 253–275, 1999.

Kwasniewski, A., Rubino, J.-L., Gariteai, T., Lescanne, M., and Mascle, A.: Stratigraphic Variability of tide dominated depositional systems within Miocene sandy succession of Bas Dauphiné basin (Miocene Peri-Alpine foreland basin) SE France, in: IAS congress, 18–22 August 2014, Geneva, Switzerland, 2014.

Lacassin, R., Tapponnier, P., and Bourjot, L.: Culminations anticlinales d'échelle crustale et imbrication de la lithosphère dans les Alpes, apports du profil ECORS-CROP, Comptes rendus l'Académie des Sci. Série 2, Mécanique, Phys. Chim. Sci. l'univers, Sci. la Terre, 310, 807–814, 1990.

Lamiraux, C.: Géologie du Miocène des chainons jurassiens méridionaux et du Bas-Dauphiné nord oriental entre Chambéry et La Tour du Pin: étude stratigraphique, sédimentologique et tectonique, PhD thesis, Université Scientifique et Médicale de Grenoble, 174 pp., 1977.

Latreille, G.: La sédimentation détritique au Tertiaire dans le Bas-Dauphiné et les régions limitrophes, PhD thesis, University of Lyon 1, 340 pp., 1969.

Laubscher, H.: Jura kinematics and the Molasse Bassin, Eclogae Geol. Helv., 85, 653–675, 1992.

Lickorish, W. H., Ford, M., Burgisser, J., and Cobbold, P. R.: Arcuate thrust systems in sandbox experiments: A comparison to the external arcs of the Western Alps, Geol. Soc. Am. Bull., 114, 1089–1107, 2002.

Lirer, F., Maria, F. L., Maria, I. S., Gianfranco, S., Elena, T., Claudia, C., Javier, S. F., and Antonio, C.: Mediterranean Neogene planktonic foraminifer biozonation and biochronology, Earth-Sci. Rev., 196, https://doi.org/10.1016/j.earscirev.2019.05.013, 2019.

Looser, N., Madritsch, H., Guillong, M., Laurent, O., Wohlwend, S., and Bernasconi, S. M.: Absolute Age and Temperature Constraints on Deformation Along the Basal Décollement of the Jura Fold-and-Thrust Belt From Carbonate U-Pb Dating and Clumped Isotopes, 40, e2020TC006439, https://doi.org/10.1029/2020TC006439, 2021.

Mastrangelo, B. and Charollais, J.: Nouvelle conception de la structure du Salève, Arch. des Sci., 70, 43–50, 2018.

McArthur, J. M., Howarth, R. J., and Shields, G. A.: Strontium isotope stratigraphy, in: Geol. time scale, edited by: Gradstein, F. M., Ogg, J. G., Schmitz, M. D., and Ogg, G. M., Elsevier, Amsterdam, Vol. 1, 127–144, 2012.

Mein, P.: A new direct correlation between marine and continental scales in rhodanian Miocene, in: VIII Congr. RCMNS., Hungar. Geol. Survey., Budapest, 377–379, 1985.

Menard, G. and Thouvenot, F.: Balanced cross-sections at crustal scale-methods and application to the western Alps, Geodin. Acta, 1, 35–45, 1987.

Miller, K. G., Kominz, M. A., Browning, J. V., Wright, J. D., Mountain, G. S., Katz, M. E., Sugarman, P. J., Cramer, B. S., Christie-Blick, N., and Pekar, S. F.: The phanerozoic record of global sea-level change, Science, 310, 1293–1298, https://doi.org/10.1126/science.1116412, 2005.

Mock, S., von Hagke, C., Schlunegger, F., Dunkl, I., and Herwegh, M.: Long-wavelength late-Miocene thrusting in the north Alpine foreland: implications for late orogenic processes, Solid Earth, 11, 1823–1847, https://doi.org/10.5194/se-11-1823-2020, 2020.

Mortaz-Djalili, D.: Sédimentologie des formations détritiques du Néogène du plateau de Chambaran (Bas-Dauphiné, France), PhD thesis, Université Scientifique et Médicale de Grenoble, 153 pp., 1977.

Mortaz-Djalili, D. and Perriaux, J.: Le Néogène du Plateau de Chambaran (Bas-Dauphiné, France), Géologie Alp., 55, 133–152, 1979.

Mugnier, J. and Marthelot, J.: Crustal Reflections Beneath the Alps and the Alpine Foreland: Geodynamic Implications, Geodynamic, 22, 177–183, 1991.

Mugnier, J., Arpin, R., and Thouvenot, F.: Balanced cross-sections through the subalpine massif of the Chartreuse, Geodin. Acta, 1, 125–137, 1987.

Mugnier, J.-L., Guellec, S., Menard, G., Roure, F., and Tardy, M.: A crustal scale balanced cross-section through the external Alps deduced from the ECORS profile, Mémoires la Société géologique Fr., 156, 203–216, 1990.

Mujito, S.: Les sédiments tertiaires dans le Jura méridional et les Bauges occidentales: Savoie, Haute Savoie (France)-Alpes françaises, PhD thesis, Université Scientifique et Médicale de Grenoble, 221 pp., 1981.

Nelson, C. S. and Smith, A. M.: Stable oxygen and carbon isotope compositional fields for skeletal and diagenetic components in New Zealand Cenozoic nontropical carbonate sediments and limestones: a synthesis and review, New Zeal. J. Geol. Geophys., 39, 93–107, 1996.

Nicolas, A., Polino, R., Hirn, R., Nicolich, R., and ECORS-CROP Working group: ECORS-CROP traverse and deep structure of the western Alps: a synthesis, in: Deep structure of the Alps, edited by: Roure, F., Heitzmann, P., and Polino, R., Mém. Soc. Geol. France, NS, 15–27, 1990.

Nicolet, C.: Le Bas-Dauphiné septentrional: étude stratigraphique et sédimentologique, PhD thesis, Université Scientifique et Médicale de Grenoble, 150 pp., 1979.

Ogg, J. G. and Lowrie, W.: Magnetostratigraphy, in: The Geologic Time Scale 2012, edited by: Gradstein, F. M., Ogg, J. G., Schmitz, M., Ogg, G., Elsevier, Amsterdam, 85–114, 2012.

Ogg, J. G., Ogg, G. M., and Gradstein, F. M.: A concise geologic time scale: 2016, Elsevier, Amsterdam, 2016.

Ori, G. G. and Friend, P. F.: Sedimentary basins formed and carried piggyback on active thrust sheets, Geology, 12, 475–478, 1984.

Pelin, S.: Etude géologique du bassin de Pont-en-Royans Vercors-Alpes françaises, PhD thesis, Université Scientifique et Médicale de Grenoble, 68 pp., 1965.

Pfiffner, O.-A., Lehner, P., Heitzmann, P., Mueller, S., and Steck, A.: Deep structure of the Swiss Alps: results of NRP 20, Birkhäuser, Basel, 380 pp., 1997.

Pfiffner, O. A.: Geology of the Alps, John Wiley & Sons, Wiley-Blackwell, Sussex, UK, 368 pp., 2014.

Philippe, Y.: Rampes latérales et zones de transfert dans les chaînes plissées: géométrie, condition de formation et pièges structuraux associés, PhD thesis, Université de Savoie (Chambéry), 1995.

Philippe, Y., Colletta, B., Deville, E., and Mascle, A.: The Jura fold-and-thrust belt: a kinematic model based on map-balancing, Mémoires du Muséum Natl. d'histoire Nat., 170, 235–261, 1996.

Philippe, Y., Deville, E., and Mascle, A.: Thin-skinned inversion tectonics at oblique basin margins: example of the western Vercors and Chartreuse Subalpine massifs (SE France), Geol. Soc. Lond. Spec. Publ., 134, 239–262, 1998.

Posamentier, H. W. and Allen, G. P.: Siliciclastic sequence stratigraphy: concepts and applications, SEPM (Society for Sedimentary Geology) Tulsa, Oklahoma, Vol. 7, https://doi.org/10.2110/csp.99.07, ISBN 101-5-6576-0700, 1999.

Rangheard, Y., Demarcq, G., Muller, C., Poignant, A., and Pharisat, A.: Donnees nouvelles sur le Burdigalien du Jura interne; paleobiologie, biostratigraphie et evolution structurale, Bull. la Société Géologique Fr., 6, 479–486, 1990.

Ricketts, B. D. and Evenchick, C. A.: Evidence of different contractional styles along foredeep margins provided by Gilbert deltas: examples from Bowser Basin, British Columbia, Canada, B. Can. Petrol. Geol., 55, 243–261, 2007.

Rigassi, D.: Le Tertiaire de la région genevoise et savoisienne, Bull. der Vereinigung Schweizerisches Pet. und-Ingenieur, 24, 19–34, 1957.

Roure, F., Howell, D. G., Guellec, S., and Casero, P.: Shallow structures induced by deep-seated thrusting, Pet. Tectonics Mob. Belts, Technip., Paris, 15–30, 1990.

Rubino, J. L., Lesueur, J. L., and Clauzon, G.: Le Miocène inférieur et moyen du bassin rhodanien: stratigraphie séquentielle et sédimentologie, Field Trip Guidebook: Special Publication of the Association des Sédimentologistes Français, ASF, 67 pp., 1990.

Saltzman, M. R. and Thomas, E.: Carbon isotope stratigraphy, in: The Geologic Time Scale 2012, edited by: Gradstein, F. M., Ogg, J. G., Schmitz, M. D., and Ogg, G. M., Vol. 1, Elsevier, Amsterdam, 207–232, 2012.

Schlunegger, F. and Kissling, E.: Slab rollback orogeny in the Alps and evolution of the Swiss Molasse basin, Nat. Commun., 6, 8605, https://doi.org/10.1038/ncomms9605, 2015.

Signer, C. and Gorin, G. E.: New geological observations between the Jura and the Alps in the Geneva area, as derived from reflection seismic data, Eclogae Geol. Helv., 88, 235–265, 1995.

Simon-Labric, T., Rolland, Y., Dumont, T., Heymes, T., Authemayou, C., Corsini, M., and Fornari, M.: $^{40}Ar/^{39}Ar$ dating of Penninic Front tectonic displacement (W Alps) during the Lower Oligocene (31–34 Ma), Terra Nova, 21, 127–136, 2009.

Sinclair, H. D.: Tectonostratigraphic model for underfilled peripheral foreland basins: An Alpine perspective, B. Geol. Soc. Am., 109, 324–346, 1997.

Sinclair, H. D. and Allen, P. A.: Vertical versus horizontal motions in the Alpine orogenic wedge: Stratigraphic response in the foreland basin, Basin Res., 4, 215–232, https://doi.org/10.1111/j.1365-2117.1992.tb00046.x, 1992.

Sissingh, W.: Tertiary paleogeographic and tectonostratigraphic evolution of the Rhenish Triple Junction, Palaeogeogr. Palaeocl., 196, 229–263, 2003.

Smeraglia, L., Looser, N., Fabbri, O., Choulet, F., Guillong, M., and Bernasconi, S. M.: U–Pb dating of middle Eocene–Pliocene multiple tectonic pulses in the Alpine foreland, Solid Earth, 12, 2539–2551, https://doi.org/10.5194/se-12-2539-2021, 2021.

Steininger, F. F., Berggren, W. A., Kent, D. V, Bernor, R. L., Sen, S., and Agusti, J.: Circum-Mediterranean Neogene (Miocene and Pliocene) marine-continental chronologic correlations of European mammal units, in: The Evolution of Western Eurasian Neogene Mammal Faunas, edited by: Bernor, R. L., Fahlbusch, V., Mittmann, H.-W., Columbia Univ. Press, New York, 7–46, https://doi.org/10.7916/D86D63B1, 1996.

Suppe, J., Chou, G. T., and Hook, S. C.: Rates of folding and faulting determined from growth strata, in: Thrust tectonics, edited by: McClay, K. R., Springer, Dordrecht, 105–121, 1992.

Wade, B. S., Pearson, P. N., Berggren, W. A., and Pälike, H.: Review and revision of Cenozoic tropical planktonic foraminiferal biostratigraphy and calibration to the geomagnetic polarity and astronomical time scale, Earth-Sci. Rev., 104, 111–142, 2011.

Watkins, H., Butler, R. W. H., and Bond, C. E.: Using laterally compatible cross sections to infer fault growth and linkage models in foreland thrust belts, J. Struct. Geol., 96, 102–117, 2017.

Young, J. R., Bown, P. R., and Lees, J. A.: Nannotax3 website, International Nannoplankton Association, available at: http://www.mikrotax.org/Nannotax3 (last access: January 2021), 2017.

Ziegler, P. A.: Evolution of the Arctic-North Atlantic and the Western Tethys: A visual presentation of a series of Paleogeographic-Paleotectonic maps, AAPG Mem., 43, 164–196, 1988.

Ziegler, P. A.: Geological atlas of western and central Europe, Shell Iternationale Petroleum Maatschappij BV, Mijdrecht, the Netherlands, 1990.

Ziegler, P. A.: Cenozoic rift system of Western and Central-Europe – an overview, Geol. en Mijnb., 73, 99–127, 1994.